DOCTORAL THESIS

UNIVERSITAT POLITÈCNICA DE VALÈNCIA

MODELLING OF HEAT LOSSES THROUGH COATED CYLINDER WALLS AND THEIR IMPACT ON ENGINE PERFORMANCE

PRESENTED BY
Johan Enrique Escalona Cornejo

SUPERVISED BY
Xandra Marcelle Margot

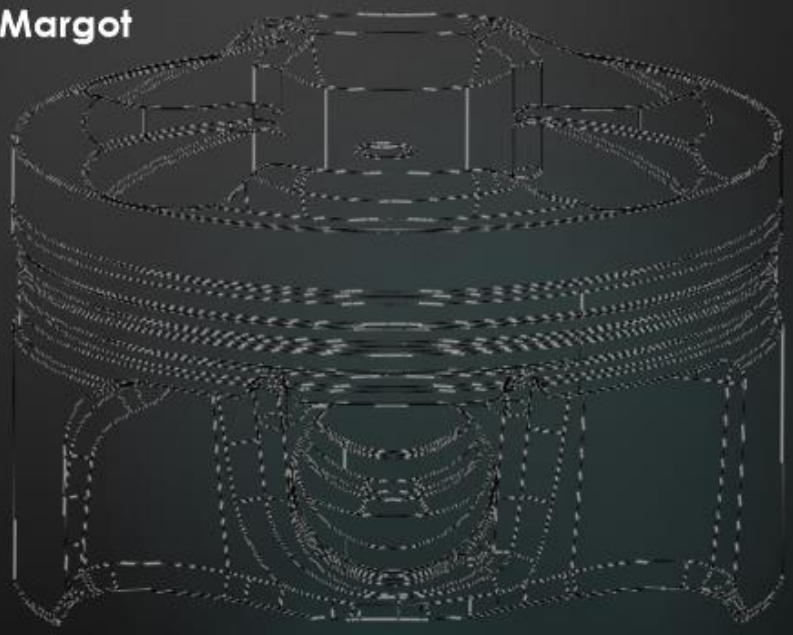

February 2021
DEPARTAMENTO DE MÁQUINAS Y MOTORES TÉRMICOS

UNIVERSITAT POLITÈCNICA DE VALÈNCIA
DEPARTAMENTO DE MÁQUINAS Y MOTORES TÉRMICOS

DOCTORAL THESIS

MODELLING OF HEAT LOSSES THROUGH COATED CYLINDER WALLS AND THEIR IMPACT ON ENGINE PERFORMANCE

PRESENTED BY

Johan Enrique Escalona Cornejo

SUPERVISED BY

Dr. Xandra Marcelle Margot

FOR THE DEGREE OF

Doctor of Philosophy

February 2021

DOCTORAL THESIS

"Modelling of heat losses through coated cylinder walls and their impact on engine performance"

Presented by: Johan Enrique Escalona Cornejo
Supervised by: Dr. Xandra Marcelle Margot

THESIS EXAMINERS

Dr. Pablo Fernandez-Yánez Luján
Dr. Federico Millo
Dr. Angelo Onorati

DEFENSE COMMITTEE

Chairman: Dr. Antonio José Torregrosa Huguet
Secretary: Dr. Octavio Armas Vergel
Member: Dr. Federico Millo

Valencia, February 2020

To all who have supported me on this endeavor

Abstract

Currently, vehicles powered by internal combustion engines (ICE) are targeted as contributing largely to environmental pollution. In this regard, there has been significant international cooperation to enact laws that regulate the polluting emissions. Hence, the car manufacturers have oriented efforts to the development of cleaner and more eco-friendly technologies. In order to face this situation, electrified vehicles have emerged as one of the most promising projects in the automotive industry for the coming years.

However, this target still seems far on the horizon. In this sense, hybridization with thermal and electric engines seems to be the path to follow in the short term. Consequently, ICEs will continue to be one of the important sources of terrestrial propulsion in the coming years.

To mitigate the inherent polluting effects of internal combustion engines, different technologies have been proposed to develop more efficient engines. Among them, the application of thermal coatings on the combustion chamber walls. This technology aims at reducing the heat losses in the engine, and thus increase its thermal efficiency.

The main objective of this thesis is to study the impact of coating the combustion chamber walls of an engine on heat losses and thermal efficiency. The experimental definition of the heat fluxes through the walls is complex and not very reliable because it requires the measurement of wall temperatures. For this reason, CFD-CHT (Computational fluid dynamics-Conjugate Heat Transfer) is used.

The first step was to validate the computational tool employed for CFD-CHT calculations in internal combustion engines. For this, a preliminary study in simple geometries such as a circular pipe or a rectangular channel was performed. Heat transfer models were evaluated and the relevance of certain parameters such as roughness was determined. To reinforce the study, a thermal analysis in a more realistic geometry such as the piston of a

CI engine was carried out. The temperature values calculated by the software were almost the same as the experimental measurements. Consequently, the reliability of the computational tool was verified.

Next, a methodology was proposed to address the problem of modeling very thin layers of thermal coating for three-dimensional CFD-CHT calculations. The methodology consists in defining an "equivalent material" with a thickness and number of nodes that allow a computationally realistic mesh. For this, a DoE in combination with a multiple regression analysis was employed.

The first CFD-CHT simulations in ICEs were carried out for a gasoline engine. The study was performed for two configurations: metallic engine and engine with coated piston and cylinder head. An exhaustive heat transfer analysis was made in order to determine the impact of applying the thermal coating on the engine. Comparison with experimental data proved the suitability of the CHT calculations to evaluate heat losses in ICEs. However, no improvement on engine efficiency was observed in the gasoline engine due to the type of coating applied on the combustion chamber walls.

Experience with the gasoline engine calculations showed that CHT calculations were very time consuming. In this regard, some strategies aimed at optimizing the calculations were analyzed in order to reduce calculation times. The most successful methodology was based on AMR cell refinement to optimize the mesh and reduce significantly the computational costs. This approach was used to study the impact of applying a new generation thermal coating on the piston top of a Diesel engine. The results obtained indicated that this type of coating allows for some improvement in the thermal efficiency of the engine without affecting its performance.

Resumen

Actualmente, los vehículos propulsados por motores de combustión interna alternativos (MCIA) constituyen uno de los mayores agentes contaminantes para el medio ambiente. En este sentido, ha existido una importante cooperación internacional para promulgar leyes que regulen las emisiones contaminantes. De manera que los fabricantes de coches han impulsado el desarrollo de tecnologías más limpias y amigables con el medio ambiente. Ante esta situación, ha surgido recientemente la electrificación, como uno de los proyectos más ambiciosos de la industria automotriz para los próximos años. Sin embargo, esta meta parece aún lejana en el horizonte. En tal sentido, la hibridación con motores térmicos y eléctricos parece ser el camino a seguir en el corto plazo. Por consiguiente, los MCIA seguirán siendo la principal fuente de propulsión terrestre durante los años venideros.

Para mitigar los inherentes efectos contaminantes de los motores de combustión interna, se han propuesto diferentes tecnologías para desarrollar motores más eficientes. Entre ellas, la aplicación de recubrimientos térmicos en las paredes de la cámara de combustión apuntan a reducir las pérdidas por calor en el motor, y así aumentar su eficiencia térmica.

El objetivo principal de esta tesis es estudiar el impacto de aplicar recubrimientos térmicos en las paredes de la cámara de combustión en motores de combustión interna. En este sentido, determinar los flujos de calor experimentalmente a través de las paredes es complicado y no del todo fiables, debido a que dependen de la medición de las temperaturas de pared. Por este motivo, el CFD-CHT es utilizado.

El primer paso fue validar la herramienta computacional que es utilizada para los cálculos en motores de combustión interna. Para ello se realizó un estudio preliminar en geometrías sencillas como una tubería circular o un canal rectangular. Se evaluaron los modelos de transferencia de calor y se determinó la relevancia de ciertos parámetros como la rugosidad. Para complementar el estudio, se realizó un análisis de las temperaturas en una ge-

ometría más realista como el pistón de un MCIA. Los valores de temperatura calculados por el software fueron casi iguales a las medidas experimentales. Por consiguiente, la fiabilidad de la herramienta computacional fue verificada.

Seguidamente, se plantea una metodología para abordar al problema de modelar capas muy finas de recubrimientos térmicos en el espacio tridimensional. Para de esta manera poder simular las paredes recubiertas en la cámara de combustión. La metodología consiste en definir un material equivalente con un espesor y número de nodos que permitan un mallado computacionalmente realista. Para ello se utilizó un DoE en combinación con un análisis de regresión múltiple.

Los primeros estudios se llevaron a cabo en un motor de gasolina. El modelado se llevó a cabo para dos configuraciones: motor con paredes metálicas y motor con pistón y culata recubiertos. A través de un análisis exhaustivo de la transferencia del calor, se evaluó el impacto que tenía aplicar el revestimiento térmico en el motor. La comparación con datos experimentales demuestran la utilidad del cálculo CHT para evaluar las pérdidas de calor en un MCIA. Sin embargo, ninguna mejora fue observada en el motor de gasolina debido al tipo de recubrimiento aplicado en las paredes de la cámara de combustión.

Las simulaciones llevadas a cabo en el motor de gasolina permitieron determinar que los cálculos CHT son computacionalmente largos. En este sentido, una serie de estrategias diseñadas a optimizar los cálculos han sido analizadas con el fin de reducir los tiempos de cálculo. A través de este estudio, se encontró una metodología para optimizar la malla del dominio computacional. Esta última, emplea un refinamiento AMR basado en la distancia de pared. Este método es utilizado para modelar el impacto de aplicar un revestimiento térmico de última generación en la parte superior del pistón de un motor Diesel. Los resultados obtenidos indican que este tipo de recubrimientos permiten una mejora en la eficiencia térmica del motor sin efectos negativos.

Resum

Actualment, els vehicles propulsats per motors de combustió interna alternatius (MCIA) constitueixen un dels majors agents contaminants per al medi ambient. En aquest sentit, ha existit una important cooperació internacional per a promulgar lleis que regulen les emissions contaminants. De manera que els fabricants de cotxes han impulsat el desenvolupament de tecnologies més netes i amigables amb el medi ambient. Davant aquesta situació, ha sorgit recentment l'electrificació, com un dels projectes més ambiciosos de la indústria automotriu per als pròxims anys. No obstant això, aquesta meta sembla encara llunyana en l'horitzó. En tal sentit, la hibridació amb motors tèrmics i elèctrics sembla ser el camí a seguir en el curt termini. Per consegüent, els MCIA continuaran sent la principal font de propulsió terrestre durant els anys esdevenidors.

Per a mitigar els inherents efectes contaminants dels motors de combustió interna, s'han proposat diferents tecnologies per a desenvolupar motors més eficients. Entre elles, l'aplicació de recobriments tèrmics en les parets de la cambra de combustió apunta a reduir les pèrdues per calor en el motor, i així augmentar la seua eficiència tèrmica.

L'objectiu principal d'aquesta tesi és estudiar l'impacte d'aplicar recobriments tèrmics en les parets de la cambra de combustió en motors de combustió interna. En aquest sentit, determinar els fluxos de calor experimentalment a través de les parets és complicat i no del tot fiable, pel fet que depenen del mesurament de les temperatures de paret. Per aquest motiu, el CFD-CHT (Computational fluid dynamics-Conjugate Heat Transfer) és utilitzat.

El primer pas va ser validar l'eina computacional que és utilitzada per als càlculs en motors de combustió interna. Per a això es va realitzar un estudi preliminar en geometries senzilles com una canonada circular o un canal rectangular. Es van avaluar els models de transferència de calor i es va determinar la rellevància de certs paràmetres com la rugositat. Per a

complementar l'estudi, es va realitzar una anàlisi de les temperatures en una geometria més realista com el pistó d'un MCIA. Els valors de temperatura calculats pel software van ser quasi iguals a les mesures experimentals. Per consegüent, la fiabilitat de l'eina computacional va ser verificada.

Seguidament, es planteja una metodologia per a abordar el problema de modelar capes molt fines de recobriments tèrmics en l'espai tridimensional, per a d'aquesta manera poder simular les parets recobertes en la cambra de combustió. La metodologia consisteix a definir un material equivalent amb una grossària i nombre de nodes que permeten un mallat computacionalment realista. Per a això es va utilitzar un DoE (Design of experiments) en combinació amb una anàlisi de regressió múltiple.

Els primers estudis es van dur a terme en un motor de gasolina. El modelatge es va dur a terme per a dues configuracions: motor amb parets metàl·liques i motor amb pistó i culata recoberts. A través d'una anàlisi exhaustiva de la transferència de la calor, es va avaluar l'impacte que tenia aplicar el revestiment tèrmic en el motor. La comparació amb dades experimentals demostren la utilitat del càlcul CHT per a avaluar les pèrdues de calor en un MCIA. No obstant això, cap millora va ser observada en el motor de gasolina a causa de la mena de recobriment aplicada en les parets de la cambra de combustió.

Les simulacions dutes a terme en el motor de gasolina van permetre determinar que els càlculs CHT són computacionalment llargs. En aquest sentit, una sèrie d'estratègies dissenyades per a optimitzar els càlculs han sigut analitzades amb la finalitat de reduir els temps de càlcul. A través d'aquest estudi, es va trobar una metodologia per a optimitzar la malla del domini computacional. Aquesta última, empra un refinament AMR (Adaptive mesh refinement) basat en la distància de paret. Aquest mètode és utilitzat per a modelar l'impacte d'aplicar un revestiment tèrmic d'última generació en la part superior del pistó d'un motor Dièsel. Els resultats obtinguts indiquen que aquest tipus de recobriments permeten una millora en l'eficiència tèrmica del motor sense efectes negatius.

List of publications

The work presented in this doctoral thesis has outcome in the publication of the following papers:

[1] A. Broatch, P. Olmeda, X. Margot, and J. Escalona. "New approach to study the heat transfer in internal combustion engines by 3D modelling". International Journal of Thermal Sciences 138, 2019, pp. 405–415.

[2] A. Broatch, X. Margot, J. Garcia-Tiscar, and J. Escalona. "Validation and Analysis of Heat Losses Prediction Using Conjugate Heat Transfer Simulation for an Internal Combustion Engine". In: 14th International Conference on Engines & Vehicles. SAE International, 2019.

[3] P. Olmeda, X. Margot, P. Quintero, and J. Escalona. "Numerical approach to define a thermodynamically equivalent material for the Conjugate Heat Transfer simulation of very thin coating layers". International Journal of Heat and Mass Transfer 162, 2020, p. 120377.

[4] A. Broatch, P. Olmeda, X. Margot, and J. Escalona. "Conjugate Heat Transfer study of the impact of "thermo-swing" coatings on Internal Combustion Engines heat losses". International Journal of Engine Research 138, 2020, pp. 405–415.

[5] X. Margot, J. Escalona, and A. Bianco. "Development of a Novel Numerical Methodology for the Assessment of Insulating Coating Performance in Internal Combustion Engines". Submitted to SAE WCX World Congress Experience, 2021.

[6] P. Olmeda, X. Margot, P. Quintero, and J. Escalona. "Reply to short communication 'Comment on "Numerical approach to define a thermodynamically equivalent material for the conjugate heat transfer simulation of very thin coating layers" by P. Olmeda, X. Margot, P. Quintero, J. Escalona, International Journal of Heat and Mass Transfer, Vol. 162(2020) 120377 " by Jaal Ghandhi and Georgios Koutsakis". International Journal of Heat and Mass Transfer, 2021.

Additionally, one more manuscript has been submitted for publication and is undergoing peer-review:

[7] X. Margot, J. Gomez-Soriano, P. Quintero, and J. Escalona. “Implementation of 1D-3D integrated model for thermal prediction in internal combustion engines ”. Submitted to Applied Thermal Engineering, 2020.

Funding and acknowledgments

The author wishes to acknowledge the financial support received through contract FPI-2018-S2-1205 of the Programa para la Formación de Personal investigador (FPI) 2018 of Universitat Politècnica de València .

Parts of the work presented in this thesis have received funding from the European Union's Horizon 2020 research and innovation programme under grant agreement No 724084.

The author wishes to thank IFPEN for their permission to use their single cylinder engine geometry and experimental results, as well as Saint Gobain Research Provence for providing the coating characteristics.

The respondent wants to express its gratitude to CONVERGENT SCIENCE Inc. and Convergent Science GmbH for their kind support for performing the CFD-CHT calculations using CONVERGE software.

Acknowledgements

I would like to thank my supervisor Xandra Margot for giving me the chance to be part of the CMT, and for her support throughout all these years. I really appreciate your willingness to collaborate to face all the problems that came up. Similarly, I want to express my gratitude to all the CMT staff, who collaborated in one way or another during this stage. Above all, to Amparo and the administration staff that helped me to solve many administrative problems.

I also want to thank Professors. Alberto Broatch and Pablo Olmeda for the knowledge provided. In particular, the latter is responsible for developing the lumped model, which was an important element for my work. Likewise, I thank Josep Gomez-Soriano for sharing with me his knowledge about CFD modeling, which helped me to establish the basis to carry out this investigation.

In this recognition, I also want to include all my colleagues who shared with me this journey and made it less stressful during all these years, Barbara Diesel, Shusma Artham, Amin Dreif, Arturo Arcila, Josep Salvador. I also wish to express a special acknowledgment to Ferran Roig for his willingness to collaborate and help all the time.

This thesis would not have been possible without the collaboration of all the people who made my arrival in Spain possible. Therefore, I want to record my infinite gratitude towards Oscar Suescun, Oscar Burguillos, Lorena Aular and Alejandro Viacaba. Although you are far away, you will always be like family. I also want to thank Margarita Jiménez for her attention and support in the last years.

I cannot name them all, but I thank all my friends who were part of this process and were a source of energy and support during the hard times.

I also wish to include in this recognition the company POWERTECH PWT, for allowing me to carry out an international cooperation work. In particular, I thank Andrea Bianco and Enrico Pautasso for giving me this opportunity.

I am also infinitely grateful for the unconditional support of my parents and my brother, for their advice and strength to overcome the difficulties.

Finally, I want to express my huge gratitude to Karolina Sobas, for always being there in the difficult moments and make me see the light when the things turned complicated.

"If you can't fly then run, if you can't run then walk, if you can't walk then crawl, but whatever you do you have to keep moving forward."

Martin Luther King Jr, *United States*

Contents

List of Figures

List of Tables

List of Symbols

Latin

c	Volumetric heat capacity
c_p	Molar constant pressure specific heat for species k
h	Depending on the context, height or heat transfer coefficient
k	Thermal conductivity
Nu	Nusselt number
Q	Transferred heat
P	Pressure
Pr	Prandtl number
R	Depending on the context, universal gas constant or thermal resistance
Re	Reynolds number
T	Temperature

Greek

α	Void fraction
δ	Crevice clearance
η	Efficiency
λ	Air-fuel ratio
μ	Dynamic viscosity
ρ	Density
σ	Surface tension
ω	Depending on the context, gas temperature period or oscillating velocity of the cooling oi

Sub- and superscripts

CoO	Referred to cooling oil
conv	Referred to convection

comb	Referred to combustion
eff	Referred to effective area
embed	Referred to embedded
exh	Referred to exhaust
ext	Referred to external wall temperature
ThO	Referred to thermal oil
in	Referred to inlet
ind	Referred to indicated
int	Referred to intake
opt	Referred to optimal
out	Referred to outlet
sat	Referred to saturation
tot	Referred to total resistance
vap	Referred to vaporization
vol	Referred to volumetric

Acronyms

0D	Zero-dimensional
1D	One-dimensional
2D	Two-dimensional
3D	Three-dimensional
AMR	Adaptive Mesh Refinement
ARPA-E	Advanced Research Projects Agency - Energy
BMEP	Brake Mean Effective Pressure
CAD	Depending on the context, crank angle degrees or Computer-Aided Design
CFD	Computational fluid dynamics
CFL	Courant-Friedrichs-Levy
CHT	Conjugate heat transfer
CI	Compression-ignition
CMT	Centro de Motores Térmicos
CPU	Central Processing Unit
CO	Carbon monoxide
CO2	Carbon dioxide
DoE	Design of experiments
EB-PVD	electron beam-physical vapor deposited
EVO	Exhaust Valve Opening
FEA	Finite Element Analysis
HC	Hydrocarbon
HRIC	High Resolution Interface Capture
HT	Heat transfer
HTC	Heat transfer coefficient

HTM	Heat transfer model
HVLP	High Velocity Low Pressure
ICE	Internal Combustion Engine
IFPEN	IFP Energies Nouvelles
IMEP	Indicated Mean Effective Pressure
IVC	Intake Valve Closing
KH	Kelvin-Helmholtz
LIP	Lifetime of laser-induced phosphorescence
LHR	Low Heat Rejection
MCIA	Motores de Combustión Interna Alternativos
MFB50	Mass Fraction Burnt 50%
MFB10-90	Mass Fraction Burnt 10%-90%
NO_x	Nitrous oxides (NO and NO_2)
PSZ	Zirconia partially stabilized
R&D	Research and development
SI	Spark ignited
Si4N3	Silicon nitride
SiC	Carbide silicon
SiRPA	Silica Reinforce Porous Anodized Aluminum
TACOM	s Tank Automotive Command
TBC	Thermal barrier coating
TSWIN	Temperature Swim Insulation Coating
U.S.	United States
VOF	Volume of fluid
ZrO2	Zirconia
PISO	Pressure implicit with splitting of operators method
RANS	Reynolds averaged Navier-Stokes
RNG	Re-Normalized Group
RoHR	Rate of Heat Release
RT	Rayleigh-Taylor mechanism
URANS	Unsteady Reynolds averaged Navier-Stokes
RAM	Random-access memory

CHAPTER 1

Introduction

Since the very beginning of its history, the automobile industry has led its efforts to achieve better and more efficient powertrains. Along all these years of evolution many changes have been introduced in the market, mainly motivated by the human needs and environmental concerns. Nowadays, most of the vehicles are powered by an internal combustion engine based on the development of Nicolaus Otto in the XIX century. Currently, the world is looking for new technologies that help to beat the global warming by reducing the pollutant emissions. In this regard, the manufacturers point to electrify the vehicles in the coming decades. However, the commercialization of full electrified cars has still a long way to go. Then, hybridization seems to be the solution in the short time.

Many years in the market are guaranteed for the internal combustion engines that are currently present in most of the passenger's automobiles. Then, the new engine designs should adapt to the regulations to protect the ecosystem and particularly, fulfill the more stringent CO2 emissions limits. It is estimated that European countries will reduce their CO2 emission per km at least by 37.5% in 2030 [8]. The target is to develop fuel saving solutions that allow to reduce the losses during the energy conversion process of the engine. In Fig. 1.1 is shown the CO2 target emissions by country in the coming years.

In particular, thermal losses through the combustion chamber walls represent around 20-30% of the overall heat energy balance in an engine. Different alternatives have appeared during the last years to increase the thermal efficiency of internal combustion engines. Hence, thermal losses are an important concern considered for the development of innovative approaches to improve the efficiencies of the engines.

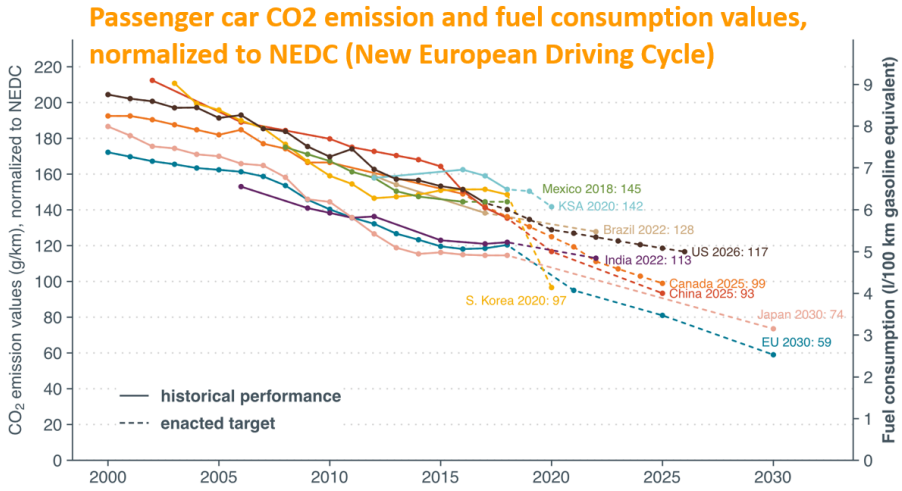

Figure 1.1: *CO2 target emissions by country. Solid dots and lines represent the historical performance, solid dots and dashed lines indicate the enacted targets and solid dots and dotted lines represent the proposed target [8].*

Among the solutions that have been studied recently to increase the thermodynamic efficiency are: using ultra-lean mixtures, downsizing the engines and coating the combustion chamber walls with advanced insulation materials.

However, the prediction of the heat losses through the combustion chamber walls by means of experimental and numerical tools remains still challenging due to the complexity of the physical processes involved in an internal combustion engine.

1.1. Internal Combustion Engines

The first invention of the internal combustion engine is attributed to the Italian engineers Eugenio Bersanti and Felice Matteucci in 1853 [9]. However, the concept of engine as we know it today would not come until the first four stroke engine developed by Otto in 1876 based on the studies of Alphonse Beau de Rochas [10].

The basic operation of the current engines consists in converting the power of a fuel in mechanical energy. Diesel and spark ignited (SI) engines have dominated the power plants in transportation [11] since their invention. Though the compression engines provide a lot of benefits in terms of performance in comparison to the SI engine, they present several drawbacks

regarding the NOx and particulate matter emissions [12]. On the other hand, many aftertreatment emission systems have been developed to clean up the Diesel engines without the expected success. In addition, these equipments yield an increase of the production cost with a final impact in the consumer. In the other way round, petrol engines were considered until few years ago as more polluting since their CO2 emissions are higher than those of the compression ignition engines. Nonetheless, the NOx emissions of gasoline engines are significantly lower than its Diesel relative and different studies have determined that they are more toxic than CO2 for the humans [13].

Even that gasoline engines provide some benefits for the human health, high CO2 emissions have a high impact on the planet because they are responsible for the global warming. In this regard, electrification of the powertrains is currently the challenge for automotive manufacturers. However, this migration will take time and the internal combustion engines will keep playing a key role as a propulsive system in transportation during the next years by means of ICE vehicles or hybrid powertrains.

Nowadays, Diesel engines still occupy an important part of the worldwide marketplace. However, gasoline engines will represent major part in the future and some R&D efforts need to be focused on thermal engines to further improve the efficiency of new hybridized powertrains.

1.2. Heat losses in ICEs

Since their invention, internal combustion engines have been the responsible of the propulsion of many kind of power plants. Their use is not limited only for vehicles and they have been employed, among others, in trucks, power generation and marine propulsion.

An ICE is a thermal machine that transforms the heat coming from the combustion in useful work. The high temperature and pressure that result from the chemical reaction between a fuel and an oxidant yield a force that causes the displacement of a solid component, that in reciprocating engines is a piston. The linear translation of the pistons is transformed in rotational motion by means of connecting rods and a crankshaft that provide the movement of the vehicle wheels.

Unfortunately, the whole thermal energy generated in the engine is not converted in power and the thermal efficiency in a ICE in the best case scenario and best-in class powertrains can reach up to 45 % [14]. The performance of the engine is limited mainly by the losses that take place in the engine as the mechanical friction, pumping losses, cooling and exhaust

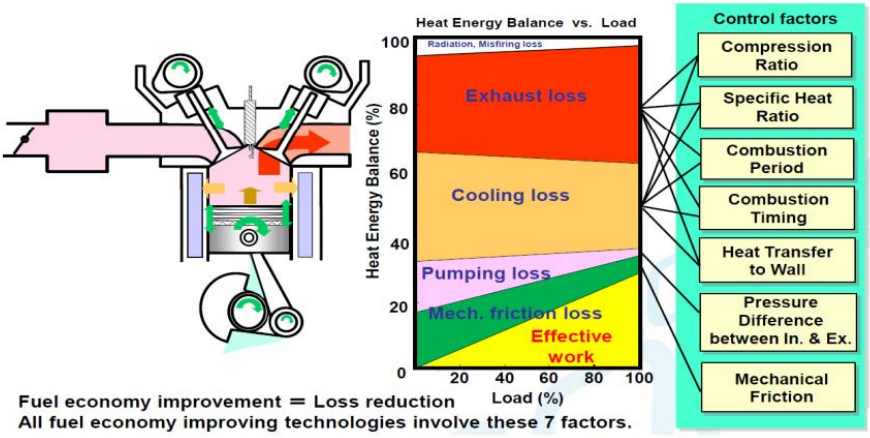

Figure 1.2: *Heat energy balance of an internal combustion engine [8].*

losses. Moreover, an important part of the heat generated during the engine cycle is lost through the combustion chamber walls, so that decreases the efficiency. The heat energy balance of an ICE is illustrated in Fig. 1.2

Hence, the automobile industry has given a particular attention to the reduction of the thermal losses through the combustion chamber walls in an ICE. Especially, after the second world war when the target of an adiabatic engine arises as a solution to increase the low thermal efficiencies of 20-30%, in the vehicles back then.

However, it was not until 1975 when the U.S Army's Tank Automotive Command (TACOM) along with Cummins Inc. began the first works to develop an adiabatic engine. The idea consisted in the creation of an engine with components made with ceramic materials. Along the years the approach was evolving and the concept of Low Heat Rejection (LHR) engine was introduced in the 1980s based on coating the combustion chamber walls with insulation materials. This invention was inspired in the thermal barrier coatings (TBC) used in the aviation for gas turbines to enhance their performance. TBCs usually have low thermal conductivity and high heat capacity that allow working at very high temperatures at the same time that they increase the durability of the components.

At first sight, this innovation would decrease the thermal losses by decreasing the thermal gradient between the combustion gas and the walls. However, some studies carried out later found several drawbacks that limited the suitability of the TBC in internal combustion engines.

However, the manufacturers kept addressing their efforts in developing new and more suitable insulation solutions. Hence, in XXI century, it emerged new advanced insulation materials to enhance the performance of ICE. Unlike the TBCs, these improved coatings have low thermal conductivity and low heat capacity. These properties allow to the coated combustion chamber walls to follow the temperature of the combustion gas in order to reduce the thermal losses. Nonetheless, the tools available currently in the industry are limited to develop a new efficient coating and there is still a long way to go through.

1.3. Objetives

The objective of this thesis is to study the heat transfer through the combustion chamber walls in an ICE by means of 3D computational calculation tools, as well as determine the suitability of applying thermal insulation coatings on solid walls of the piston and cylinder head to increase the engine efficiency. In order to comply with this target, additional objectives have been defined:

- Validation of the conjugate heat transfer 3D-CHT calculation to study the heat transfer through the solid regions in an internal combustion engine and determine what parameters will allow achieving good results.
- Developing new numerical strategies to study the behavior of advanced insulation coatings applied on the combustion chamber walls in an ICE. Since the knowledge regarding this topic is limited to few works available in the literature, the contributions on this matter will help to further studies on coated engines.
- Optimization of the 3D calculation tools for saving computational resources. The simulation of physical processes in the 3D space tends to embrace an important consumption of resources that sometimes limit the performance of the simulations. Then, improvements in this regard will permit to carry out a wider parametric research for a better understanding of the heat transfer in an ICE.

1.4. Thesis outline

This thesis comprises seven chapters. The introduction presented here constitutes the Chapter 1. Then, in Chapter 2 a comprehensive literature review on the heat losses in internal combustion engines is carried out. This chapter starts introducing fundamentals regarding the thermal management and the heat transfer in ICE. Afterwards, the most extended coating applications on ICE to reduce the heat losses will be presented. Finally, the different numerical methods to study the heat transfer in ICE are described.

In order to validate the 3D computational tool employed in this work to analyze the heat transfer in ICEs, preliminary simulations in simplified geometries are performed in Chapter 3. The results are compared with analytical solutions available in the literature. Furthermore, it is studied the effect of the roughness on the heat transfer to determine if this parameter needs to be considered to model the ICE in the 3D simulations in the following chapters. In addition, a validation with experimental measurements in the piston of a Diesel engine is carried out to confirm the reliability of the tool for engine geometries.

Chapter 4 describes the methodology employed to study the application of thin insulation coatings on the combustion chamber walls. The chapter introduces the 1D numerical lumped model developed in CMT to study the heat transfer in ICEs. Subsequently, the results of the proposed, elaborate method are explained.

The developed methodology will be used in combination with the 3D computational tool to study the heat transfer in ICE by means of CHT calculations in Chapter 5. First, the geometry, models and boundary conditions are described for a gasoline engine. The simulations will be performed for two engine configurations: uncoated and coated. Then, the results will be compared with experimental data and 1D numerical tools.

In Chapter 6 is presented a strategy to optimize the computational time of the 3D-CHT simulations in ICE. The simulations will be performed in a Diesel engine and similar as the previous chapter the model set-up along with an exhaustive analysis of the results will be presented.

Finally, Chapter 7 summarizes the main conclusions as result of the investigation carried out in this thesis. In addition, future works that could contribute to this line of investigation are highlighted.

CHAPTER 2

Literature review

Heat losses are an important issue to take into account to enhance the performance of internal combustion engines. All the improvement that manufacturers may try to implement in the powertrains need to be evaluated previously with engineering tools in order to guarantee their suitability.

In this chapter, a literature review of the thermal management in ICE and the heat transfer through the combustion chamber walls in internal combustion engines is presented. In particular, it is focused on the techniques that have been used to predict the heat losses and estimate spatial temperature distributions in the solid components of the engine.

Furthermore, a state of the art about the strategies employed to reduce the thermal losses in ICE is provided. Emphasizing the application of insulation coatings on the engine cylinder walls. The overview of this new technology that points out to improve the engine efficiency will allow a better understanding of the complexity to assess experimental and computationally the behavior of these innovative materials.

Finally, the literature review is extended to the numerical tools employed in the industry to determine the heat losses in ICE. An especial attention is given to coupled conjugate heat transfer models, since they will give the bases to develop numerical solutions concerning to the heat transfer in ICE.

2.1. Thermal management in ICE

The combustion process that takes place in the combustion chamber is responsible of the power generation in fossil fuel vehicles. This chemical reaction where the fuel is burnt occurs in thousandths of seconds and it implies an important increase in pressure and temperature as consequence of the energy release.

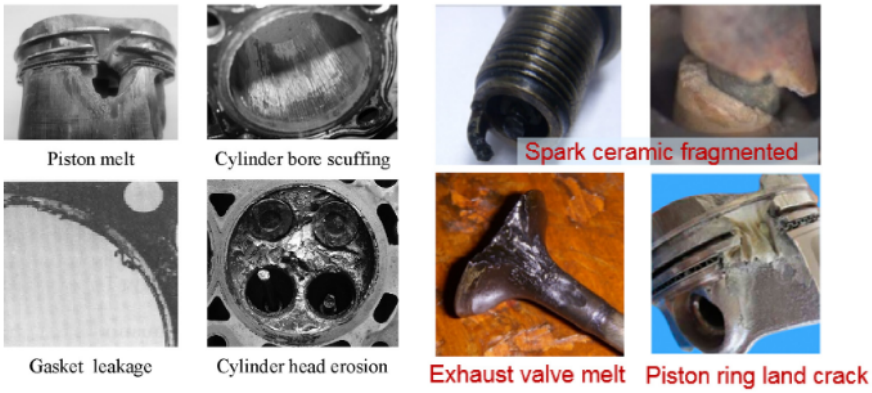

Figure 2.1: *Typical damage caused by engine knock [17]. Illustration of the effects of conventional knock (left) adapted from [18] and representation of the effects of super-knock (right) reprinted from [19]*

Very high temperatures in the combustion chamber are related to pollutant emissions and fuel consumption over the limits [15]. In addition, in gasoline engines, high temperatures on the combustion chamber walls can lead to knock occurrence and in a worst case scenario to more damaging phenomenon known as super-knock [16].

Thermal management in internal combustion engines is oriented to the control of the warm-up of the engine according to the operating conditions. In this regard, the cooling system plays a key role in the performance of the engine [20] . One of the main functions of the cooling system is to limit the highest temperature of the solid surfaces.

Some works have determined that thermal stresses and deformations due to high temperature can affect negatively the performance of the components [21]. For instance, the hottest spot on the engine piston must not be greater than 66 % of melting point temperature of the material [22]. In addition, thermal management by cooling oil minimizes the chances of formation of carbon on the piston that may induce appearance of hot spots on the surface [23]. This fact could be harmful for the engine due to the hot zones in the combustion chamber is one of the causes that leads to pre-ignition of the mixture.

For many years, some efforts in the automotive marketplace have been focused on developing strategies that allow a better thermodynamic performance on the engines [24]. Vagenas et al. [25] propose an innovative cooling jet system able to keep the temperatures in the critical range of the exhaust valve or cylinder head. In 2006, Wagner et al. [24] presented a

thermal management system denominated as “coolant rail” aimed to reduce the presence of hot spots through the cylinder. Tanaka et al. [26] developed an oil-cooled Diesel engine with no fins on the block achieving better performance than a water-cooled engine at warming operation with lower emissions.

Summarizing, the cooling systems are implemented to provide heat dissipation in the engine at high power operation conditions [27]. Moreover, the efficiency of thermal management system to warm up the engine at cold start improves the fuel consumption and reduces the pollutant emissions [28].

Despite that most of the heat generated for an ICE occurs in the combustion chamber, there is an interaction between all the systems intended for the thermal management in the engines. In typical configurations, the engines are cooled by a jacket with passages through the block and the cylinder head while the piston is oil jet cooled. Therefore, all the solid components as piston, head, valves and engine block are affected by the thermal conditions of the cooling system. Furthermore, these considerations need to be taken into account for the experimental and numerical assessment of the heat transfer through the combustion chamber walls as will be shown in Chapter 5.

2.2. Heat transfer in ICE

The heat transfer through the combustion chamber walls results from the interaction of the several thermal systems integrated in an internal combustion engine. Reducing the heat losses due to this interaction is currently one of the main goals for future vehicles. Understanding the heat transfer through the engine components has been an issue widely studied since the early engine inventions [18, 29, 30].

In order to predict the heat transfer from the fluid to the solid regions some researchers have developed empirical correlations [31] with the main target to approach numerical solutions as close as possible to the experiments. However, due to the complex thermodynamics during the engine operation, heat transfer modeling in ICEs is a challenging task. [32].

In this regard, during the last decades of XX century some authors achieved important findings. Woschni found important correlations taking into account the piston motion and the combustion [33]. Nowadays, Woschni contributions are still used to calculate the heat transfer in ICE.

In the early 1970s Seale et al. [34] were able to identify the location of the maximum heat transfer coefficient in the combustion chamber. In addition, they presented a correlation for the cooling oil heat transfer on the piston. Few years later Sinkei continues looking for a heat transfer universal correlation using the dimensional analysis [35]. Prasad et al. [36] carried out numerical simulations in a Diesel engine to study the heat losses through the combustion chamber by a finite difference method.

Along the last three decades it has been remarkable the work of Rakopoulus [37] concerning the heat transfer in internal combustion engines. One of his first contributions consisted in using a 0D turbulence model to evaluate the heat transferred from the fluid to the solid walls on the combustion chamber with results very close to experimental data. Subsequently, he would use a two zones combustion model to assess the impact of the ambient temperature on the performance of a Diesel engine [38]. Later, by using 2D-3D numerical strategies he was able to determine the temperature distribution and heat flux in the piston and liner in a CI engine [39].

In 1998, he presented a 3D model based on finite elements for the thermodynamic analysis of an insulated Diesel engine in steady conditions. This approach was able to estimate the heat fluxes and the temperatures on the gas exposed surfaces in the combustion chamber [40]. In subsequent works this was used to study the heat transfer in transient operation conditions [41]. For instance, an experimental research where thermocouples and sensors were used and let him to assess the heat fluxes in the cylinder head and exhaust manifold [42].

During the arrival of the XXI century, he kept leading important investigations in Diesel engines. Experimental tests and numerical simulations allowed him to estimate the temperature wall evolution on the solid surfaces of the combustion chamber walls [43]. These findings constitute a relevant reference to study the heat transfer through the solid surfaces in ICE and to evaluate the denominated “Wall temperature swing”. Moreover, an experimental methodology was presented to study local heat transfer effects on the engine [44]. Among the most relevant results, this work highlights the significant differences that exist between local heat transfer coefficient (HTC) along the combustion chamber domain and the mean HTC value.

Other authors have led experimental simulations to determine the temperature of the combustion chamber walls. Alkidas et al. [45] investigated the effects of the equivalence air-fuel ratio and the volumetric efficiency on the heat transfer. For their experiments the heat flux was measured on the liner and cylinder head in a gasoline engine. The results concluded that

the heat flux was higher in a stoichiometric air fuel mixture than in a lean or rich mixture. Enomoto et al. [46] used thermocouples to measure the wall temperature evolution of 100 points in the chamber and the values were employed to estimate the heat fluxes. Similar approaches have been used to assess the transient wall temperature and heat flux on the piston top exposed to the combustion chamber [47].

In general, experimental methods to study the heat transfer from the gas to the walls consist in using sensors as thermocouples in the solid regions of the piston, liner and cylinder head. These devices measure the temperature or the heat flux in specific points of the combustion chamber walls in an engine. Since the sensors provide reliable values they allow to develop and validate empirical correlations to evaluate the heat transfer in combustion engines.

While some authors have analyzed the heat transfer in ICE using experimental approaches, other researchers have developed analytical correlations to predict the heat losses. However, predicting the thermal behavior in an ICE is not trivial due to the multiple variables interacting during the engine operation, especially when unusual phenomena as knock or super knock take place in the engine. This fact has been demonstrated by some authors. Recently, Broekaert et al. [48] led an investigation to study the impact of the pressure oscillations caused by knocking combustion on the heat transfer in the combustion chamber. They used sensors to measure the heat flux in the engine and compare the results with the correlations of Annand [31] and Woschni [33]. Moreover, they found that the empirical equations are not able to model properly the variations of the heat transfer due to the knock. Finally, they proposed a modification of Annand's correlation able to estimate the heat transfer during knocking combustion. In this regard, many authors have presented variations of the most extended correlations available in the literature in order to improve them and achieve a more accurate prediction of the heat losses.

In spite of the important contributions on heat transfer in combustion engines, the ICE are evolving constantly. Therefore, some models or strategies used some years ago may lead to inadequate results to assess the engine performance. In other cases, they need to be adapted to the new powertrain systems. Anyway, experimental measurements are always desirable to study the heat transfer from the fluid to the combustion chamber walls. However, in order to achieve this target sophisticated techniques with measuring

devices and test benches are required. Hence, the numerical simulations become highly relevant for the car's manufacturers during early designing stages of new prototypes.

2.3. Insulation coatings applied in ICE

Coating the combustion chamber walls has been one of the alternatives to improve the thermal management in the reciprocating engines and reduce the heat losses. There is a whole field in the industry only committed with the development of new insulation materials with better properties.

The employment of insulation coatings in ICE has two main objectives. First, they are used to increase the endurance of the components to the high thermal conditions that take place in the engine. Also, they are applied to enhance the durability of the engine by protecting the parts of the damages due to wear, such as oxidation and corrosion. The other widely used application of the coatings is the reduction of the heat loss through the combustion chamber walls. The target is to reduce the thermal gradient between the temperatures of the combustion gas and the chamber walls. They are commonly applied to coat partially or wholly the surface of the combustion chamber walls (piston, liner, cylinder head and valves).

Insulation materials should avoid over heating the walls during the intake gas phase of the engine cycle. In addition, their physical properties need to allow the adherence to the metallic components of the engine. On the other hand, detachment and decomposition of the coating may affect the air-fuel mixture in detriment of the engine performance.

The application of insulation materials to coat the combustion chamber walls in both spark ignition and compression engines have been studied using experimental methods along with numerical simulations.

2.3.1. Adiabatic engines

During the 1970s, many global factors such as the oil crisis and high fuel costs encouraged manufacturers to improve the efficiency of the vehicles [49]. Then, it came up the first ideas about the possibility of developing an adiabatic engine by TACOM and Cummins Inc. in 1975 [50]. The concept evolved in the following years, and it mainly consisted of using the thermal energy that is normally lost through the walls of the combustion chamber to obtain better efficiencies. In the early 1980s, LHR (Low Heat Rejection) engines were born as result of these investigations.

LHR engine investigations were conducted mainly on Diesel engines. This concept was based on an engine with the combustion chamber walls made from a ceramic material. At first instance, these materials can increase their temperature higher than the metallic materials such as aluminum or steel. In these works, the authors mainly used zirconia [51] as insulation material.

There were high expectations for the development of this technology due to the benefits they could offer in internal combustion engines. The hypothesis suggested that the high temperatures in the walls would reduce the thermal gradient with the combustion gas, and therefore the heat losses. Moreover, this had a positive impact on the engine performance. Among other things, this technology was thought to increase thermal efficiency and improve the fuel consumption [52].

In order to evaluate the advantages of this application, several numerical and experimental studies were carried out. In this regard, Miyairi et al [53] developed a model for an LHR Diesel engine with different insulating materials such as PSZ (Zirconia partially stabilized) and ZrO2 (Zirconia). His results would lead him to conclude that materials with low conductivity and low thermal capacity could induce improvements in the thermal efficiency and the emissions. At the same time, other numerical tests developed by different authors showed optimistic results in LHR engines [54, 55]. However, other researchers began to doubt the effectiveness of this approach and the reliability of the models employed to study the heat transfer [56].

On the other hand, some experimental results where constant operating conditions were maintained also suggested an improvement in thermal efficiency, fuel consumption and emissions reduction. For instance, Wade et al. [57] found improvements of 4 to 7 % in the fuel consumption of a Diesel engine with ceramic coatings on the cylinder head, valves, piston and liner. Thring et al. [49] also reported improvements in a Diesel engine coated with ceramic materials. In a turbocharged engine, the fuel consumption improved by 7 %, while in a turbocompound engine it was up to 15 %. However, NOx emissions increased by 15 %. Hence, the first contradictions with the numerical results about the possible benefits of LHR engines emerged. In this matter, Cheng and Wong [58] used ceramic materials in the piston and part of the cylinder head of an engine. Among the results, they found a significant deterioration in fuel consumption and higher wall temperatures, in addition to a negative effect during the combustion process.

It is important to remark that the most of those works were carried out on Diesel engines, since an important sector of the automotive industry focused their efforts to improve this kind of engines. Nonetheless, according to the results obtained in compression engines, it can be assumed that this LHR approach would lead to several drawbacks in gasoline engines.

Although there was a significant support to finance the development of LHR engines, many disadvantages were found in applying this technology in internal combustion engines.

Most of the authors agreed on a deterioration in the volumetric efficiency due to the high temperatures in the combustion chamber walls. However, there was not a clear consensus on the effect of ceramic coatings on the thermal efficiency in LHR engines, due to some authors claimed a gain [49, 59], while others noted a reduction [60–62]. Regarding fuel consumption, the investigations pointed to higher consumption in atmospheric engines, which improved in turbocharged and turbcompound engines. Finally, many experimental results indicated a deterioration in pollutant emissions such as NOx, HC and CO [63, 64].

All these negative findings in LHR engines were mainly due to the high temperatures in the combustion chamber walls, as a consequence of applying thick ceramic coatings with low thermal conductivities and high heat capacity such as Si4N3 (silicon nitride), SiC (carbide silicon), zirconia and PSZ. So that, the research centers working in this field began to rethink the use of ceramic coatings in ICEs.

2.3.2. Thermal Barrier Coatings

Considering the drawbacks found in LHR engines with thick coatings, the authors led their efforts to study the application of thinner thermal coatings. Again, TACOM and Cummins Inc. would be the pioneers for this approach. In the first studies conducted in the late 1980s, Kamo et al. [65] used thermal coatings with thicknesses less than 200 microns in a spark ignition engine. Their results allowed them to associate the temperature swing in the combustion chamber walls with the physical properties of the material. In addition, they also detected a significant difference in the temperature swing of coatings with thin thicknesses with respect to the thick layers of insulating materials, used until then in LHR engines. Thus, the interest of the scientific community was encouraged to study thermal barrier coatings TBCs (Thermal Barrier Coatings) in internal combustion engines.

TBCs are thermal coatings that have been used for many years in aeronautics to extend the life of components, such as turbines and burners [66]. Therefore, they must be resistant and withstand the high temperatures to which they are subjected during their operation. In particular, this application is useful for turbines, as it allows working with fluids at higher temperatures, with a positive impact on their performance.

Plasma-coated PSZ coatings (Plasma-sprayed and yttria-stabilized zirconia) and EB-PVD (electron beam-physical vapor deposited) ceramic coatings are between the most widely used TBCs in aeronautics [67].

Some authors suggested that TBCs would lead to some improvements in engine power and emissions. Furthermore, they would extend the life of engine components [68]. In this sense, Kamo et al. [69] carried out experimental studies on a Diesel engine with different configurations applying coatings on the combustion chamber walls. Their results indicated that applying TBCs on the piston and cylinder head surfaces was more effective than coating the liner.

Beyond that some experiments had shown some positive trends, there were not strong enough arguments to certify the application of TBCs to reduce the heat losses in the combustion chamber. Then, with the arrival of the new millennium, some authors considered the possibility of using TBCs with lower thermal conductivities [70]. However, in the first studies there were problems concerning the durability of the coating materials, since they had a short life cycle [71]. Furthermore, the fact that the coatings could disintegrate would affect the air-fuel mixture due to contamination with ceramic material waste.

As is widely known by engine manufacturers, high temperatures in the combustion chamber can promote auto-ignition of the mixture and generate knock on gasoline engines. For this reason, the literature on spark ignition engines with TBCs is quite limited. However, some experimental tests applying 0.10 to 0.27 mm thickness coatings in the combustion chamber of a gasoline engine, led to improvements in the power and the fuel consumption without the presence of knock [72]. Then, after many years of research to improve that concept of "adiabatic engine", the results indicated that the path was in thin coatings with low thermal conductivity and low heat capacity.

Moreover, some recent works have shown that the the use of TBCs such as Yttria-Stabilized Zirconia [73] offers an opportunity to develop cleaner engines that may comply with the stringent regulations to limit CO2 emissions [74]. The use of these insulating materials allows achieving higher exhaust

temperatures and this improves the performance of the aftertreatment systems, accelerating the catalyst light-off. Furthermore, the application of TBCs in combination with new calibration strategies can promote improvements in fuel economy [75, 76].

2.3.3. New generation of Insulation coatings

Over the past decade environmental regulations have become more stringent, and the need for more efficient engines has increased considerably. Consequently, during the 2010s, the authors did not stop searching for more effective coatings for ICEs that can optimize fuel consumption, increase engine efficiency, and do not affect the emissions. In the case of gasoline engines, it is particularly important to avoid auto-ignition and knock.

In 2013, researchers from Toyota Corp. research center introduced what they called "Temperature Swing Insulation Coating (TSWIN)" [77]. This consisted in coating the engine combustion chamber walls with a materials that allow wall temperature to follow the gas temperature during the engine cycle. This would reduce the temperature gradient between the gas and the solid walls. Therefore, it should increase the thermal efficiency of the engine without affecting the performance.

Other authors [78], through numerical simulations, confirmed the hypotheses stated by Toyota that a coating capable of following instantaneously the temperature of the combustion gases would lead to a gain in the thermal efficiency. In particular, both works agree that the "ideal" material should have 1/32 times the properties of the zirconia, typically used in TBCs. Fig. 2.2 shows a comparison between the metallic engine configurations with the TBCs and the TSWIN coatings. In addition, the same figure displays the influence of the thickness and the compression ratio on the thermal efficiency of the TSWIN coatings

However, developing a material with such physical properties is not possible yet with the current technology. Even though the investigations on this topic point to coatings with physical properties closer to this "ideal material", advances in TSWIN coating concept have been carried out by developing more realistic coatings.

For 2016, Toyota presented a material called SiRPA (Silica Reinforce Porous Anodized Aluminum), with a thermal conductivity of $0.67 W/(mK)$ and a heat capacity of $1300 kJ/(m^3 K)$. This material was used to coat the piston of a turbocharged Diesel engine, specifically in the TSWIN 2.4 GD and 2.8 GD engines, reaching a maximum efficiency of 44% % [79]. However, in these models the entire surface was not coated and the piston cavity was excluded.

So that, the coated portion on the piston is quite small. In addition, other improvements in the intake and exhaust systems have been included on this engine. Hence, the 1 % reduction in the heat losses reported in their work does not allow to reach a conclusion on the suitability of the SiRPA as a thermal coating.

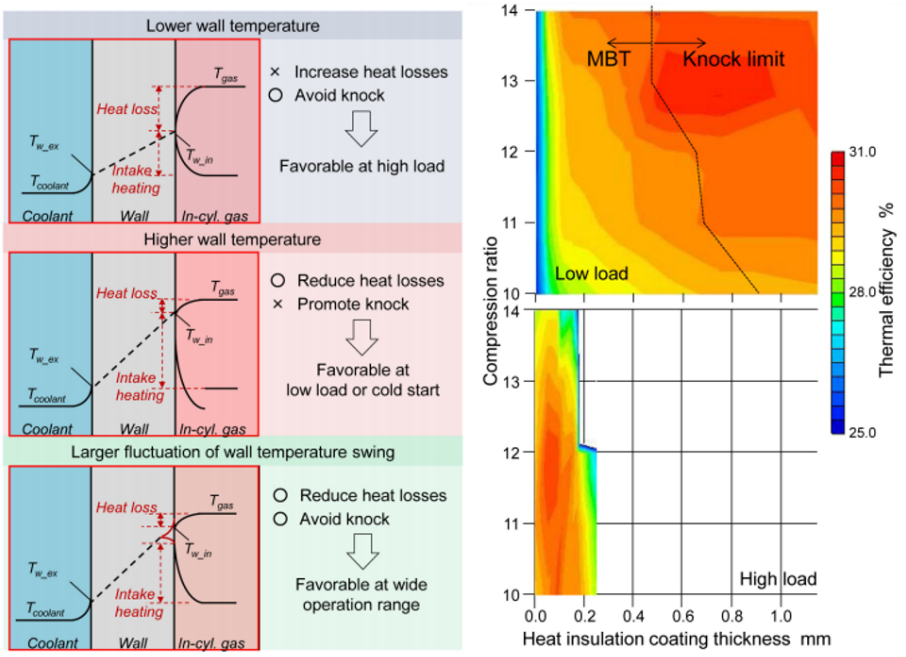

Figure 2.2: *The effect of the combustion chamber wall surface temperature and its swing on heat losses and knock (left): Lower wall temperature for metallic walls, higher wall temperature for typical ceramic TBC and larger fluctuation of wall temperature swing for TSWIN coatings. Thermal efficiency contour maps for different compression ratios and heat insulation coating thicknesses (right) [78].*

Toyota Corp. has stated that a 100 microns SiRPA coating layer generates a temperature swing enough to reduce the thermal gradient between combustion chamber walls and the gas. However, validating these claims through traditional experimental techniques is quite complicated. On the one hand, due to the characteristics of the coating, it is difficult to place thermocouples on the surfaces of the combustion chamber walls, and it is necessary to use other techniques to measure the temperature on the solid surfaces. In order

to solve this problem, Fukui et al. [80] presented a method to measure the instantaneous temperature in the coated walls through optical techniques. The process was called LIP (lifetime of laser-induced phosphorescence) and they were able to measure a temperature swing at a point on the surface of the piston. They also determined a higher temperature gradient for a coated piston compared to an aluminum base piston. However, there were some uncertainties about the effectiveness of this technology. In particular, the temperature swing measured on the surface of the aluminum piston is considerably higher than that found by several authors through different numerical and experimental tests.

Nevertheless, the researchers have not declined in their efforts to find a "TSWIN" material that allows reducing the heat losses in the combustion chamber. In this sense, the United States Department of Energy (U.S. Dept of Energy) and ARPA-E (Advanced Research Projects Agency - Energy) have opened the way for a new generation of TBCs with better benefits [81]. The coatings developed under this project improved significantly the physical properties of Toyota's SiRPA, since they have thermal conductivities less than $0.40 W/(mK)$ and heat capacities less than $500 kJ/(m^3 K)$. This work was carried out in cooperation with the University of Madison Wiscosin and they used binders mixed with aluminosilicate, metals and oxide powders to decrease the conductivity, density and specific heat capacity. For this, they used the HVLP (High Velocity Low Pressure) spray technique on the surfaces of the piston, cylinder head and valves.

The application of coatings by HVLP as its initials indicate, consists of spraying a binder on the surfaces at high speed and low pressure. The authors have identified two binders that offer great durability and capacity to resist high temperatures. Therefore, they can be used as thermal coatings: organic polysilazane binder and metal phosphate binder.

This technology has been evaluated with different coated configurations on a SI engine. The results presented the polysilazane coatings as the best candidate to serve as an insulating material in ICEs. Furthermore, there was a reduction of 4% in the heat losses, as well as an improvement in the thermal efficiency of the engine about 1.1-1.3%. In addition, they managed to prevent the engine from entering in knocking regime.

From the economic point of view, the development of this technology implies a high cost, due to expensive manufacturing processes and the need for complex experimental measurements to validate the reliability of the materials. Hence, the efforts also seem to be oriented to lower the high cost of developing better coatings. In this regard, some authors [82] have applied

this new generation of TBCs to the piston of a gasoline engine, reducing the production cost by 23%. Moreover, they achieved benefits in the thermal efficiency, related to the temperature swing on the piston surface.

The investigations regarding the application of thermal coatings on the combustion chamber walls are expected to continue during the coming years. Likewise, it is necessary to optimize the numerical and experimental methods to evaluate the impact of these thermal coatings on the performance of ICEs.

2.4. Numerical methods

Nowadays, the automotive industry has a strong interest in improving ICEs and vehicles in general. Any modification in the engine will have an effect on the heat transfer directly or indirectly. For this reason, it has become important for the manufacturers to have tools at hand that allow them to study the physical processes that take place inside the engine.

A priori, experimental techniques are the most suitable, due to their reliability. However, they need an accurate calibration the building of expensive and complex test benches. Though there are necessary, or even mandatory, numerical methods are extremely useful during the early stages of the engine design. Especially, considering the wide range of possibilities that they offer to study the ICEs. Numerical simulations offer several advantages over experimental tests, among others, we can highlight:

- No dependence on physical measurement equipment.
- The possibility of conducting multiple tests with different configurations and input parameters, which in many cases is not possible experimentally.
- Depending on the type of simulation, the results can be obtained in a reasonable time.

Numerical methods for studying the heat transfer in ICEs comprise the simplified 0D-1D models to more detailed and complex 3D models. The convenience of using any of them depends on the objectives of the research, as well as the sought accuracy target.

2.4.1. One dimensional models

The 1D models to study the heat transfer take into account several hypotheses, and the physical processes are considered to occur in a one-dimensional plane. Consequently, the equations that govern the system are significantly simplified. In general, unlike 3D modeling, these models yield results in a very short time. However, they require an accurate and detailed calibration.

Currently, most of the manufacturers dedicate significant resources to the development of 1D computational tools that allow studying the heat transfer in ICEs. This interest comes from the fact that one-dimensional models are less expensive and allow to model in an integrated way all the components acting in the operation of an engine, such as the cooling, lubrication, friction and combustion systems, among others.

Over the past years, 1D models have been improved due to the extensive data obtained with 3D models and experimental simulations. Therefore, many of these models produce reliable results and they have been included into different computational tools employed in the industry. Thus, one-dimensional models have become in an important mean for modeling the heat transfer in ICEs.

The 1D models developed until now have made possible to obtain a good prediction of the temperatures on solid surfaces of an engine. In this regard, the contributions made by different authors in terms of thermal management and heat transfer in ICEs have been essential. In general, most of the computational tools for 1D simulations use the most well-known empirical correlations (Woschni [33], Colburn [83], Gnielinki [84], Ditus-Boelter [85], Sider-Tete [86]).

The use of 1D lumped models is widely applied to study the heat transfer through the solid walls of an ICE. In these models, the solid regions are discretized in a finite number of nodes considering certain assumptions to simplify the system. The main hypothesis considered by these models is that the heat flow is one-dimensional. This is supported by different investigations, where it is shown that the radial temperature distribution is negligible compared to the axial distribution [87]. Torregrosa et al. [88] have presented a model to predict the wall temperatures in the combustion chamber. The model consisted of only three nodes: piston, liner, and cylinder head. The convection coefficient between the gas and the solid walls was calculated with the Woschni general equation of [33]. The temperatures determined with the model were successfully validated with experimental measurements.

Based on the fundamentals of this lumped model, Olmeda et al. [89] have achieved a remarkable progress in evaluating the heat transfer in ICEs. Among other things, they developed a methodology to calculate the heat flow inside a turbocharger for a Diesel engine, considering the working fluids and the turbocharger components. Furthermore, they have used the lumped model to integrate it with a 0D model for combustion calculations [90, 91].

Besides their use to determine heat fluxes and temperatures in conventional engines, the 1D models play an important role in evaluating the behavior of thermal coatings. In this sense, Kikusato et al. [78] performed one-dimensional simulations to evaluate the behavior of different insulating materials in order to determine an optimal coating to improve the performance of ICEs. From this work, it is remarkable the physical properties that were defined for the ideal coating, since they have been the target values considered by the researchers:

- Thermal conductivity: $0.1 W/(mK)$
- Heat capacity; $100 kJ/(m^3 K)$
- Thickness: 100 microns

This kind of numerical approximations allow to evaluate the heat transfer in ICE in a general way. However, to study phenomena that are more complicated such the heat transfer in all directions, the spatial temperature distribution or the local effects of the wall temperatures in the combustion chamber, more advanced numerical methods are needed.

2.4.2. 3D Conjugate heat transfer

3D heat transfer models allow to study with higher detail the physical processes that take place in ICEs. However, the fact of involving more variables implies a more exhaustive calibration of the inputs, as well as significantly longer calculation times compared to the one-dimensional models. In particular, the main 3D approaches for evaluating the heat transfer in engines are summarized below:

- CFD (Computational Fluid Dynamics): Isothermal conditions are considered for the solid surfaces in contact with the gas. So that only the fluid region is calculated.
- Finite Element Analysis (FEA): Only the solid regions are calculated, imposing thermal conditions on each surface of the solid domain.

- Conjugate calculation CHT (Conjugate Heat Transfer): It can be considered as the most complete of the methods since it allows to solve the fluid and solid regions in only one simulation. In general, the fluid domain is calculated by CFD, while the solid is solved by numerical approximations similar to the FEA.

Although the CFD calculations yield accurate information about the fluid in the engine (temperature, pressure, velocities), the fact of assuming constant temperatures on the engine walls throughout the full cycle can affect the combustion and lead to inaccuracies. On the other hand, this approach might not be the best one to analyze the heat transfer in the engine. As an alternative to this problem, decoupled heat transfer models have been proposed [92–94]. These consist in calculating the fluid regions by means of CFD, assuming constant temperatures; while solid regions are solved by FEA. The heat flux and gas properties calculated with the CFD are used as boundary conditions to calculate the thermal conduction through the solid domain. Wall temperatures are updated in a new CFD calculation, and the process is repeated until the temperatures converge. However, this methodology may be computationally inefficient due to the exchange of information between different calculation tools.

Instead, CHT simulations aim to be one of the most suitable methods to study the heat transfer in ICEs. The conjugate calculation allows to study local variables such as the spatial temperature distribution of any solid surface, the local and temporal heat transfer coefficient and the gas velocities close to the solid walls. Moreover, it is also possible to determine the thermal stresses to improve the solid components and optimize the cooling system [95]. In addition, the CHT simulations improve the modeling of the boundary layer, since the transient and non-homogeneous wall temperature improves the boundary layer of vaporization, which has an impact on calculating the emissions [96].

Even though the CHT calculations seem to be the most suitable approach to analyze the heat transfer in ICEs, it has some disadvantages compared to CFD and FEA calculations. Indeed, due to the meshing of both the fluid and the solid domains, it has a significant computational cost. In addition, the convergence of the solid regions is much slower than the fluid regions. Therefore, it may take many cycles to ensure full convergence of the computational domain.

In recent years, technological advances in the computational field has allowed the development of powerful tools for 3D modelling, in particular for CHT calculations. However, even though the investigations on this matter increased significantly during the last decade, the information available in the literature is still quite limited.

Xin et al. [97] were between the first authors to apply the 3D-CHT calculation in ICEs, demonstrating that the heat flux and the temperature of the combustion chamber walls are not uniform. A few years later, Urip et al. [98] implemented numerical equations to couple the fluid and solid regions of an ICE into a computational model. In this study, they used the KIVA code to investigate the transient heat transfer process in a Ford 5.4-L V8 engine. Subsequently, Yuanhong et al. [96] coupled the transient heat conduction calculations in the solid components of the combustion chamber of a Diesel engine with fluid calculations by finite volumes and central differentiation schemes. This calculation approach was employed to model the combustion process in the combustion chamber and the heat transfer through the solid walls of the piston and cylinder head.

Some experimental studies have validated the CHT calculations. In this regard, Iqbal et al. [99] compared the temperatures obtained by means of the CHT simulations with experimental measurements from thermocouples located in specific sections in the intake and exhaust ports of the engine. Other authors [100] that modeled by CHT the heat losses throughout the cycle of a Diesel engine for marine applications have used similar techniques. In this case, for the validation they used thermocouples located on the surface of the piston. In addition, with this methodology they were able to estimate with thermal resistances, the impact of ceramic TBCs in ICEs.

Recently, most of the works on CHT in ICEs has been mainly focused on numerical simulations including certain engine components such as the piston, cylinder head or valves. Full-integrated simulations, including all the engine systems are not common, since it implies a significant investment in computational resources.

Although important advances have been achieved to model the heat losses in ICEs by CHT calculations, there are some applications that remain unexplored, as the analysis of the heat transfer in engines with the combustion chamber walls coated with the new generation of insulating materials. In this regard, most of the investigations [101] are limited to evaluate the influence of insulating coating, ignoring the thermal inertia of the material, which leads to an inaccurate prediction of the heat transfer through the combustion chamber.

2.5. Summary

After reviewing several works on thermal management, heat transfer in ICEs, the application of thermal coatings on the combustion chamber walls and numerical methods to study the heat transfer in ICEs, some general conclusions about the state of the art are summarized:

- The combustion process in ICEs leads to significant variation in temperature and pressure in the engine. This also has a direct effect on the engine components. Thus, thermal management in ICEs allows to optimize the engine operation, assuring the life of the parts and without affecting the combustion process itself.
- The heat transfer in ICE is the result of interaction between the different systems for the thermal management of the engine with the combustion chamber. For many years, several authors have studied this process in order to design more efficient engines. As result of these investigations, empirical correlations have been developed and they are currently used to study the heat losses in ICEs.
- All the calorific power of the fuel is not transformed into useful work due to the different losses that take place in the ICE. In this regard, the heat losses through the combustion chamber walls represent about a third of the total losses.
- During the last decades, the application of thermal coatings on the walls in contact with the air-fuel mixture has emerged as an alternative to reduce the heat losses through the combustion chamber walls.
- According to the most recent studies, to achieve a gain in the thermal efficiency of an ICE, the new generation of thermal coatings must be insulating materials with low thermal conductivity and low heat capacity. Therefore, the wall temporal evolution of the gas exposed surfaces can instantly follow the gas temperature and thus reduce the thermal gradient.
- In spite of the usefulness of the experimental research, numerical simulations have an important interest to the automotive industry, due to their flexibility and low resource consumption. In particular, the development of computational tools that allows to model the performance of the ICEs is a priority. In this sense, different approaches are used to study the heat losses in ICEs such as one-dimensional models and 3D models.

- In general, one-dimensional models are used to simplify the physical processes in the engine and obtain results in short periods of time. On the other hand, 3D models are used to carry out more detailed and complete studies in ICEs.
- The CHT calculation is one of the most suitable approach to study heat transfer in ICEs, since they couple the fluid and solid regions of the engine in a single simulation.

CHAPTER 3

Conjugate heat transfer validation

The main objective to the work described in this chapter is to perform a preliminary parametric study on simplified geometries to assess the computational tool to calculate the heat transfer in solid regions. This study establishes the first step before performing the CHT calculations in ICEs along the following chapters. The chapter starts with a study of the heat transfer in a cylindrical geometry in steady state, varying the heat transfer models available in the computational tool. The results are compared with an analytical solution. Moreover, a transient study is performed in a 2D channel. In both cases, the wall roughness was considered in order to determine its impact on the heat transfer. This study will allow to conclude if the roughness parameter needs to be taken into account when modelling the thermal coatings.

To validate the computational tool in a more realistic geometry as that of an ICE, the oil jet system of a Diesel engine in steady state was studied. The results are compared with experimental measurements carried out at the CMT facilities.

3.1. Super-Cycling approach

As explained in the previous chapter, the CHT calculations combine the fluid and solid domains in only one simulation. However, most of the time the heat conduction in the solid is slower than the simulated time in the fluid.

Then, taking into account that it takes much longer to converge the solid region than the fluid one, the super-cycling approach of CONVERGE [102] has been used in this and the next chapters to solve the 3D conjugate heat transfer problem . This method solves both fluid and solid phases using the transient solver. During a defined cycle it stores periodically the heat transfer

coefficient and the near wall temperature at the fluid/solid interface cells in stages at defined time-step intervals. After that cycle (stages number*time interval), CONVERGE asolves the solid heat conduction using time averaged boundary conditions from the stored fluid temperature and HTC (Heat transfer coefficient). It then uses the new wall temperatures to solve the fluid and solid with the transient solver. The code freezes the fluid solver at the super-cycling time step interval and solves the steady-state solid temperature. This is updated to recalculate the solid and fluid with the transient solver. The process is repeated until the solid temperature has converged. This strategy reduces the time needed to reach the convergence of the solid temperature. The time step interval to store the heat transfer variables will depend on each application.

More stages means that supercycling after the first one will be performed more frequently. 12 stages for 4-stroke ICEs are typically used (60 CAD averaging windows). All in all it is an option meant to speed up convergence by not having to wait the full 720 CAD between supercyclings. CONVERGE uses sort of a moving average consisting of stages where each performed supercycle omits the first stage from the previous one. For other applications, as steady-state flow pipes one stage supercycling may be enough [102].

3.1.1. Validation on simple geometries

In this section, preliminary calculations of the heat transfer from the flow to the walls on simple geometries performed using the CFD-CHT technique are presented.

First, a gas flow through a cylindrical geometry is modeled. The results are validated by comparing the solution with a theoretical model from the literature, the analytical Dittus-Boelter correlation [85].

$$Nu = 0.023 Re_{Dh}^{0.8} Pr^{0.4} \tag{3.1.1}$$

where:

- $Dh[m]$: is the hydraulic diameter.
- $Re[-]$: is the Reynolds number.
- $Pr[-]$ is: the Prandtl number.
- $Nu[-]$ is: the Nusselt number.

The geometry of the circular cylinder shown in Fig. 3.1 is defined as follows:

- Length $L = 100mm$
- Internal diameter $D_{int} = 50mm$
- Aluminum wall thickness = 5 mm

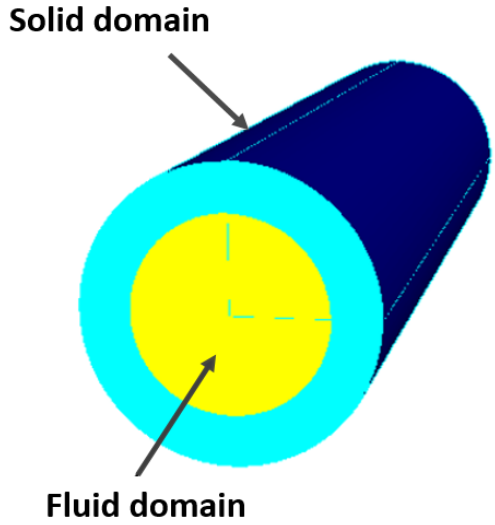

Figure 3.1: *Cylindrical geometry used for the preliminary calculations in steady state.*

Considering the axisymmetric geometry, only a quarter of the cylinder was meshed. The boundary conditions considered for the validation were:

- Aluminium solid material with thermal conductivity $k = 237W/mK$
- Inlet airflow velocity $V = 80m/s$
- Reynolds number $Re = 105300$
- Gas inlet temperature $T_g = 375K$
- External wall temperature $T_{ext} = 325K$
- Super-Cycling time step interval = $0.05s$
- Super-Cycling stages number = 1

The steady-state CHT calculations were performed with the RNG (Re-Normalized Group) k-ϵ turbulence model [103] and a law of the wall, and with all 3 different Heat Transfer (HT) models available in the program CONVERGE [102]: O'Rourke and Amsden [104, 105], Angelberger [106] and Han Reitz [107].

The roughness is taken only into account in the turbulence model via the law of the wall. The equations used by CONVERGE are written below, and follow Cousteix and Cebeci [108].

Law of mean velocity (u) in the boundary layer modified for roughness:

$$u = \frac{1}{\kappa}\ln\left(Ey^{+}\right) - \beta \tag{3.1.2}$$

where $\kappa = 0.4187$ and $E = 9.8$

$$y^{+} = \frac{y\rho u_{\tau}}{\mu} \tag{3.1.3}$$

In equation 3.1.3 y is the absolute distance from the wall, while ρ, u_{τ} and μ are the density, the sheer speed velocity and dynamic viscosity, respectively.

$$\beta = \frac{1}{\kappa}\ln(f_r) \tag{3.1.4}$$

The roughness function f_r quantifies the shift of the intercept due to roughness effects. The β value depends on the type of roughness (uniform sand, rivets, ...) and is correlated to the non-dimensional roughness height:

$$k^{+} = \frac{\rho u K_s}{\mu} \tag{3.1.5}$$

where K_s is the physical roughness height, known as the Ra (arithmetic average of the absolute values of the profile heights over the evaluation length) value.

For values of Ra or K_s ranging between 0 and 100μm, the value of the dimensionless roughness height ranges between 0 and $3.47 \cdot 10^{8}$ for the case studied here. Since $k^{+} > 90$, this is a fully rough regime, and in this case the value for β is given by:

$$\beta = \frac{1}{\kappa}\ln\left(1 + r_s k^{+}\right) \tag{3.1.6}$$

This equation is used to evaluate the shear stress at the wall and the wall functions for the mean temperature and turbulent quantities. The roughness constant (r_s) depends mainly on the type of roughness. The

default roughness constant is 0.5. For non-uniform sand-grains, ribs, or wire-mesh roughness, a larger value (0.5 to 1.0) is more appropriate. For the calculations performed in this chapter the default r_s value was employed.

A mesh independence study was performed for this geometry which is presented in Appendix 3.A, and based on the results obtained, a mesh of 60873 cells was used with a 1 mm base grid size.

The mean heat transfer coefficient is obtained from the CHT calculation, which in this study case is $h = 226W/(m^2K)$. The heat transfer rate was compared with the solution of Dittus-Boelter. The heat transfer rates calculated with all HT models are compared with the analytical solution in Fig. 3.2. As shown in the figure, for this simple case the O'Rourke Amsden heat transfer model is closer to the analytical solution, while the Angelberger model yields clearly a much lower value and the Han Reitz model over-predicts the Dittus-Boelter solution.

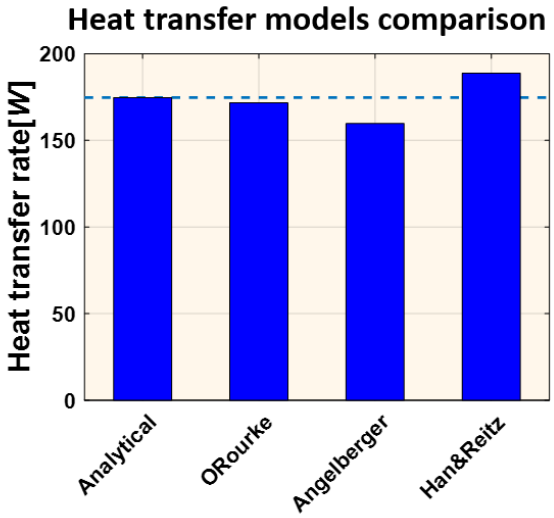

Figure 3.2: *comparison of the heat transfer rate with the different heat transfer models.*

In the following calculations, it was decided to use the O'Rourke and Amsden model, because, according to different investigations it seems that this is the model that yields the best results for the realistic calculations in the combustion chamber [109–114]. However, it is important to remark that

the physics of the steady low turbulence flow inside the circular cylinder is quite different from that of the highly turbulent unsteady flow in the combustion chamber.

Once validated, the impact of internal wall roughness on the heat transfer to the walls in steady state conditions is analyzed. The following study is carried out in order to determine if the roughness has to be considered to model coated walls of ICEs. New calculations were performed with the same geometry and the same boundary conditions, just changing the internal wall roughness height Ra in a range of values between 0 (smooth wall) and 100 μm (very rough). The results are presented in Fig. 3.3, in terms of heat transfer rate versus surface roughness (left) and heat transfer percentage difference relative to the smooth surface versus roughness (right). For Ra roughness values ranging from 0 to 14 μm there is no difference on the heat transfer, and consequently on the external wall temperature. For Ra $>$ 14 μm the heat transfer rate increases slightly with roughness, with a maximum HT rate increase of about 10% obtained for the highest value of roughness. Considering that a realistic wall roughness for the coating should be around Ra $= 6\mu$m, the conclusion is that the wall roughness has no impact on the heat transfer rate, at least in steady state flow conditions.

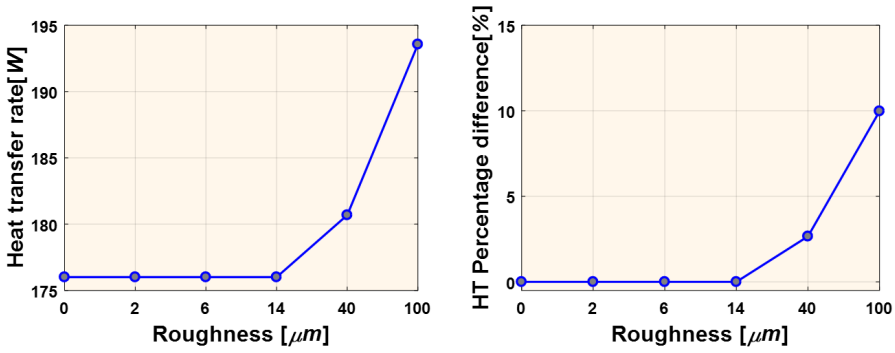

Figure 3.3: *Effect of roughness on the heat transfer rate to the walls in the cylindrical geometry for steady state: heat transfer rate for different roughness values (left) and percentage error respect to the smooth case (right).*

3.1.2. Impact of roughness in transient conditions

Recognizing that the low turbulence steady state flow is not representative of the highly turbulent flow inside a combustion chamber, it was decided to evaluate the impact of wall roughness on the heat transfer to the walls

in transient conditions and for Reynolds numbers closer to those existing in the vicinity of the combustion chamber walls when there is combustion. The previous study showed that the CHT calculations are computationally expensive and time-consuming. For this reason, it was decided that to perform the transient flow parametric study, it would be more efficient to select a two-dimensional channel geometry, as shown in Fig. 3.4. Its characteristics are:

- Channel length L= 100 mm
- Height = 10 mm
- Upper wall thickness = 2 mm

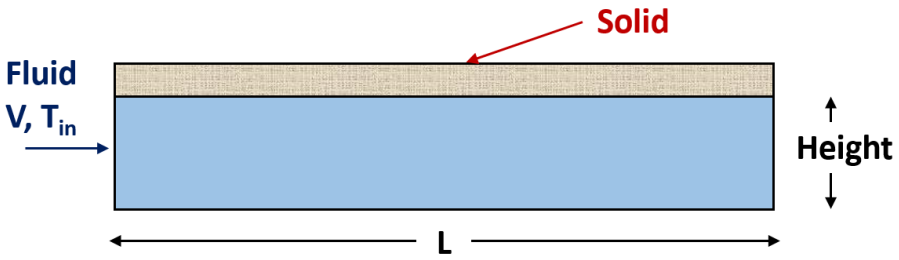

Figure 3.4: *Rectangular channel used as geometry for basic transient study.*

The boundary conditions considered for this case were:

- Coating material with thermal conductivity $k = 0.1\ W/(mK)$ and thermal heat capacitance $c = 100\ kJ/(m^3K)$
- Inlet airflow velocity V varied as shown in Table 3.1
- Inlet gas temperature with varying profile similar to that of an engine. Figure 3.5 displays the gas temperature profile at the channel inlet imposed as boundary condition for the calculations.
- External wall temperature $T_{ext} = 380K$
- Bottom wall adiabatic

The transient CHT calculations were performed with the RNG k- turbulence model and a law of the wall, and with the O'Rourke and Amsden heat transfer model. A mesh of 1200 cells was employed, using the base grid size from the previous section (1 mm). The reduction in the mesh size is due to the 2D simplification.

Table 3.1: *Transient cases studied.*

Case	Roughness $[\mu m]$	Inlet velocity $[m/s]$	Average Re
1	0	15	2844
2	150	15	2844
3	0	80	15168
4	150	80	15168

Four cases were run changing the inner wall roughness and the inlet velocity (hence the Reynolds number) as shown in in Table 3.1. It is important to clarify that this study is just a gross approximation of the transient flow that takes place in the engine. The main idea is to verify if there is some influence of either the wall roughness or the Reynolds number, or both, on the heat transfer. Clearly, the value of roughness is exaggerated and the Reynolds number has been chosen to consider both low and high turbulence flow.

In Fig. 3.6 is clearly seen that the curves of cases 1 and 2 on one hand, and 3 and 4 on the other hand, are practically the same, showing that roughness has no significant impact on the heat transfer to the walls. For cases 3 and 4, which correspond to the higher Reynolds number, the wall temperature is higher. As expected, the heat transfer rate increases for higher flow velocity close to the walls. Table 3.2 shows the total heat transferred from the gas to the wall for each case. For a lower Reynolds (cases 1 and 2) the roughness has a impact of 0.49% with respect to the smooth wall on the heat transfer. Meanwhile, for higher Reynolds (cases 3 and 4) the effect is about -1.55%.

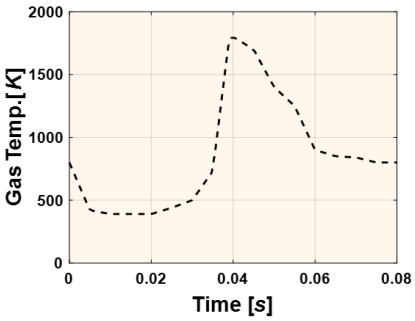

Figure 3.5: *Gas temperature profile imposed at the channel inlet.*

Based on these results, it can be concluded that the roughness has no significant impact on heat transfer during the transient process, even for high velocity and roughness values. It is important to remark that there exists no analytical solution to compare the latter results. The case was

modeled giving velocity and temperature conditions close to the ones found in an engine. However, the flow conditions are quite different, as there is no parallel flow in a combustion chamber.

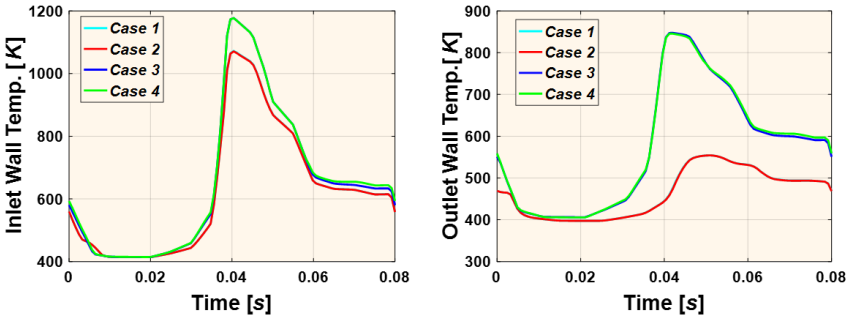

Figure 3.6: *Wall temperature evolution on the inlet (left) and on the outlet of the channel (right).*

Table 3.2: *Heat transfer for transient cases in the rectangular channel.*

Case	Q [J]	Diff. respect to smooth [%]
1	275.4	—
2	274.0	0.49
3	481.1	—
4	488.6	-1.55

3.2. Experimental validation

In order to ensure the suitability of the computational tool to study the heat transfer in ICEs, CHT calculations on the piston of a Diesel engine have been compared with experimental measurements carried out at CMT facilities. The experiment was performed in 2010 by Torregrosa et al. [115] in steady-state conditions without piston motion. This analysis aims at verifying that the CHT calculation can be used in more complex geometries such as those of an ICE. In addition, it will allow to check the reliability of the CHT results.

3.2.1. Test equipment

In the work presented by Torregrosa et al. [115] the cooling system of a CI engine piston was studied by changing parameters such as the pressure and temperature of the cooling oil. For this investigation, 480 tests with different configurations were performed. However, for the validation presented in this section, only 4 tests were considered due to the computational times of the CHT.

The experimental equipment consisted of 3 electric heaters (Oil heaters) that heat a thermal oil stored in a tank (Thermal oil Tank). The system is also completed with an oil pump and an expansion tank and has the capacity to deliver flow up to $6.5 m^3/h$ at temperatures up to $573 K$.

Table 3.3: *Main engine specifications.*

Bore $[mm]$	55
Stroke $[mm]$	88
Number of intake valves	2
Number of exhaust valves	2
Compression ratio	17.9:1
Inection system	Common rail

To characterize the piston cooling, the original engine cooling system was employed. The main features of the engine are listed in Table 3.3. The system comprises an oil jet (oil jet system) that is injected just below the inlet of the piston gallery. In the experiment, the pressure and the temperature of the cooling oil were varied, as well as the distance between the piston gallery and the oil jet.

Finally, K-type thermocouples were used to measure the temperature at 6 different points on the piston. Fig. 3.7 shows a schematic of the experimental equipment used, as well as the location of the thermocouples on the engine piston.

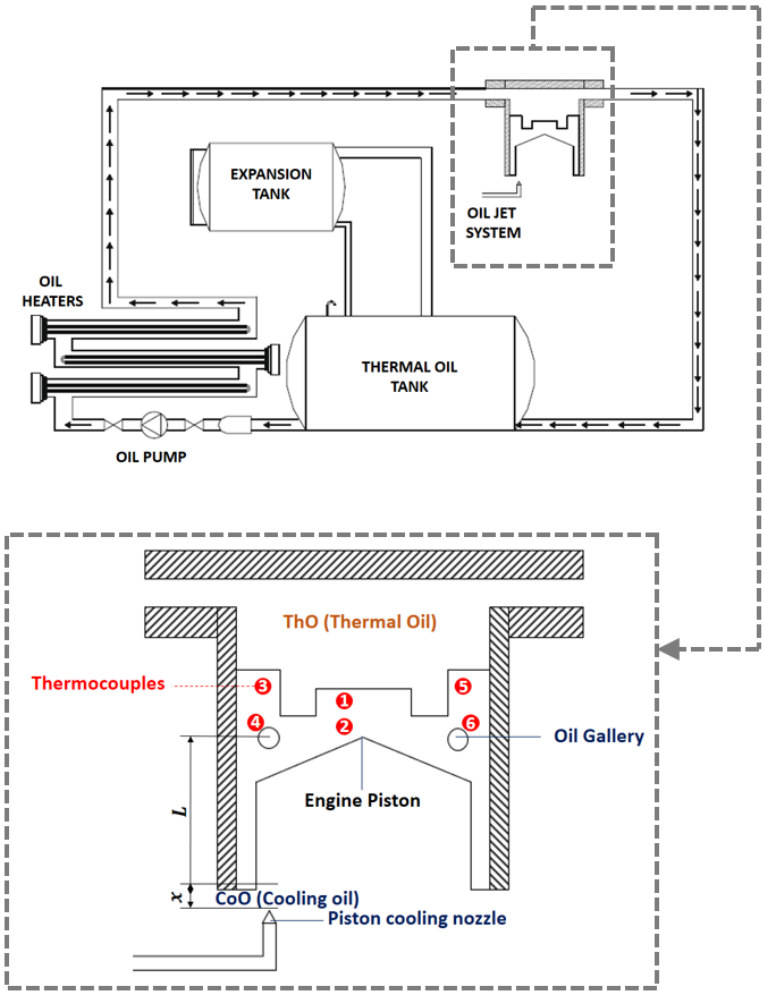

Figure 3.7: *Scheme of the experimental equipment. The full system is integrated by a thermal oil tank, an expansion tank, an oil pump, oil heaters and by the original oil jet system of the engine (top). The oil jet system is equipped with 6 K-type thermocouples to measure the temperature in the solid piston (bottom).*

3.2.2. Coolant fluid characterization

The following considerations were taken into account to model the cooling fluid of the oil jet system:

- The distance considered between the oil jet and the piston gallery is $x = 0$. This value was taken into account due to a larger mesh is required at greater distances.
- The cooling oil temperature $T_{CoO} = 298$ K was considered. At this temperature the oil is more stable since it is far from its critical temperature.
- The cooling oil pressure P_{CoO} was varied from 1 to 4 bar.

In the computational software it is necessary to define a liquid for the fluid domain. However, there is no data available for the oil used in the experiments. In addition, there is no information in the literature for all the properties needed to define a fluid in CONVERGE, which are:

- $\mu[Ns/m^2]$: Dynamic Viscosity
- $\sigma[N/m]$: Surface tension
- $H_{vap}[J/kg]$: Heat of vaporization
- $P^{sat}[Pa]$: Vapor pressure
- $\rho[kg/m^3]$: Density
- $c_p[J/(kgK)]$: Specific heat
- $k[W/(mK)]$: Thermal conductivity

As an alternative to this problem, the values of ρ, μ, k, c, P^{sat} were obtained by using the GT-Power library [116] for a SAE5W30 oil [117] and are shown in Fig. 3.8 as function of temperature. However, this library does not provide information about H_{vap} and σ values.

To obtain the value of H_{vap} the Clausius Clapeyron [118] equation was used:

$$\ln \frac{P_2}{P_1} = -\frac{\Delta H_{\text{vap}}}{R}\left(\frac{1}{T_2} - \frac{1}{T_1}\right) \tag{3.2.1}$$

where the sub-index 1 and 2 refer to different stages of the fluid.

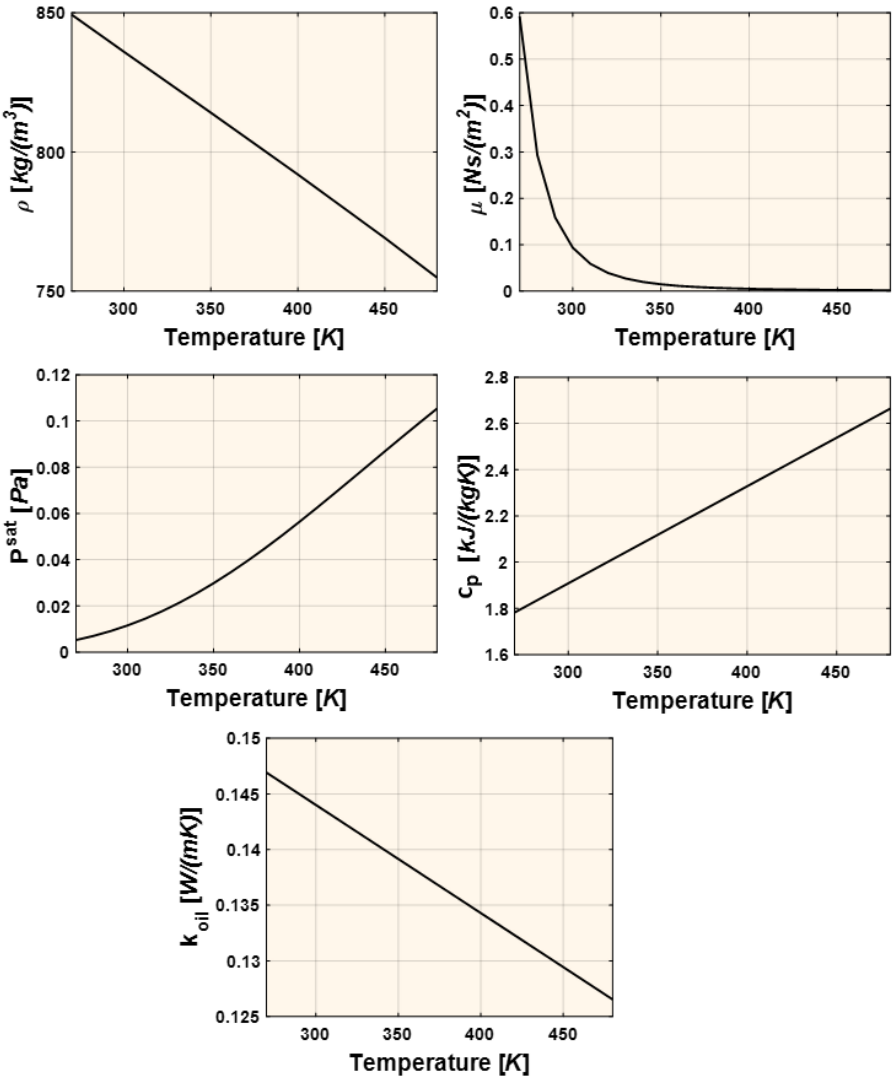

Figure 3.8: *Cooling oil properties obtained with GT-Power library: density ρ, dynamic viscosity μ, vapor pressure P^{sat}, specific heat c, conductivity k_{oil}.*

The values of σ were approximated using the Yaws equation [119]:

$$\sigma = \exp(\mathrm{A}) \cdot \{1 - (T/T_c)\}^n \tag{3.2.2}$$

The parameters A and n depend on the properties of the liquid, while T_c denotes the temperature of the oil at its critical point($T_c = 473.15$) [116]. As the values of A and n are unknown, the value of $n = 1.22$ was taken for the Ethylene glycol, as proposed by Yaws et al.[120] since this organic compound is also employed as a cooling fluid [121]. The value of $A = -2.17$ was estimated from equation 3.2.2 using T and σ as reference values [116]:

$$0.0406 = \exp(\mathrm{A}) \cdot \{1 - (270/T_c)\}^{1.22} \tag{3.2.3}$$

Fig. 3.9 shows the H_{vap} and σ values in function of temperature calculated with the Clausius Clapeyron and Yaws equations, respectively.

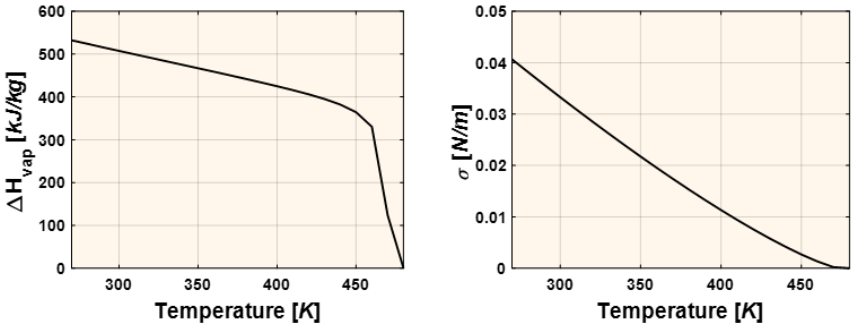

Figure 3.9: *Calculated cooling oil properties: heat of vaporization H_{vap} (left) and surface tension σ (right), calculated with the Clausius Clapeyron and Yaws equations, respectively.*

3.2.3. Modeling approach

The piston cooling system for Diesel engines is a complex problem, as the piston is in motion and a liquid-gas fluid composed of oil and air circulates through the piston galleries [122]. In addition, the oil splashes the walls of the piston cavity, affecting the heat transfer. Consequently, the heat transfer through the piston is not completely symmetrical. Then, for modeling the oil jet system, accurate models and characterization of the cooling oil properties are needed.

Multi-phase flows can be simulated in CONVERGE with the volume of fluid (VOF) method [123]. The VOF method locates and tracks the free surface in a liquid-gas flow or the interface in a liquid-liquid flow. It is an Eulerian method that reconstructs the interface location and orientation within each

fluid cell. Coupled with Adaptive Mesh Refinement (AMR), CONVERGE tracks these interfaces accurately and efficiently. The VOF method can be used with both compressible and incompressible fluids.

Moreover, this approach tracks the volume of fluid within each cell. The volume of fluid is represented by the void fraction α, which is the fraction of the cell's volume that is occupied by the gas phase:

$$\begin{gathered} \alpha = 0 \quad \text{(the cell contains only liquid)}, \\ 0 < \alpha < 1 \quad \text{(the cell contains both liquid and gas)}, \\ \alpha = 1 \quad \text{(the cell contains only gas)} \end{gathered}$$

Preliminary studies performed to model the oil jet system indicated that the oil splashed in the piston cavity wall remains unevenly adhered to the solid. In addition, it overcooled the piston diverging from the solution. Thus, there could be inaccuracies with any of the calculated properties. However, the only way to verify this hypothesis is measuring the physical properties of the oil.

To face the problem at hand, a methodology was developed to determine the spatial temperature distribution of the piston. The methodology displayed in Fig. 3.10 consists of 2 configurations:

- In the first set-up, the piston oil jet is modeled using the VOF method with the HRIC (High Resolution Interface Capture) [124]. This approach builds an interpolated curved interface using information from neighboring cells. Though that the piston geometry is employed in this configuration, the piston temperatures are not considered. Although the HRIC approach is recommended for complex geometries, such as piston galleries, it cannot solve an interface as sharply as other models. From this configuration the pressure and temperature of the oil at the piston gallery inlet are determined. In addition, the temperature and the heat transfer coefficient near the piston cavity wall are also obtained. These values are used as inputs in the second configuration. Table 3.4 shows the values obtained with set-up 1.

- In set-up 2, the super-cycling approach is employed to perform the CHT calculations on the piston. In this case, the VOF method does not track the gas in the adjacent cells ($\alpha = 0$). HRIC method is not necessary since it can be assumed that the fluid entering to the piston gallery inlet is completely liquid. This assumption is possible because the experiment is performed in a steady state. However, for the transient case, where the piston is in motion, this methodology may not be applicable.

Table 3.4: *Inputs for the CHT calculations with set-up 2 obtained with set-up 1.*

$P_{CoO}[bar]$	$P_{inlet}[bar]$	$T_{inlet}[K]$	$h_{splashed}[W/(m^2K)]$	$T_{splashed}[K]$
1	1.017	338.9	1185	329.5
2	1.019	319.2	2528	328.0
3	1.124	318.9	4124	327.9
4	1.143	318.5	5342	327.6

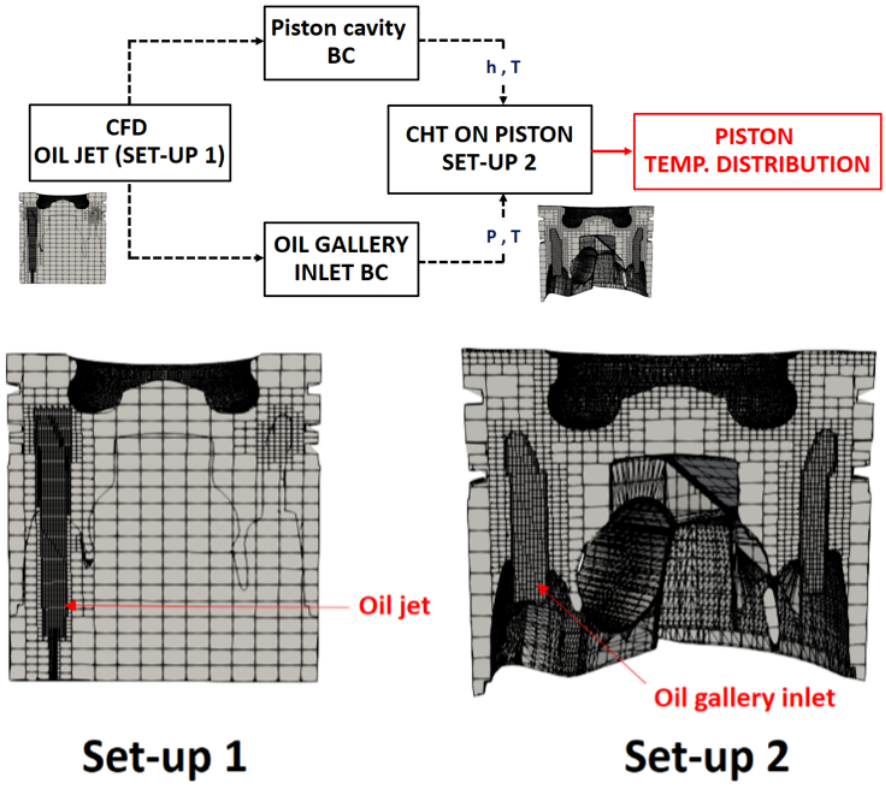

Figure 3.10: *Scheme of the methodology employed for the CHT calculations on the Diesel engine piston (top) and the zoom of the mesh employed for the 2 configurations considered (bottom).*

The employed mesh has a base grid size of 4 mm in both configurations, with 281702 and 146832 cells in the mesh of the configuration 1 and 2, respectively. Since the piston geometry is very narrow, a refinement

of 0.5 mm was applied on the gallery walls and on the piston top. In addition, an Adaptive Mesh Refinement (AMR) algorithm has been used for the calculations. This approach refines the mesh in regions where changes in the thermodynamic properties take place. An AMR refinement of 1 mm was used for velocity changes of 0.06 m/s and 0.5 mm for changes of 0.001 in the void fraction. Fig. 3.11 shows the piston geometry with the different regions considered in the domain. The boundary conditions applied in each region for the steady state calculations are summarized:

- Piston top: Convection ($h = 3700W/(mK)$ and $T_{ThO} = 473K$)
- Piston cavity: Convection ($h_{splashed}$ and $T_{splashed}$)
- Oil gallery inlet: Inflow (P_{in}, T_{in})
- Oil gallery outlet: Outflow ((P_{out}, T_{out}) calculated by the software)
- Piston gallery: Interface wall (calculated by the software)
- Isolated wall: Adiabatic

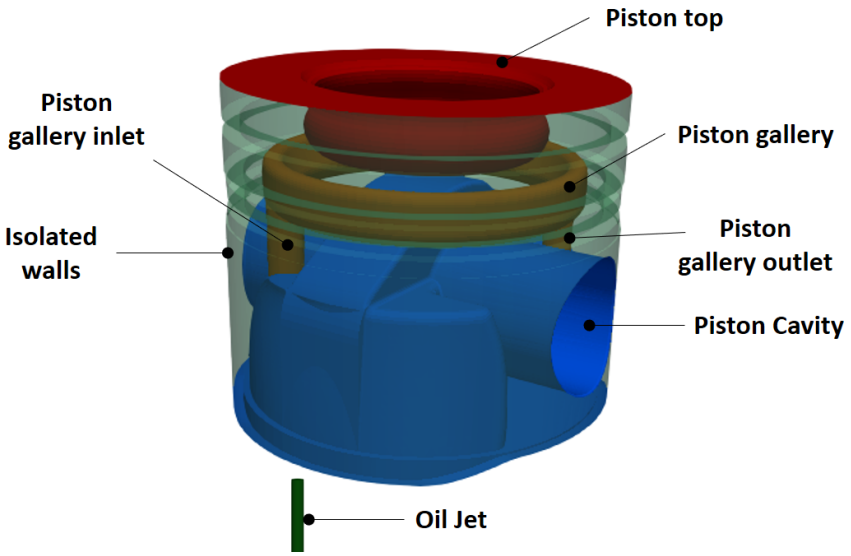

Figure 3.11: *Regions considered for the CHT calculations of the Diesel engine piston.*

The CHT calculation yielded the spatial temperature distribution of the piston. As shown in Fig. 3.12 the piston is hotter when the pressure of the coolant oil is lower. It can be clearly seen that the hottest part of the solid is the periphery of the piston top. However, the bowl in the piston top is colder due to its proximity to the oil gallery.

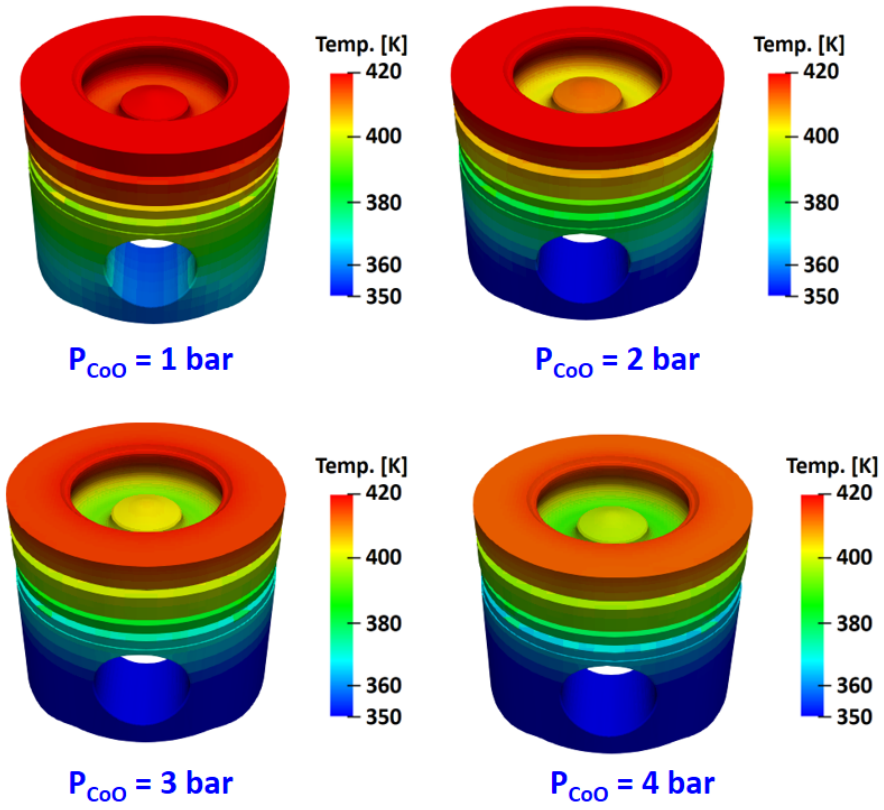

Figure 3.12: *Spatial temperature distribution of the Diesel engine piston for different cooling oil pressures.*

To validate the reliability of the results, the calculated dimensionless temperatures at symmetrical locations on the piston were compared with experimental measurements of the thermocouples. The dimensionless temperature is defined as:

$$\theta_{\mathrm{i}} = \frac{T_i - T_{\mathrm{CoO}}}{T_{\mathrm{ThO}} - T_{\mathrm{CoO}}} \tag{3.2.4}$$

where, T_i is the measured temperature for the thermocouples (Fig. 3.7).

The comparison is shown in Fig. 3.13. The solid line indicates the case where the heat transfer is axisymmetric (slope = 1). The experimental measurements show that the heat transfer in the piston is not completely symmetrical. However, the measurements are very close to the axisymmetric trend. In the case of the calculated temperatures with the CHT, the values fit with the slope 1 line. Therefore, the heat transfer is axisymmetric in the simulations performed since the splashed oil has not been modeled.

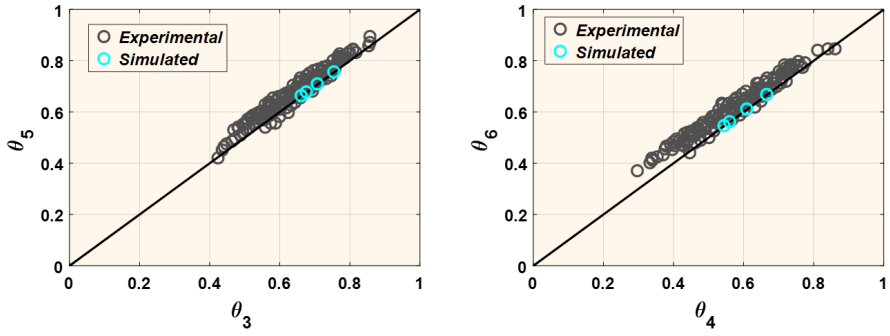

Figure 3.13: *Measured and calculated dimensionless temperature comparison at symmetry locations of the piston: on the top of the piston (left) and on the sides of the cooling oil gallery (right). The solid black line indicates the case where the heat transfer is axisymmetric.*

Finally, the differences between the experimental and calculated dimensionless temperatures were studied. Fig. 3.14 confirms what is shown in Fig. 3.12, that the temperatures in the piston are higher at lower pressures of the cooling oil. Furthermore, it can be seen that the calculated values are very close to the experimental measurements with a maximum difference of 2%, for a pressure in the cooling oil of 2 bar.

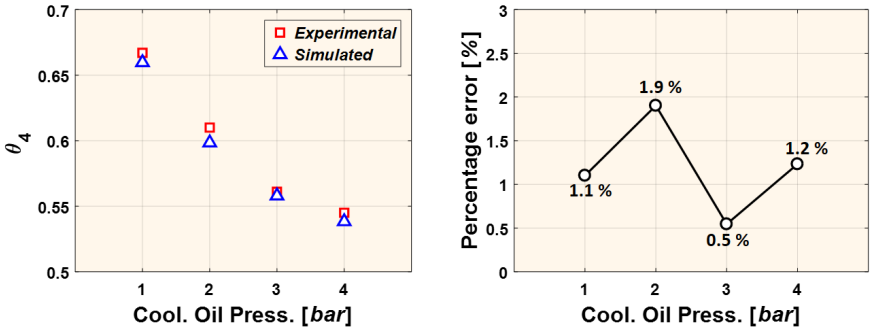

Figure 3.14: *Difference between the measured and calculated dimensionless temperature on the sides of the cooling oil gallery for the considered cooling oil pressures (left) and percentage error at each considered pressure (right).*

3.3. Summary

In this chapter, preliminary CHT calculations in simple geometries are presented. The main objective is to validate the suitability of the computational tool to study the heat transfer through the combustion chamber walls in an ICE.

As first validation approach, the simulations performed for two simplified geometries (cylinder and 2D channel) allowed setting up and validating the CFD-CHT calculations. In the models, the roughness is taken into account in the turbulence model via the law of the wall. The main conclusions from this study are:

- The heat transfer through the cylindrical geometry was compared with the analytical solution of Dittus-Boelter for turbulent flow in pipes. The calculated heat transfer is in the same order of magnitude as the theoretical solution for all the heat transfer models available in CONVERGE.
- The O'Rourke and Amsden heat transfer model is closest to the analytical solution. According to the results, it seems that Angelberger model under-predicts the heat transfer while Han Reitz model over-predicts it.
- A parametric study made by varying the surface roughness indicated that this has no effect on heat transfer for reasonable values of roughness, neither in the steady state study (cylindrical geometry) nor in the transient study (2D channel).

Finally, a second validation with a realistic geometry of a Diesel engine was performed by comparing steady state calculations with some experimental measurements available for the oil jet cooled piston. A methodology was developed to determine the spatial temperature distribution of the piston. The approach consists in determining the boundary conditions at the piston gallery inlet and at the surrounding wall of the piston cavity. Then, the estimated values are introduced in the CHT calculation without modelling the oil splashed to the piston cavity. From these calculations, it can be concluded that:

- The periphery on the piston top is the hottest region of the domain. However, the bowl at the piston top is colder due to its proximity with the piston gallery.
- The results yielded a symmetric temperature distribution on the piston. Although the heat transfer is not completely symmetrical in the experimental cases, the approximation fits very well with the experimental data.
- For lower values of the oil jet pressures the temperatures on the piston are higher. The calculations show that the hottest piston walls are mainly due to the low heat transfer coefficient at the piston cavity wall.

3.A. Appendix: Mesh independence study for simple geometries

In order to verify that the the solution is not dependent on the mesh, the base grid size of the mesh for the simple geometries was varied from 5 - 0.5 mm in the cylindrical pipe. Fig. 3.15 shows that the heat transfer rate changed by less than 0.4% when reducing the base grid size from 1 to 0.5 mm. Therefore, for the CHT calculations on simple geometries a base cell size of 1 mm was employed.

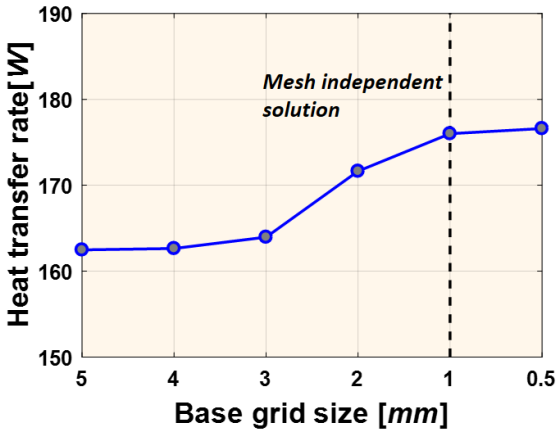

Figure 3.15: *Mesh independence study to define the base grid size for the CHT calculations on simple geometries. Dashed line indicates the base grid size selected.*

CHAPTER 4

Equivalent coating

Though 1D models can be used to study the heat transfer of the insulating coatings, they cannot yield detailed information about the wall temperature distribution, for instance. Especially, in the case of SI engines it is interesting to determine the wall temperature distribution on the combustion chamber surfaces, in order to identify possible hot spots. These are known to induce knocking phenomenon affecting the engine performance.

Experimental measurements of the possible performance improvements in coated engines are very difficult to obtain, mainly because the techniques available to measure wall temperature are limited. Therefore simulations are typically used to investigate insulated combustion chambers. Nevertheless, the new generation of insulating coatings is posing challenges to numerical modelling, as layer thickness is very small ($\sim$ 100 µm). Indeed, a detailed modelling would require additional cells refinement for the coating layer and therefore significant increase in computational effort and simulation time. In this regard, in this chapter a methodology is presented whereby a 1D heat transfer model is used in combination with a multi-factorial DoE and a multiple regression analysis to define the thermodynamic properties (conductivity and heat capacitance) of an equivalent coating material with reasonable thickness for 3D calculations. The target is to achieve that the equivalent "thick" insulating layer behaves as the real very thin coating

Work on this chapter has been partly published in the following paper:

- Numerical approach to define a thermodynamically equivalent material for the Conjugate Heat Transfer simulation of very thin coating layers [3]

layer in terms of heat fluxes and wall temperature evolution. The defined equivalent material layers will be used to study the heat transfer in coated ICEs by 3D-CHT in the next chapters.

4.1. Methodology

Currently, in the literature there are many studies about the application of TBC (Thermal Barrier Coatings) in ICE. Few of them deal with Computational Fluid Dynamics (CFD) studies of ICE with coated combustion chamber walls [100, 125, 126]. However, to my knowledge there are no CHT studies about the new generation of insulating coatings mentioned in Chapter 1. This is probably due to the difficulties linked mainly to the computational cost involved in coupling the calculation of the gas flow with the heat transfer through the solid walls [127, 128].

In the recent studies mentioned above the exposed gas surfaces are insulated with a very thin coating layer (of the order of 100 μm). For these cases, the mesh to calculate the heat transfer to the coated walls using CHT needs to be extremely fine to represent the coating layers adequately, thus increasing drastically the total number of cells, and hence the computational time. Indeed, it is practically impossible to mesh such thin layers for numerical as well as cost reasons.

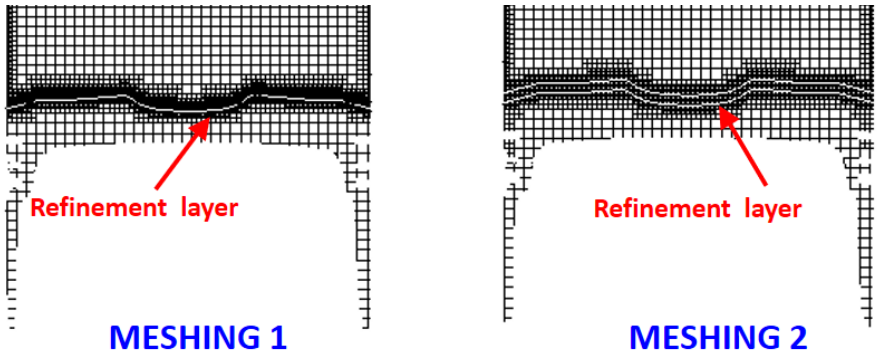

Figure 4.1: *3D-CHT mesh for an engine piston with 100 μm coating layer (left) and for 2 mm coating layer (right).*

In order to illustrate how significant is the increase in total number of cells in the combustion chamber of an ICE with 2 coating layers on the piston surface, Fig. 5.2 shows the mesh for two different coating thicknesses. The coating in mesh 1 is 100 μm thick, and the necessary near wall and wall

mesh fineness yields a total of 50 million cells approximately, which is quite impossible from the computational point of view. On the other hand in mesh 2, a 2 mm coating layer is modeled on the piston wall and the total number of cells is reduced to about 1.5 million cells, which is a perfectly reasonable mesh for 3D CHT calculations. This limitation could be overcome by defining an equivalent insulating layer of viable thickness (meaning a thickness that could be meshed) that would behave like the real coating layer. In this regard, this work proposes a methodology that consists in modelling a very thin layer of coating material of defined thermal characteristics by a 'reasonably' thick layer of virtual coating material, whose thermal response would be equivalent to those of the thin real coating layer.

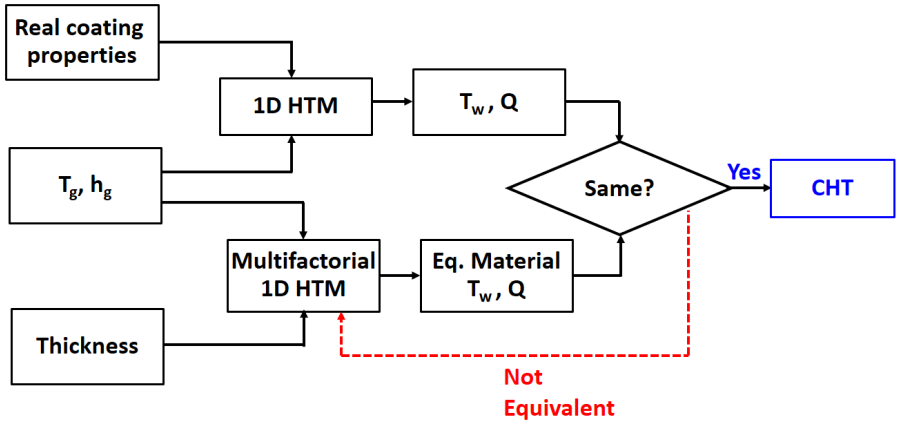

Figure 4.2: *Equivalent material scheme methodology.*

The proposed methodology is shown in Figure 4.2. First, the heat transfer coefficient (h) and the gas near-wall temperature (T_g) coming from a 0D-1D combustion model or from experimental data are used as boundary conditions for the 1D heat transfer model considering the real coating. This calculation yields the thermal swing in wall temperature during an engine cycle (T_w) and the instantaneous heat flux on the surface. Simultaneously, using the same boundary conditions a multi-factorial test is carried out to find an equivalent coating of acceptable thickness, by trying different combinations of heat capacitance and conductivity. The instantaneous heat flux and the wall temperature swing of the 'equivalent material' obtained with these tests are compared with the values of the real coating. Finally, the chosen equivalent coating material will be the coating with the lowest error in positive and negative heat fluxes. In addition, it is also checked that

the thermal swing of this material has a similar behavior to that of the real coating. The properties of the best equivalent material are determined by a multiple regression analysis. This 'equivalent material' material with its acceptable thickness will then be used in the 3D CHT simulations, replacing thus the real coating and allowing for very substantial computing savings.

4.2. 1D Numerical model

The 1D numerical lumped model used in this work has been developed in the CMT to study the heat transfer in ICEs [129]. In this section a description of this numerical tool is presented, since it is employed often in the thesis to estimate the wall temperatures in the combustion chamber.

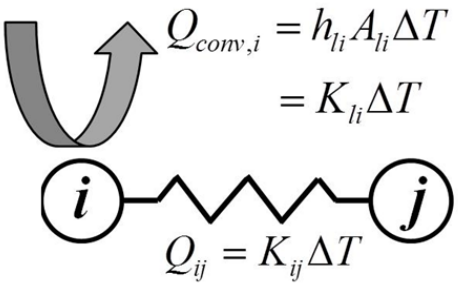

Figure 4.3: *Node of a lumped model with all its possible interactions(conduction to other nodes,convection to a fluid and heat sources).*

In this model, the engine is regarded as a thermal network consisting of a finite number of nodes, whose thermal inertia is characterized by a thermal capacitance, and linked to other nodes by means of thermal conductances. Once the structure is divided into nodes, the energy conservation equation can be written for each node. Figure 4.3 represents a node and all its possible interactions: conduction to other nodes, convection to a fluid, and heat sources. The energy balance on a node leads to:

$$m_i c_v \frac{T^i_{t+\Delta t} - T^i_t}{\Delta t} = \sum_j K_{ij}(T^j_{t+\Delta t} - T^i_{t+\Delta t}) + \sum_k q_{k\to i} + \sum_l h_{li} A_{li}(T_l - T^i_{t+\Delta t}) \tag{4.2.1}$$

Here, m_i is the mass of node i, c_v its heat capacity, K_{ij} the conductance between nodes i and j, h_{li} the heat transfer coefficient between node i and a boundary l and A_{il} the corresponding contact area. The temperatures on the right-hand side are computed at time $t + \Delta t$ with an implicit formulation in order to ensure the stability of the calculation when considering transient processes. Writing Eq. 4.2.2 for each of the nodes gives an implicit set of linear equations of the form:

$$[K][T^t] - [C][T^t] = [T^{bc}] - [C][T^{(t-t)}] \tag{4.2.2}$$

Where:

- $[T^t]$: is a temperature vector (unknown)
- $[K]$: is the conductance matrix
- $[C]$: is the capacitance matrix
- $[T^{bc}]$: is the temperature vector of boundary conditions
- $[T^{t-\Delta t}]$: is the temperature vector at the previous time step

The diagonal elements of the conductance matrix are the sum of all the conductances connected to the corresponding node, whereas off-diagonal elements K_{is} represent the conductance between nodes i and j with a minus sign. Conductive conductances are calculated according to the geometry of the connection between nodes planar $\left(k_v A_v / x_{ij}\right)$ or radial $\left(2\pi k_{ij} l_{ij} / \ln\left(r_j / r_i\right)\right)$, whereas convective conductances are computed as the product of the heat transfer coefficient and the contact area $\left(h_{ij} A_{ij}\right)$. Thus, assuming that all conductances are linear their expression becomes:

$$\begin{aligned} K_{ij} &= \sum jk_{ij}A_{ij}/x_{ij} + \sum lh_{li}A_{li} if\, i = j \\ K_{ij} &= -k_{ij}A_{ij}/x_{ij} or K_{ij} = -h_{ij}A_{ij} if\, i \neq j \end{aligned} \tag{4.2.3}$$

In cycle to cycle calculations with conventional engines (metallic components), even though the heat fluxes through the combustion chamber walls change periodically with time, a steady state is assumed. Hence cycle averaged values are used. This assumption is reasonable considering that the expected change in gas temperature is of the order of 700°C, while the wall temperatures may change by about $10-15$°C maximum [1]. The same assumption is valid for the exhaust and intake gases. Obviously this approach does not permit to identify the thermal fatigue, nor the instantaneous wall temperature on the material.

Since in steady-state conditions $T^t_{t+\Delta t} = T^t_t$, Eq. 4.2.2 reduces to

$$\left[T^t\right] = [K]^{-1}\left[T^{bc}\right] \tag{4.2.4}$$

When using coated walls, the steady-state assumption made in the latter equation should not be used, since an important wall temperature swing is expected for this case. Therefore, depending on the approach considered (steady or unsteady), either Eq. 4.2.2 or Eq. 4.2.4 is solved implicitly for the temperature vector [T'] by using a Gaussian elimination procedure.

Equations 4.2.5, 4.2.6, 4.2.7 and 4.2.8 shows the expansion of each term of Eq. 4.2.2 in which all the elements of the matrixes used for calculating the heat transfer with coated walls are specified.

In Eq. 4.2.5 the first matrix corresponds to the stationary part of Eq. 4.2.2 in which the first two rows refer to the boundary conditions, while the following rows represent the connections between the different nodes. This first matrix is the one that will be used also when using Eq. 4.2.4. On the other hand, the second matrix (vector) represents the temperatures of all the nodes at the current time (unknown). The matrix in Eq. 4.2.6 takes into account the transient state of heat transfer. The original model has been modified to calculate the transient evolution of all the temperatures in a time step defined by the user. This temporal evolution can be calculated using the capacitance of each node that is implemented in the diagonal of the mentioned matrix. The first term on the left hand side of Eq. 4.2.5 is a vector containing the boundary conditions at the time step which is being calculated (Eq. 4.2.7). The second term is the capacitance matrix multiplying the vector of the previous time step temperatures ((Eq. 4.2.8).

In addition to including the capacitance matrix in this equation, the size of all the matrixes was changed to take into account the coating nodes, as explained in the following section.

$$[K][T^t] = \begin{bmatrix} I_{\text{conv}} & 0 & 0 & 0 & 0 & 0 \\ 0 & I_{\text{gases}} & 0 & 0 & 0 & 0 \\ K_{\text{cv-ln}} & K_{gs-\text{ln}} & K_{\text{ln-ln}} & K_{ps-ln} & 0 & K_{f-ln} \\ K_{cv-ps} & 0 & K_{ln-ps} & K_{ps-ps} & 0 & K_{f-ps} \\ K_{cv-ch} & 0 & 0 & 0 & K_{ch-ch} & K_{f-ch} \\ K_{cv-f} & 0 & K_{ln-f} & K_{ps-f} & K_{hd-f} & K_{f-f} \end{bmatrix} \cdot \begin{bmatrix} T^t_{\text{conv}} \\ T^t_{\text{gases}} \\ T^t_{\text{liner}} \\ T^t_{\text{piston}} \\ T^t_{\text{cyl-head}} \\ T^t_{\text{fluid}} \end{bmatrix} \tag{4.2.5}$$

$$[C][T^t] = \begin{bmatrix} 0 & 0 & 0 & 0 & 0 & 0 \\ 0 & 0 & 0 & 0 & 0 & 0 \\ 0 & 0 & C_{ln} & 0 & 0 & 0 \\ 0 & 0 & 0 & C_{ps} & 0 & 0 \\ 0 & 0 & 0 & 0 & C_{ch} & 0 \\ 0 & 0 & 0 & 0 & 0 & C_f \end{bmatrix} \cdot \begin{bmatrix} T^t_{conv} \\ T^t_{gases} \\ T^t_{liner} \\ T^t_{piston} \\ T^t_{cyl-head} \\ T^t_{fluid} \end{bmatrix} \tag{4.2.6}$$

$$[T^{bc}] = \begin{bmatrix} T^t_{conv} \\ T^t_{gases} \\ -Q^t_{gen,ln} \\ -Q^t_{gen,ps} \\ -Q^t_{gen,ch} \\ -Q^t_{gen,f} \end{bmatrix} \tag{4.2.7}$$

$$[C][T^{(t-t)}] = \begin{bmatrix} 0 & 0 & 0 & 0 & 0 & 0 \\ 0 & 0 & 0 & 0 & 0 & 0 \\ 0 & 0 & C_{ln} & 0 & 0 & 0 \\ 0 & 0 & 0 & C_{ps} & 0 & 0 \\ 0 & 0 & 0 & 0 & C_{ch} & 0 \\ 0 & 0 & 0 & 0 & 0 & C_f \end{bmatrix} \cdot \begin{bmatrix} T^{t-\Delta t}_{conv} \\ T^{t-\Delta t}_{gases} \\ T^{l-\Delta t}_{liner} \\ T^{t-\Delta t}_{piston} \\ T^{t-\Delta t}_{cyl-head} \\ T^{t-\Delta t}_{fluid} \end{bmatrix} \tag{4.2.8}$$

4.2.1. Model validation

For an engine, the following boundary conditions have to be taken into account for the calculation of the instantaneous heat transfer through a solid surface:

- The heat transfer through the solid is three dimensional.
- On one side of the solid (in cylinder combustion chamber), both the heat transfer coefficient h and the gas temperature (T_g) vary with time during a thermodynamic cycle.
- On the other side (coolant side), both the heat transfer from gas to walls and the coolant temperature can be assumed to be constant with time during a thermodynamic cycle.

However, this problem has no analytical solution and hence, as a first approximation it is necessary to define a simple approach for which the analytical solution may be obtained. The 'equivalent' theoretical problem [130] considered here is presented in the scheme of Figure 2-1, for which the following hypotheses were assumed:

- The calculation domain is a semi-infinite solid, so that the heat transfer is one-dimensional.
- The solid consists of one material with constant conductivity (k), density (ρ) and specific heat (c).
- The gas temperature (T_g) on the left hand side of the solid varies as defined by Eq 4.2.9.
- The heat transfer coefficient between the gas and the solid surface is constant.

$$T_g(t) = T_{gm} + \Delta T_g \cos(\omega t) \tag{4.2.9}$$

where t is the time, T_{gm} is the average gas temperature, ΔT_g is the amplitude of gas temperature and ω is the gas temperature period.

$$\omega = 2\pi n f_0 \tag{4.2.10}$$

where n represents the harmonic number and f_0 is the fundamental frequency.

-Boundary condition at solid surface:

$$\dot{q} = h(T_g - T_s) = -k\frac{\partial T}{\partial y}\bigg|_{x=0} \tag{4.2.11}$$

where T_s represents the solid temperature at the surface and T represents the solid temperature at any point of the solid.

The unsteady one dimensional heat conduction equation has to be solved in the semi-infinite solid:

$$\frac{\partial T(x,t)}{\partial t} = \alpha\frac{\partial^2 T(x,t)}{\partial x^2} \tag{4.2.12}$$

where α represents the thermal diffusivity:

$$\alpha = \frac{k}{\rho c_p} \tag{4.2.13}$$

and k, ρ and c_p are the conductivity, density and specific heat of the material, respectively.

The solution for the solid temperature with the proposed boundary condition is:

$$T(x,t) = T_{gm} + \Delta T_g \cdot A \cdot exp^{-\bar{x}} \cdot \cos(\omega t - \beta) \tag{4.2.14}$$

and rearranging the terms in the equation:

$$\frac{T(x,t) - T_{gm}}{\Delta T_g} = A \cdot exp^{-\bar{x}} \cdot \cos(\omega t - \beta) \tag{4.2.15}$$

where A and β are respectively the amplitude and the phase shift of the surface temperature.

The amplitude A is given by:

$$A = \frac{Bi}{(Bi^2 + 2Bi + 2)^2} \tag{4.2.16}$$

where Bi is the Biot number:

$$Bi = \frac{h}{k}\sqrt{\frac{\alpha}{\pi n f_0}} \tag{4.2.17}$$

The value of the instantaneous temperature at the solid surface holds for x=0

$$\bar{x} = \sqrt{\frac{\pi n f_0}{\alpha}}x \tag{4.2.18}$$

$$\beta = -\sqrt{\frac{\pi n f_0}{\alpha}}x - tan^{-1}\frac{1}{1+Bi} \tag{4.2.19}$$

$$\frac{T(0,t)-T_{gm}}{\Delta T_g}=\frac{Bi}{(Bi^2+2Bi+2)^2}\cdot\cos(\omega t-tan^{-1}\frac{1}{1+Bi}) \tag{4.2.20}$$

As seen above, the amplitude of the surface temperature and the phase shift depend on the Biot number, which can be rewritten as:

$$Bi=\frac{h}{\sqrt{k\rho c_p \pi n f_0}} \tag{4.2.21}$$

The maximum amplitude is obtained for $Bi\rightarrow\infty$, while $Bi\rightarrow 0$ means that $T_s \approx T_{gm}$

In this work the following values were given to the different parameters of the previous equations:

A material with optimal properties for a thermal coating [78] has been considered:

k=0.1 $Wm^{-1}K^{-1}$

ρc_p=100 $\cdot 10^3 JK^{-1}m^{-3}$

Values for the fundamental frequency and heat transfer coefficient were taken for a Diesel engine operating at 1500 RPM-8bar.

nf_0=50 Hz

h=250 $Wm^{-2}K^{-1}$

These values lead to the following results:

α=10^{-6}Wm$^2s^{-1}$

Bi=0.2

β=40^o

$$A=\frac{Bi}{(Bi^2+2Bi+2)^2}=0.128 \tag{4.2.22}$$

These show that the maximum amplitude of the mean surface temperature is about 13% of the gas temperature maximum amplitude and the phase shift between excitation and response is 40^o.

In order to analyze the penetration of the temperature oscillation into the solid, the positions at which the temperature oscillation is attenuated by respectively 10% and 1% of the surface oscillation can be calculated by the following equations:

$$0.1 = exp(-\sqrt{\frac{\pi n f_0}{\alpha}} x_1) \tag{4.2.23}$$

$$0.01 = exp(-\sqrt{\frac{\pi n f_0}{\alpha}} x_2) \tag{4.2.24}$$

which yield::

$$x_1 = 183\mu m$$
$$x_2 = 362\mu m$$

It can be concluded that the temperature oscillation vanishes very quickly within the solid, barely penetrating 10^{-3} m into the solid.

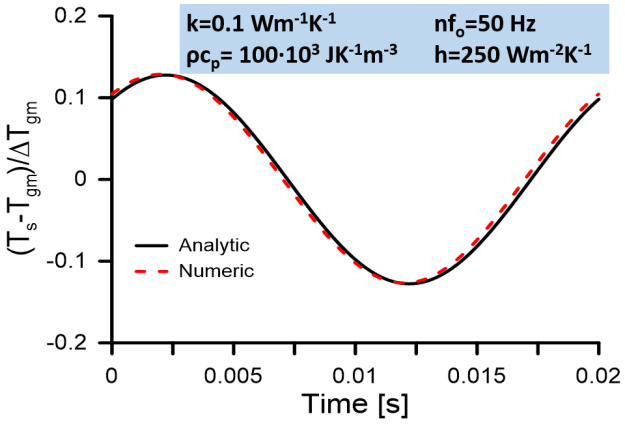

Figure 4.4: *Comparison of the wall temperature evolution calculated with the numerical model and analytic solution of the theoretical problem proposed by Bejan[130].*

Fig. 4.4 presents the comparison of the analytic solution presented above and the modified 1D-HTM lumped model solution. The good agreement between both temperatures confirms the reliability of the numerical model for predicting the evolution of the coated surface temperature. It can therefore be used with confidence to solve the coated engine heat transfer problem.

4.3. Coating definition

Once the model has been validated, the proposed methodology in section 4.1 is applied to define the equivalent coating for three insulating materials. The properties of the considered coatings are shown in Table 4.1. As seen in the mentioned section, a multi-factorial DoE must be carried out in order to find a good equivalent material that behaves as the real coating. The multi-factorial test requires as input the thickness of the equivalent material. The thickness is chosen depending on the engine geometry, taking into account the minimum realistic cell size for the mesh.

Table 4.1: *Real coating used for the definition of the equivalent coatings.*

Coating 1 [131]			
Layers	$k[W/(mk)]$	$\rho c_p\ [\frac{kJ}{m^3K}]$	$Thickness[\mu m]$
1	0.79	2596	130
2	0.83	2724	30
Coating 2 [131]			
Layers	$k[W/(mk)]$	$\rho c_p\ [\frac{kJ}{m^3K}]$	$Thickness[\mu m]$
1	0.79	2596	110
2	0.83	2724	30
Coating 3 [81]			
Layers	$k[W/(mk)]$	$\rho c_p\ [\frac{kJ}{m^3K}]$	$Thickness[\mu m]$
1	0.35	440	100

In this work three different geometries are considered to define the coating layer and the mesh size. This thickness is not added to the real engine geometry, as this would modify the compression ratio of the engine. Instead, the coated layer replaces an equivalent layer metal meshing. This has little influence on the heat transfer through the walls, since the heat transfer through metal is very low. Depending on the geometry, it may be necessary to modify the equivalent material thickness and /or the number of nodes for the coating layer for meshing purposes. Fig. 4.5 displays the engine geometries on which each coating is applied.

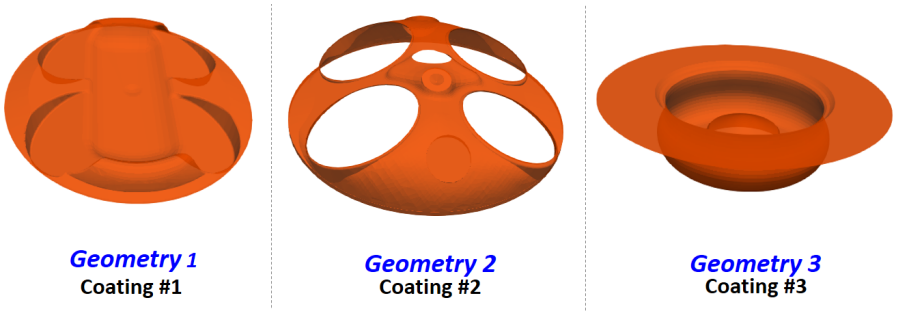

Figure 4.5: *Engine geometries on which coating materials are applied. Geometry 1 corresponds to a piston of a SI engine, geometry 2 to the cylinder head of a SI engine and the geometry 3 to the piston of a Diesel engine.*

In particular, it is important that the 'equivalent material' with a greater thickness reproduces instantaneously the thermal evolution of the real thin coating. The thickness for the equivalent coating should be minimum 500 μm, since the temperature oscillation is attenuated at 362 μm, as seen in the previous section. Then, the optimal value for the equivalent coating layer is determined by the geometry and it has to allow for a reasonable mesh size in CFD-CHT calculations. In addition, as the proposed method seeks also for the discretization step, the number of nodes needs to be defined. Therefore, a range between 4-12 nodes is considered to model the equivalent material.

Based on the geometries presented in Fig. 4.5, the equivalent coating thicknesses are chosen for the 3 insulating coatings presented in Table 4.1:

- **Coating 1**: Layer of 2 mm thickness insulating the whole surface with 4 nodes
- **Coating 2**: Layer of 6 mm thickness insulating the whole surface with 12 nodes
- **Coating 3**: Layer of 2 mm thickness insulating the piston top (rim only), as it is not common to coat the bowl of the Diesel engines. The equivalent material for this coating is discretized with 4 nodes.

For the equivalent coating layer definition the data of a Diesel engine operating at 1500 rpm and 14 bar BMEP has been employed. First, the heat flux and the temperature of the gas exposed wall are calculated for the real coatings with the 1D-HTM model. The boundary conditions, i.e. the heat transfer coefficient and the gas in-cylinder temperature of this operating condition have been previously calculated by CALMEC (a 0D combustion model based on experimental measurements) [132, 133]. The 1D heat transfer problem is illustrated in Fig. 4.6.

To model the behavior of the real materials, each coating was discretized with 1000 nodes in the 1D heat transfer model. The number of nodes was determined by a mesh independence study presented in Appendix 4.A.

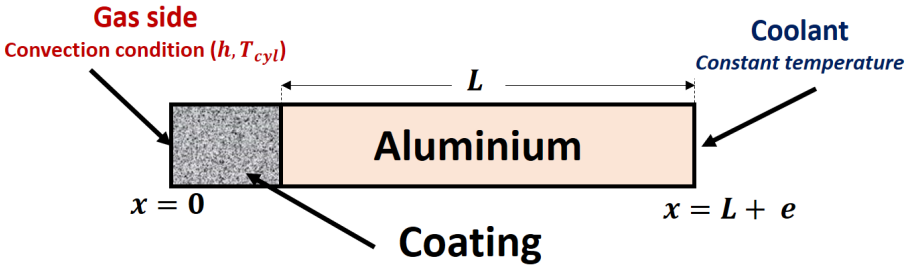

Figure 4.6: *Scheme of a 1D coated bar heat transfer problem with ICE combustion chamber boundary conditions. Gas side: transient heat transfer coefficient and in-cylinder gas temperature. Coolant side: constant temperature of the engine coolant.*

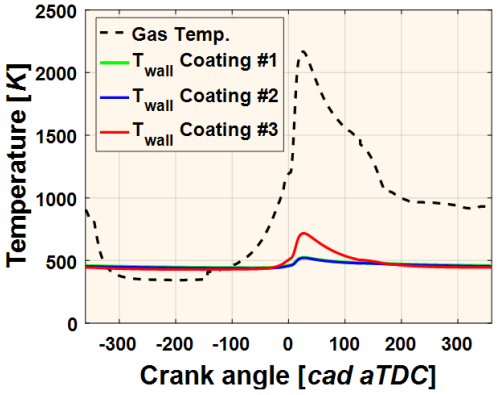

Figure 4.7: *Instantaneous temperature evolution of the gas and of the solid surfaces insulated with real thin coatings during an engine cycle.*

Fig. 4.7 shows the instantaneous temperature evolution during the full engine cycle of each insulating coating, as well as the gas temperature in the combustion chamber. The temperature of the various surfaces follows a similar trend to that of the gas temperature trace and presents a high peak during the combustion phase. Clearly, low values of the conductivity and heat capacitance are more convenient for reducing the heat transfer through the wall. In this regard, coating 3 yields the best reduction in heat transfer

rate since the swing temperature of this material is higher. Fig. 4.8 presents the instantaneous evolution of the heat transfer coefficient and Fig. 4.9 the heat flux through the wall for each material. The heat flux evolution and the wall temperature evolution are taken as references for the definition of the equivalent coating material with the multi-factorial DoE.

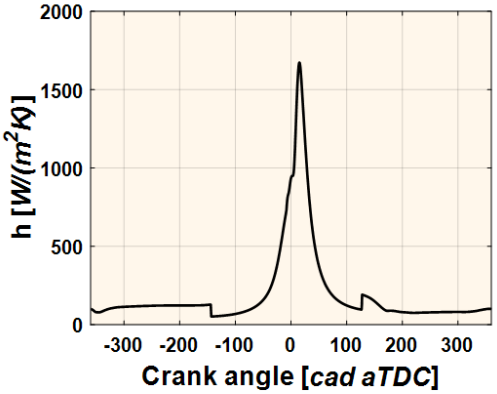

Figure 4.8: *Heat transfer coefficient during the cycle of a Diesel engine at 1500 rpm-14 bar. The trace is used as boundary condition in the 1D heat transfer model.*

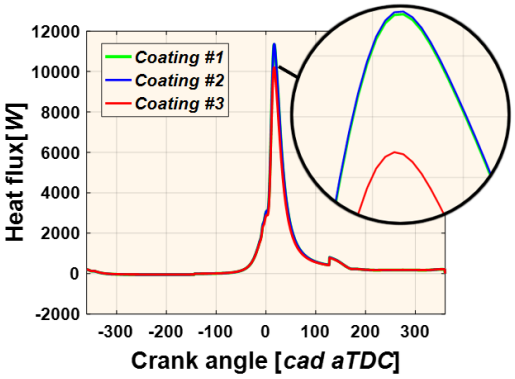

Figure 4.9: *Heat flux evolution during engine cycle for the real thin coating materials.*

The next step, a multifactorial test of possible combinations of heat capacitance and conductivity was carried out to find the instantaneous heat flux and temperature of each material.

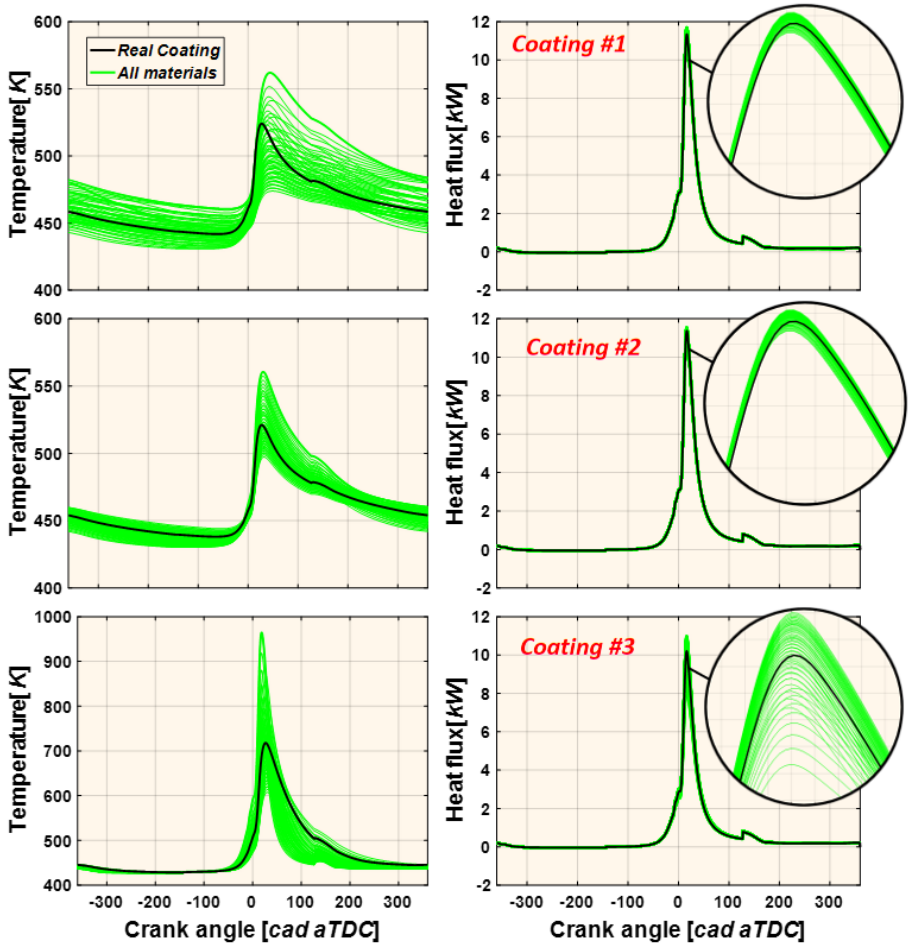

Figure 4.10: *Wall surface temperature evolution (left) and heat flux temporal evolution (right) for real coating and the coating materials obtained with the multifactorial DoE.*

Figure 4.10 displays the wall temperature evolution and the heat flux evolution obtained with the sweep of possible combinations of the material properties considered. As seen, it is quite difficult to find a solution whereby both the wall temperature and the heat flux traces match exactly the real coating material behavior. Since the coating is applied mainly to reduce the heat losses, the equivalent material should be primarily chosen to match the heat flux transient evolution. As shown in figure 4.7, the wall temperature is higher than the gas temperature during the intake stroke. Therefore,

the heat flux is negative in this part of the engine cycle. The equivalent material should also reproduce this behavior. Hence, for selecting the best material, the errors for the positive, negative and mean heat fluxes have to be minimized in the equivalent coating. Nonetheless, the wall temperature evolution was also taken into account in order to guarantee that it follows a very similar tendency to that of the real coating.

Since the possible combinations of the material properties are many, a 2D least square fitting method was employed to find the optimal properties of heat capacitance and conductivity of the material.

The 2D least square fitting method consists in determining the 2D polynomial that best fits with the data. Polynomial coefficients are obtained in the following order:

$$\begin{aligned} f(x,y) = p_1 x^n y^m + p_2 x^{(n-1)} y^m + \ldots + p_{n+1} y^m + \ldots \\ p_{n+2} x^n y^{(m-1)} + p_{n+3} x^{(n-1)} y^{(m-1)} + \ldots + p_{2(n+1)} y^{(m-1)} + \ldots \\ \ldots \\ p_{m(n+1)+1} * x^n + p_{m(n+1)+2} * x^{(n-1)} + \ldots + p_{(n+1)(m+1)} \end{aligned} \tag{4.3.1}$$

Hence, we define the error Q^{error}:

$$Q^{error} = Q^{error}_{negative} + Q^{error}_{positive} \tag{4.3.2}$$

where $Q^{error}_{negative}$ and $Q^{error}_{positive}$ are the errors of the negative and positive heat fluxes, respectively. The target is to find the materials with $Q^{error} = 0$:

$$Q^{error} = F(x,y) = F(\rho c_p, k) = 0 \tag{4.3.3}$$

Finally, by applying a multiple regression analysis the optimal equivalent material is chosen as the one that minimizes the negative and positive heat flux errors. Hence, the following expressions are defined:

$$\rho c_p = F(Q^{error}_{negative}, Q^{error}_{positive}) \tag{4.3.4}$$

$$k = F(Q^{error}_{negative}, Q^{error}_{positive}) \tag{4.3.5}$$

Then the optimal values for ρc_p and k are given for:

$$\rho c_{p_{opt}} = F(0,0) \tag{4.3.6}$$

$$k_{opt} = F(0,0) \tag{4.3.7}$$

The equivalent coating layers are indicated as a black starred dot in Figs. 4.11, 4.12 and 4.13. These maps also show the sensitivity of the solution to the changes of the parameters. Note that a small change in ρc_p or k leads to discrepancies in the solution that are of the same order of magnitude as the possible gain in engine thermal efficiency obtained with this kind of coatings.($\backsim$ 3%). The polynomials of the multiple regression analysis are presented in Appendix 4.B.

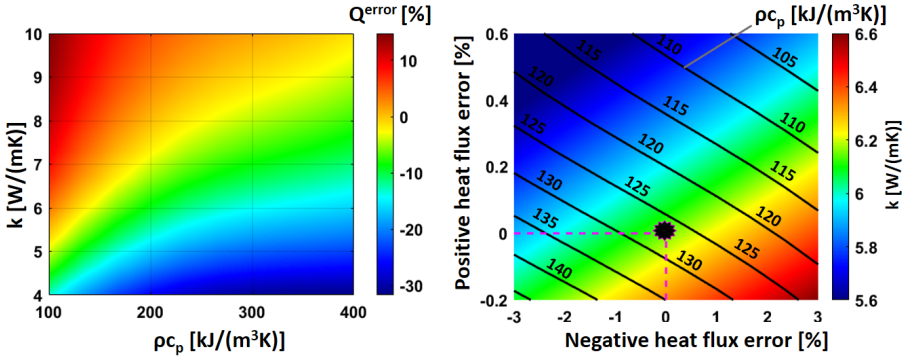

Figure 4.11: *Results of sweep of the possible combinations for the equivalent material for coating 1 determined with the regression $Q^{error} = F(\rho c_p, k)$ (left) and the multiple lineal regression to determine the $\rho c_{p_{opt}}$ and k_{opt} (right).*

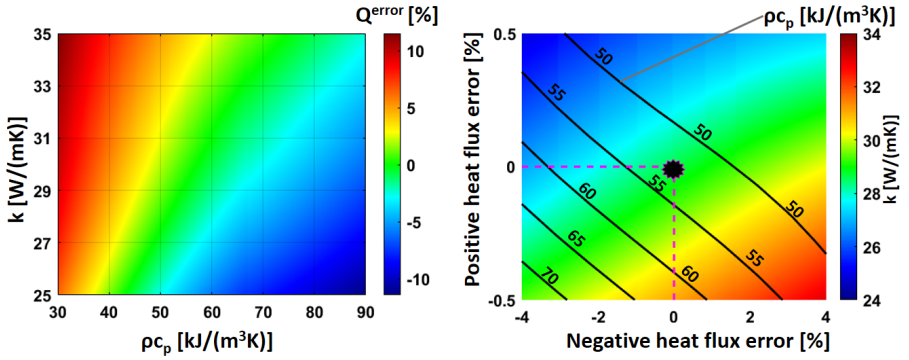

Figure 4.12: *Results of sweep of the possible combinations for the equivalent material for coating 2 determined with the regression* $Q^{error} = F(\rho c_p, k)$ *(left) and the multiple lineal regression to determine the* $\rho c_{p_{opt}}$ *and* k_{opt} *(right).*

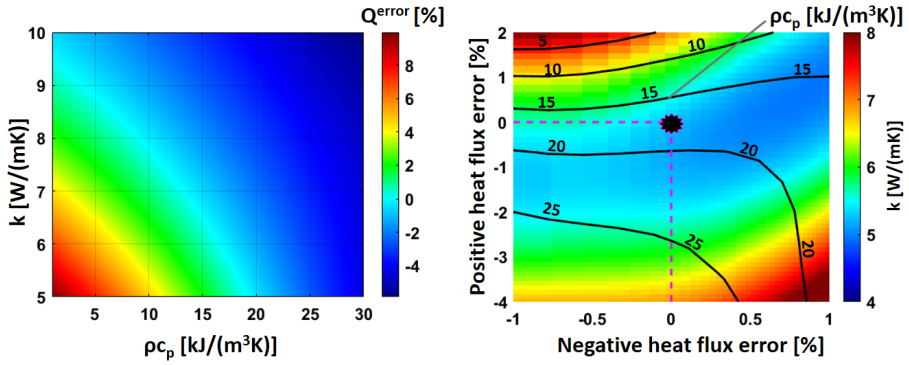

Figure 4.13: *Results of sweep of the possible combinations for the equivalent material for coating 3 determined with the regression* $Q^{error} = F(\rho c_p, k)$ *(left) and the multiple lineal regression to determine the* $\rho c_{p_{opt}}$ *and* k_{opt} *(right).*

In Table 4.2 the optimal properties for each equivalent material are summarized. Furthermore, Fig. 4.14 shows the heat flux evolution of the newly defined equivalent materials compared with the real coatings. Although there are slight discrepancies, once quantified, the differences are very small (Table 4.3) for the heat fluxes (negative, positive and mean). The results in terms of wall temperature evolution during the engine cycle, which are displayed in the same figure confirm the above statement. This error at peak temperature for each material is not really representative in terms of heat flux, so it is not significant. Nonetheless, it is important that the equivalent

material should reproduce properly the thermo-swing of the real coating. Particularly when the exact wall temperature information is required, as is the case for instance to predict knocking in gasoline engines.

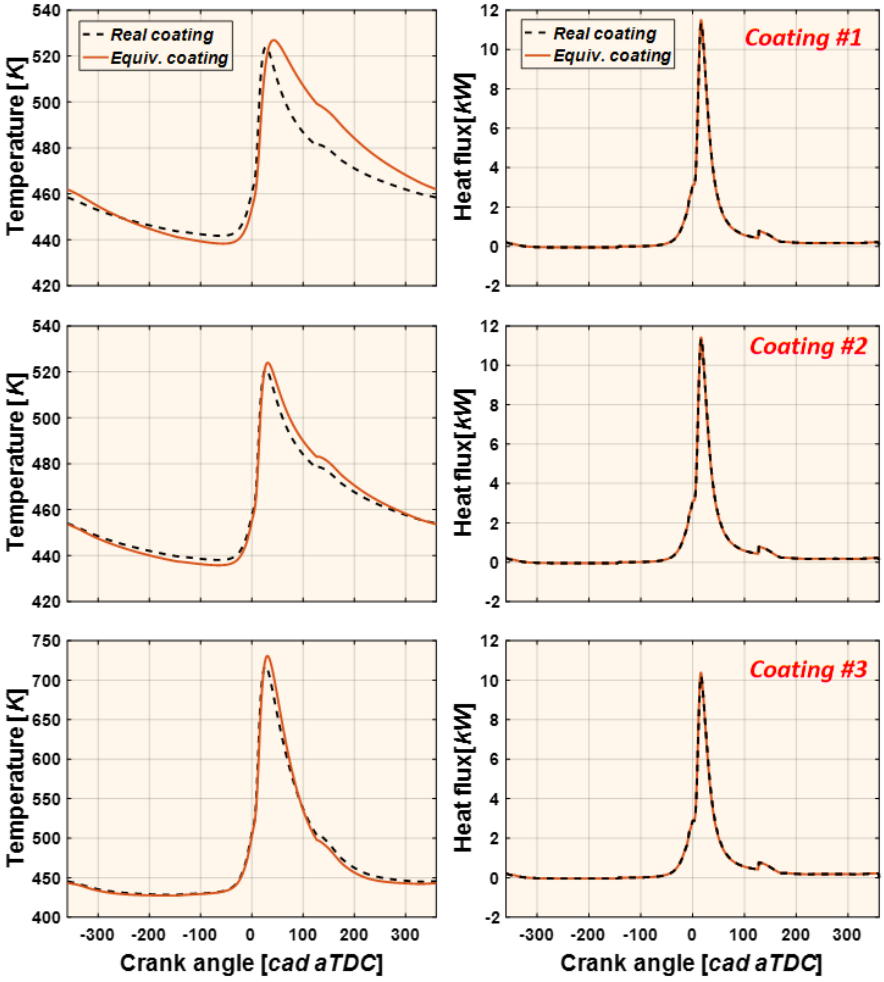

Figure 4.14: *Comparison of the surface temperature evolution (left) and heat flux evolution (right) for the real coating and the selected equivalent materials.*

The differences of the equivalent coating layers with the the real materials are displayed in Table 4.3. For all the materials the differences are lower than 1% for the negative ($Q^{error}_{negative}$), positive ($Q^{error}_{positive}$) and mean flux (Q^{error}_{mean}), respectively. In case of the wall temperature evolution, the

Table 4.2: *Material properties for the equivalent insulating coatings.*

Equiv. Coating	ρc_p $[\frac{kJ}{m^3K}]$	k $[\frac{W}{m \cdot K}]$
1	127.10	6.15
2	52.65	28.64
3	17.62	5.21

maximum difference is for the coating 1 with 4.3 %. Clearly, the coating 2 has the lowest error for all the heat transfer parameters. This probably is due to the fact that this material has been meshed with a higher number of nodes.

Table 4.3: *Differences between the real coating and the equivalent coating layers.*

Equiv. Coating	$Q^{error}_{negative}[\%]$	$Q^{error}_{positive}[\%]$	$Q^{error}_{mean}[\%]$	$T^{error}_{max}[\%]$
1	0.23	0.0014	0.04	4.31
2	-0.124	0.05	0.014	1.50
3	0.68	-0.19	-0.2	3.89

When the coated layer is meshed with different number of nodes the thermal behavior of the equivalent material changes. It does not reproduce anymore the behavior of the real insulating layer. It is also the case if the thickness considered is different. Hence in order to perform CHT calculations it is important to define the 'equivalent material' taking into account the effect of these parameters on the multi-factorial test solutions. The results of these parametric studies are described below. The reference solutions are the ones calculated above and represented in the figure with a dashed line.

Figure 4.15 displays the wall temperature evolution and the heat flux traces for the equivalent materials in function of the nodes number. In terms of heat flux, the traces are very similar, but the heat flux decreases as the number of nodes increases, especially at peak flux. On the other hand increasing the number of nodes leads to higher temperatures on the wall surface, as expected, since the heat flux is proportional to the thermal gradient between the gas and the solid surface.

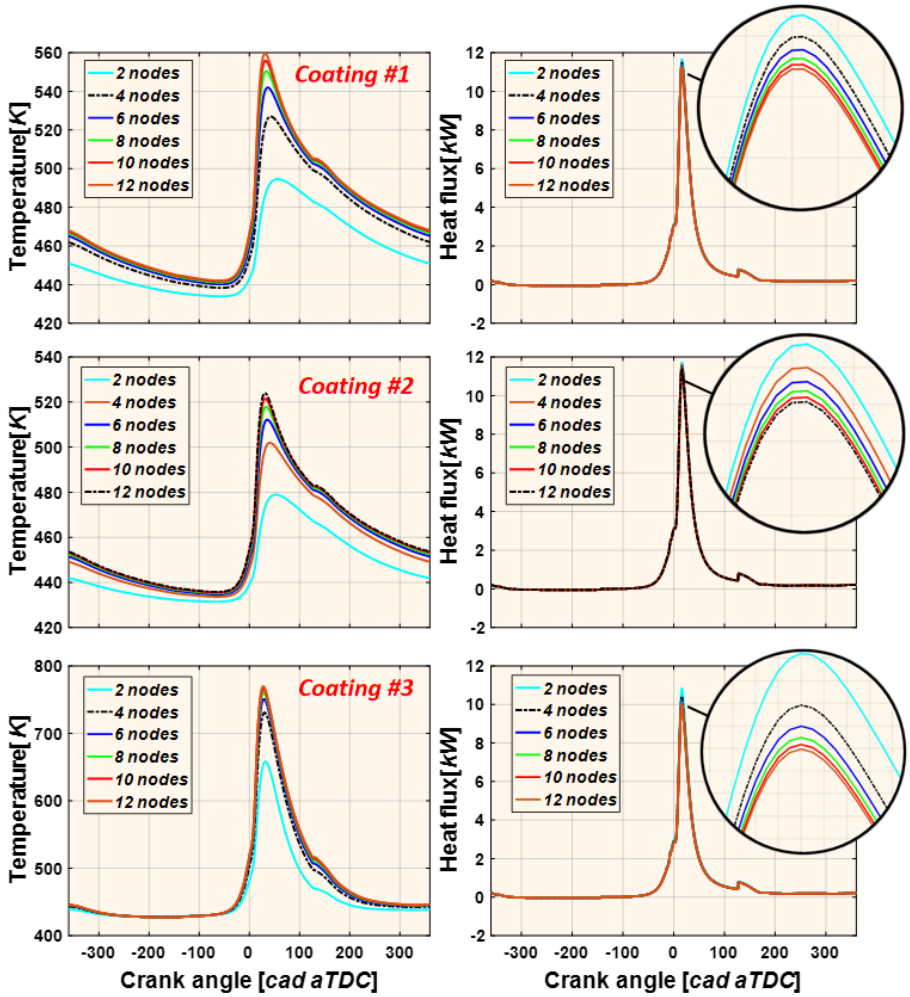

Figure 4.15: *Wall temperature evolution (left) and heat flux evolution (right) of the selected materials for different number of nodes.Black dashed traces represent the equivalent coating chosen.*

The results of the multi-factorial tests performed by varying the thickness of the equivalent materials are shown in Fig. 4.16 in terms of the wall temperature evolution and the instantaneous heat flux. The comparison of the wall temperature traces shows that these increase proportionally to the material thickness, though the peak temperature does not change significantly from 2 mm thickness onwards. The peak heat flux is not significantly affected by the thickness of the equivalent coating material. The traces

start diverging after TDC, however, during the diffusion combustion process: there is less heat flux for increasing material thickness. This study clearly illustrates the necessity of properly defining the equivalent coating thickness before performing the CHT calculation.

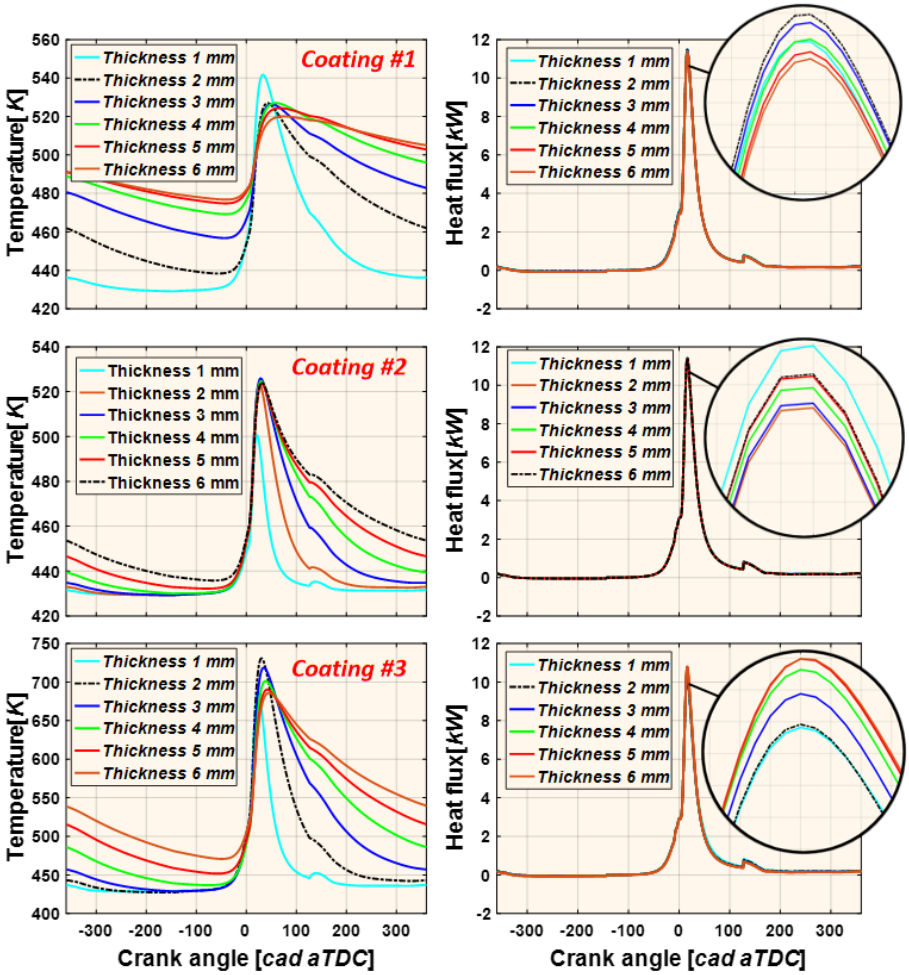

Figure 4.16: *Wall temperature evolution (left) and heat flux evolution (right) of the selected materials for different thicknesses. Black dashed traces represent the equivalent coating chosen.*

The material optimal thermal properties calculated with the proposed approach for different number of mesh nodes are displayed in Fig. 4.17 for the equivalent thickness specified for each coating layer. The results

show that the heat capacitance and thermal conductivity values increase as the number of nodes is higher. Moreover, the optimal thermal properties obtained by varying the thickness are shown in Fig. 4.18 considering the selected number of nodes for each coating layer mesh. In this case, when the thickness grows the heat capacitance should be decreased and the thermal conductivity increased.

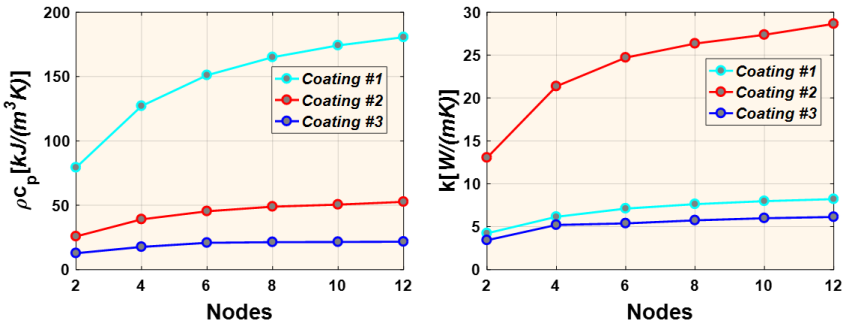

Figure 4.17: *Material properties for different number of nodes. Optimal heat capacitance (left) and optimal thermal conductivity (right). The thickness for each material are 2 mm, 6 mm and 2 mm for the coating 1, 2 and 3, respectively.*

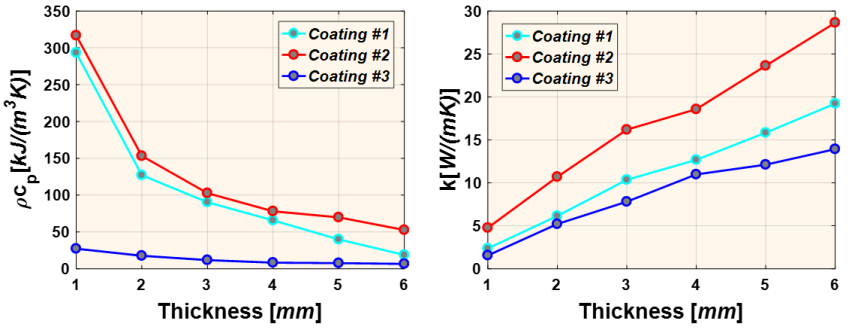

Figure 4.18: *Material properties for different thicknesses of the equivalent materials. Optimal heat capacitance (left) and optimal thermal conductivity (right). The nodes number considered for each material are 4 nodes, 12 nodes and 4 nodes for the coating 1, 2 and 3, respectively.*

4.4. Summary

In this chapter a methodology is presented whereby a 1D heat transfer model is used in combination with a multi-factorial test and a multiple regression analysis to define the thermal properties (conductivity and heat capacitance) of an equivalent coating material with reasonable thickness (e.g. 2-6 mm) that behaves as the real very thin coating layer ($\backsim$100 μm). This equivalent material can then be adequately meshed to perform the CHT calculations and predict with more accuracy the heat losses in the combustion chamber of an ICE. The most remarkable findings are summarized below:

- The prediction of the heat transfer from gas to walls in ICEs is a very complex process that does not have an analytical solution. Then, it is necessary to use numerical tools that allow estimating the heat transfer. However, these numerical models must be validated with available experimental or analytical solutions. In this chapter the 1D-HTM lumped model developed at CMT has been validated with the theoretical solution of a semi-infinite solid. The results show the suitability of the model to study the heat transfer on coated solids.
- The new generation of insulating coatings applied in ICE tends to be very thin (around 100 μm). Therefore, to model with CHT the heat transfer through the ICE coated walls the mesh needed has to be extremely fine. As solution for this problem, a thicker coating layer of 'equivalent material' can be defined that will allow reasonable meshing for the CHT calculations.
- In order to define the equivalent coating layer is required to define a material that behaves thermodynamically as the real thin coating layer. The optimal properties for heat capacitance and thermal conductivity for the new material have to minimize the error for the negative, positive and mean heat fluxes. Moreover, the selected equivalent material has to reproduce a similar wall temperature evolution as the one of the real coating. In particular, low errors in the wall temperature evolution is important for the SI engines where the hotter walls can lead to knock in the engine. Though the thermal properties of the equivalent material may not be realistic (meaning that this material does not physically exist), it does behave as the real coating material.
- The optimal properties for the equivalent coating layers are determined by using a multiple regression analysis with the data of a mutifactorial DoE of possible equivalent coatings. For the calculation of the optimal heat capacitance and conductivity the polynomial regression needs to

have a good fitting with the data (> 90%). The suitability of the polynomial regressions to match with the data determine the discrepancies between the equivalent and the real coatings (see Appendix 4.B).

- The results show that the equivalent material defined with the methodology proposed has an error lower than 1% in the heat flux while for the wall temperature evolution the maximum error is about 4%. Furthermore, the equivalent coating layer with the lowest error is the one with the highest number of nodes. Then, adding more nodes to the coating layer can reduce the error in the instantaneous temperature. However, the definition of the number of nodes for the mesh in the CHT is given by the base grid in the calculation and the geometry of the surfaces.
- A parametric study to evaluate the effect on the heat transfer of changing the number of nodes and the thickness of the equivalent materials has been performed. The study shows the importance of the definition of both parameters to mesh the equivalent coating material. Therefore, changing one of them in the CHT calculation may lead to inaccuracies.

4.A. Appendix: Mesh convergence

The objective of the methodology proposed in this chapter is to be able to assess accurately the impact of very thin coating layers on the heat losses through the engine walls using CFD-CHT. However, generating a mesh to solve adequately such thin layers leads to prohibitive mesh size. The thick 'equivalent' material with few nodes (2-12) has to reproduce the behavior of the real coating with fine mesh. Then, in the developed approach, the properties of the thick coating layer are adjusted to match the properties of the real thin coating meshed with a finer discretization. So that, the mesh independence needs to be assured for the thin coating layer. Fig. 4.19 shows that the mean temperature do not change significantly by increasing the number of cells above 200 already.

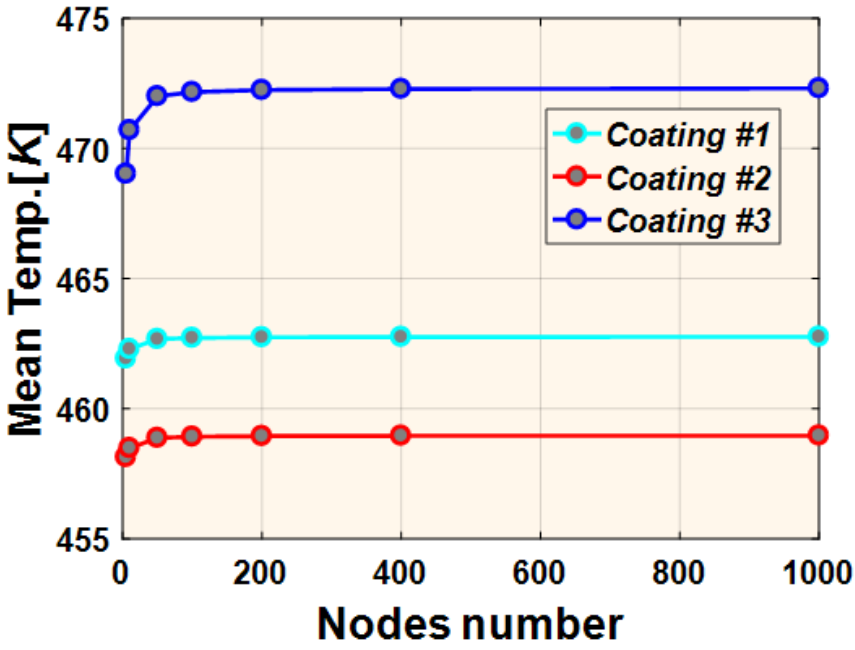

Figure 4.19: *Mesh independence study with the mean wall temperature on the real coating layer.*

4.B. Appendix: Multiple regression analysis

Table 4.4: *Multiple regression analysis to define the equivalent coatings.*

Material 1				
$F(x,y)$	∂	Coefficients	R^2	$R^2_{adjusted}$
Q^{error}	6	$[-8.13e-07$ $-2.45e-05$ 0.001 $8.95e-04$ $1.01e-03$ -0.37 0.07 -2.42 26.53 $-58.25]$	0.9989	0.9988
ρc_p	6	$[-0.87$ -1.44 10.53 0.09 1.96 37.40 0.01 0.0082 -3.27 $127.06]$	0.9999	0.9999
k	6	$[-0.03$ 0.0029 0.13 $-2.0e-04$ -0.01 -0.89 $5.45e-05$ $2.11e-04$ 0.08 $6.15]$	0.9998	0.9998
Material 2				
$F(x,y)$	∂	Coefficients	R^2	$R^2_{adjusted}$
Q^{error}	6	$[-1.72e-05$ $-1.69e-04$ 0.01 $8.32e-05$ 0.02 -1.51 $2.20e-03$ -0.24 8.12 $-60.69]$	0.9989	0.9989
ρc_p	6	$[-0.0033$ 0.19 0.13 0.58 1.96 -1.78 0.95 6.81 -16.35 $52.48]$	0.9926	0.9919
k	6	$[2.47e-04$ -0.03 -0.0065 -0.12 -0.16 0.41 -0.41 0.47 -4.50 $28.65]$	0.9996	0.9996
Material 3				
$F(x,y)$	∂	Coefficients	R^2	$R^2_{adjusted}$
Q^{error}	6	$[4,39e-05$ $-8.07e-04$ 0,007 $-0,010$ 0,24 $-1,55$ $-0,004$ 0,32 $-6,24$ $34,37$	0.9989	0.9989
ρc_p	6	$[-1.90$ 0.86 -0.53 0.17 2.17 1.78 -0.08 -0.73 -4.21 $17.62]$	0.9428	0.9401
k	6	[0.41 -0.19 0.11 -0.04 -0.47 -0.60 0.01 0.23 0.25 $5.2062]$	0.9279	0.9244

To define the equivalent coating layers were used polynomials regression of order (∂) 6 since they provide a good fitting with the multifactorial DoE test. The coefficient of determination R^2 is a measure of the suitability of the polynomial regression to fit with the data. However, this parameter may not be representative for more than one independent variable. Then, the $R^2_{adjusted}$ need to be evaluated to have a better estimation of the quality of the polynomial regressions. As seen in the Table 4.4 the polynomial regressions to define the equivalent coatings 1 and 2 have a fitting of 99 % with the DoE data. Nonetheless, for the equivalent coating 3 the fitting is about 92 and 94 % for the heat capacitance and the conductivity, respectively. This value in the coefficient of determination explains the slight lower resolution in Fig. 4.13 and the higher error for the heat fluxes for the equivalent coating in Table 4.3.

Finally, in order to define the more suitable equivalent coating the fitting of the polynomial regression have to be higher than 90 %. In the other way round, the underlying differences with the real coating material are expected to increase.

CHAPTER 5

Heat losses through uncoated and coated engines

The main objective in this chapter is to quantify by 3D CFD-CHT modelling the impact on heat losses and engine efficiency of the thermal insulation coating applied on the piston and cylinder head.

For the calculations the CONVERGE CHT tool described in Chapter 3 is employed and the equivalent coatings defined in Chapter 4. It is important to be able to quantify the heat losses during the intake and exhaust strokes in order to assess if the advantages gained during the combustion process are not outweighed by the impact of the coating during the intake and exhaust strokes. Hence, the 3D calculation of the full engine cycle considering the solid coated parts is needed.

In this chapter, the methodology followed for the CHT full cycle calculations is presented. Moreover, the mesh employed for the simulations as well as the models and boundary conditions are described. The calculations are performed for two operation conditions (low load and medium load) in a single cylinder SI engine designed by IFP Energies Nouvelles (IFPEN). The results are compared with experimental data of the engine. In addition, the temporal evolution of the average temperature solid gas exposed sur-

---

Work presented in this chapter has been partly published in the following papers:

- Validation and Analysis of Heat Losses Prediction Using Conjugate Heat Transfer Simulation for an Internal Combustion Engine [2]
- Conjugate Heat Transfer study of the impact of "thermo-swing" coatings on Internal Combustion Engines heat losses [4]

faces calculated with CHT were compared to that predicted by the CMT-1D HTM lumped model described in Chapter 4, since they cannot be measured experimentally.

The results yielded for the CHT calculations will allow to confirm the suitability of the approach to assess the heat losses in ICEs.

5.1. Methodology

In order to perform the CHT calculations to study the heat losses in ICEs through the uncoated and coated walls, a calculation methodology was developed. It consists on the two main steps described below:

- **CFD-CHT for metallic engine**

Before the CHT full engine cycle simulations, CFD calculations are performed in the metallic engine in order to calibrate the combustion model and define the set-up. In the calculations, the whole gas exchange process (GEP), starting from exhaust valve opening (EVO) is also simulated together with the closed cycle. The resulting in-cylinder pressure traces are compared with experimental data to assure the reliability of the settings.

Then, for the CHT calculations, the piston and the cylinder head geometries are also included in the meshing, since CHT will be applied to these two solid parts. The calculations were performed for two operation conditions of a single cylinder engine described in the following sections: low load operation point (2000 rpm, 4 bar IMEP) and medium load operation point (3000 rpm, 7 bar IMEP).

In order to validate the CHT results, the obtained mean temperature levels and swing on the piston wall are compared with the results of the 1D simulation performed with a 1D lumped model [134]. In addition, the fluid domain is validated by comparison of the experimental and simulated in-cylinder pressure traces.

- **CFD-CHT for coated engine**

Following the same approach as described above, CFD-CHT calculations are carried out for piston coated with equivalent material 1 and the cylinder head coated with equivalent material 2 (see Section 4.3). Since the real coating layer is too thin for modelling (Table 4.1), equivalent coating layers of 2 mm for the piston and 6 mm for the cylinder head have been defined previously in Chapter 4 corresponding to the combined properties of layers 1 and 2 (Table 4.2).

The results obtained with the coated engine are compared with those of the base aluminium engine in order to quantify the impact of the thermal insulation material, as well as the experimental data obtained from the engine.

5.2. Numerical setup

For the CFD calibration simulations only the fluid domain is considered. However, the computational domain for the CHT calculations includes both the fluid and solid zones. The fluid region includes the single cylinder geometry, as well as the intake and exhaust ports, while the solid region is formed by the piston and cylinder head. In the case of the coated configuration the layer of insulating material is integrated in the solid on the gas exposed surfaces of the piston and cylinder head, so that the engine compression ratio remains unchanged. The engine geometry was provided by (IFPEN) and its main characteristics are presented in Table 6.1.

Table 5.1: *Engine specifications.*

Engine type	4-stroke spark ignited
Number of cylinders [-]	1
Bore - Stroke [mm]	75-93
Connecting rod [mm]	150
Compression ratio	14:1
Number of valves [-]	2 intake and 2 exhaust

As mentioned in the previous section, the calculations are performed for two operation conditions that are described in Table 5.2

Table 5.2: *Specifications of the operation conditions to perform the CHT calculations.*

Operation condition	**1**	**2**
IMEP [bar]	4	7
Engine speed [rpm]	2000	3000
Air-fuel ratio $\lambda[-]$	1.2	1.4
Ignition timing [cad aTDC]	-21.5	-27

The computational domain is shown in Fig. 5.1 and includes the complete single cylinder geometry and the intake/exhaust ports for full cycle calculations.

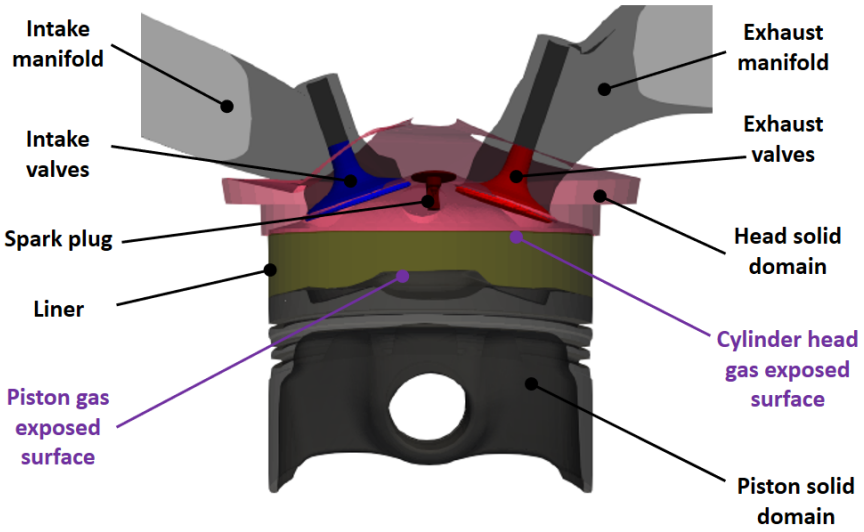

Figure 5.1: *Calculation domain for the CHT calculations formed by the combustion chamber with the intake/exhaust ports. The gas exposed surfaces of the piston and cylinder head (purple) are the fluid/solid interface walls in the CHT simulations.*

5.2.1. Mesh and model set-up

For the engine calculations performed in the SI engine the commercial CFD code CONVERGE v2.3 [102] based on the finite-volume method has been used. The engine geometry was provided by IFPEN.

The cut-cell Cartesian method available in the code was used to generate a hexahedral mesh with a base size of 2 mm. The cell size was reduced to 0.5 mm at the walls of the combustion chamber ports and valves regions to improve boundary layer prediction. In order to model the fuel injection, the mesh was refined to 0.5 mm in the injector region. Moreover, the mesh size in the chamber was decreased to 1 mm, while the region of the spark plug was prescribed to 0.125 mm to resolve both the spark and the developing primary flame kernel (see Figure 4 3). The code also employed an Adaptive Mesh Refinement (AMR) technique to increase grid resolution (up to 0.5 mm minimum cell size) based on the velocity and temperature sub grid

scales (SGS) of 1 m/s and 2.5 K, respectively. Previous Reynolds-averaged Navier-Stokes (RANS) [135–137] and large eddy simulations (LES) studies [138, 139] have demonstrated that this mesh configuration is sufficient for simulating the flame propagation and knocking in SI engines. Furthermore, in order to save computational time, the AMR was applied according to the following considerations [102]:

- SGS for the velocity in the intake ports during the full cycle
- SGS for the velocity in the in-cylinder during the full cycle
- SGS for the temperature in the in-cylinder during closed cycle (combustion)

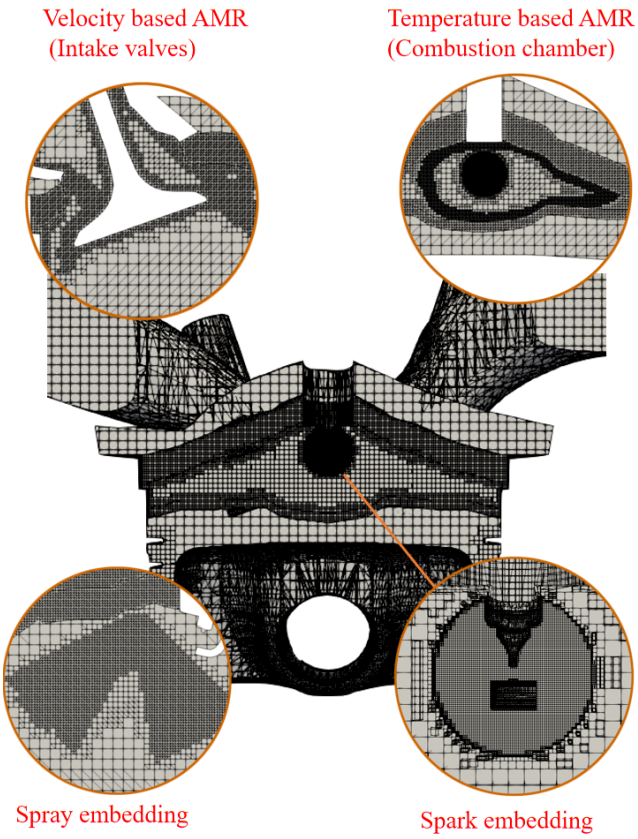

Figure 5.2: *Mesh charaterization of the SI engine.*

These considerations are based on the fact that most of the velocity fluctuations take place during the intake and the combustion, while the important temperature fluctuations occur during the combustion. Hence, activating the AMR in the whole domain for the full cycle would lead to unnecessary mesh refinement and longer computational times.

The models employed for the fuel injection follow work available in the literature [140]. In this regard, the Kelvin Helmholtz (KH)-Rayleigh Taylor (RT) breakup model was used to predict liquid atomization and drop breakup [141]. The O'Rourke collision and coalescence model is employed to estimate the droplet collisions and their outcomes [142]. In addition, the Frossling model was prescribed to reproduce the fuel evaporation [143]. In CONVERGE, the isooctane inorganic compound (C8H18) is used to model the gasoline.

To model the combustion process, the SAGE detailed chemistry solver was employed [144]. This model uses local conditions to calculate reaction rates based on the principles of chemical kinetics.[102].

The empirical Hiroyasu soot model [145] was employed for the calculation of emissions whereas the extended Zeldovich mechanism [18] was used for determining the NOx formation.

A second-order central difference scheme was chosen for spatial discretization and a first-order scheme was employed for temporal discretization. In-cylinder turbulence was modeled using the Unsteady Reynolds-Averaged Navier Stokes (URANS) based RNG k-ϵ model [103] coupled with the wall heat transfer model developed by O'Rourke and Amsden [105]. The Redlich-Kwong equation [146] was selected as the equation of state for calculating the compressible flow properties. Pressure-velocity coupling was achieved by using a modified Pressure Implicit with Splitting of Operators (PISO) method [147].

In the O'Rourke and Amsden model, the wall heat transfer is given by

$$k\frac{dT}{dx_i} = \frac{\mu_m F\left(T_f - T_w\right)}{Pr_m y} n_i \tag{5.2.1}$$

k is the molecular conductivity, μ_m is the molecular dynamic viscosity, T_f is the fluid temperature, T_w is the wall temperature, $\mathrm{Pr_m}$ is the molecular Prandtl number, y is the absolute distance from the wall and n_i is the moles amount. F value is given by:

$$F = \begin{cases} 1.0 & y^+ < 11.05 \\ F_{new} & y^+ > 11.05 \end{cases} \tag{5.2.2}$$

$$F_{new} = \frac{\left(\frac{y^+ \mathrm{Pr}_m}{\mathrm{Pr}_t}\right)}{\frac{1}{\kappa}\ln(y^+) + B + 11.05\left(\frac{\mathrm{Pr}_m}{\mathrm{Pr}_t} - 1\right)} \tag{5.2.3}$$

$$y^+ = \frac{\rho u_t y}{\mu_m} \tag{5.2.4}$$

Pr_t is the turbulent Prandtl number, κ is the Von Karman constant (0.4187) and B is a law-of-the wall constant; in this case the value is 5.5. y^+ is determined with the equation 3.1.3:

$$y^+ = \frac{\rho u_t y}{\mu_m} \tag{5.2.5}$$

A variable time-step was specified in CONVERGE. This time-step control technique performs a number of checks and calculations to determine the size of the next time-step, and takes the largest time-step that satisfies all of the applicable limiters. These limiters are given for the maximum CFL (Courant-Courant-Friedrichs-Levy) numbers for convection (5.2.6), diffusion (5.2.7) and Mach (5.2.8).

The maximum convection CFL limit max_cfl_u is defined as:

$$max\_cfl\_u \leq u\frac{\Delta t}{\Delta x} \tag{5.2.6}$$

where u is the velocity and $\frac{\Delta t}{\Delta x}$ is the time interval and Δx is the space interval.

For the maximum diffusion CFL limit max_cfl_nu, the following expression is employed:

$$max\_cfl\_nu \leq \nu\frac{\Delta t}{\Delta x^2} \tag{5.2.7}$$

here, ν is the viscosity of the fluid.

Finally, the maximum Mach CFL limit, based on the speed of sound c is given by:

$$max\_cfl\_\,\mathrm{mach} \leq c\frac{\Delta t}{\Delta x} \tag{5.2.8}$$

In order to optimize the calculation time, a time step-control strategy is defined, which consists in relaxing the Courant number [148]. Furthermore, a modification of this approach was introduced, relaxing the CFL (Courant-Courant-Friedrichs-Levy) number according to the stages of the engine cycle.

In Table 5.3 the maximum CFL limits for convection, viscosity and Mach are displayed.

Table 5.3: *Maximum CFL limits for the calculations in the SI engine.*

Intake region			
CAD	max_cfl_u	max_cfl_nu	max_cfl_mach
-610.6	2.0	5.0	80
-171.0	2.0	5.0	50
109.4	2.0	5.0	80
Exhaust region			
CAD	max_cfl_u	max_cfl_nu	max_cfl_mach
-610.6	5.0	5.0	80
-171.0	5.0	5.0	50
109.4	5.0	5.0	80
In-cylinder region			
CAD	max_cfl_u	max_cfl_nu	max_cfl_mach
-610.6	2.0	5.0	80
-171.0	1.0	2.5	50
109.4	2.0	5.0	80

To solve the CHT problem in the solid domain, the super-cycling approach of CONVERGE has been used. For this study multiple cycles were run to calculate the evolution of the temperature on the solid surface of the piston, with a time step interval of 60 CAD to store the heat transfer variables.

5.3. Boundary conditions

To model the fluid domain, isothermal wall boundary conditions are considered in the gas exposed surfaces of the combustion chamber. The temperatures were determined by using the 1D-HTM described in chapter 4 that has been used in many investigations to predict the temperature of the combustion chamber walls [149–152]. The wall temperatures obtained for the piston and the cylinder head are only used for the CFD calibration. However, these temperatures are employed for initializing the solid domain in the CHT calculations. The temperatures for the combustion chamber walls obtained with 1D-HTM are listed in Table 5.4.

Table 5.4: *Boundary conditions for the isothermal walls obtained with the 1D-HTM for CFD calibration.*

Point	$T_{piston}[K]$	$T_{head}[K]$	$T_{liner}[K]$
1	442.1	411.5	401.3
2	435.7	438.3	395.6

To model the combustion, the fuel mass and the injection rate are imposed. Furthermore, an inflow boundary condition is given at the intake ports inlet with the experimental intake pressure and temperature provided by the experimental data IFPEN. Similarly, an outflow boundary condition is considered at the exhaust outlet ports with the experimental values of pressure and temperature. The boundary conditions considered at the intake/exhaust port are displayed in Table 5.5.

Table 5.5: *Boundary conditions at the intake and exhaust ports for the multiple cycle calculations.*

Point	$P_{int}[bar]$	$T_{int}[K]$	$P_{exh}[bar]$	$T_{exh}[K]$
1	0.52	301.4	1.01	756.2
2	0.87	302.2	1.01	779.2

5.3.1. CHT solid domain

For the CHT simulation of the piston and cylinder head, boundary conditions have to be imposed on both sides of the fluid/solid interfaces [100]. The required boundary conditions for CHT at the inner solid surfaces in contact with the gas are the heat capacitance, the thermal conductivity, and the density of the wall material (aluminium or equivalent coating). The thickness of the material is directly given by the meshed geometry of the walls. It is important to set appropriate boundary conditions for the gas or fluid in contact with the walls of the piston in order to achieve the right temperature levels on the piston surface. Thus the solid piston is divided into several regions as shown in Fig. 5.3 to take into account the properties of the different fluids (gas, coolant) in contact with its surfaces. The boundary conditions imposed at the outer fluid interface are convection conditions, which require values for the near-wall heat transfer coefficient (h) and near-wall gas/fluid temperature (T) for the piston top and crown, these

parameters are directly calculated by the CFD-CHT process. For the piston ring, skirt and oil cavity values were taken from the literature. These are detailed below:

- Piston top: Contact with the combustion gas (h, T) given by the calculation itself (Convection)
- Piston crown: Contact with combustion gas near the liner wall (h, T) given by the calculation (Convection)
- Piston ring [102]: Piston segments (Convection)
- Piston skirt [153]: Contact with oil vapor (Convection)
- Piston oil cavity [154]: Contact with cooling oil

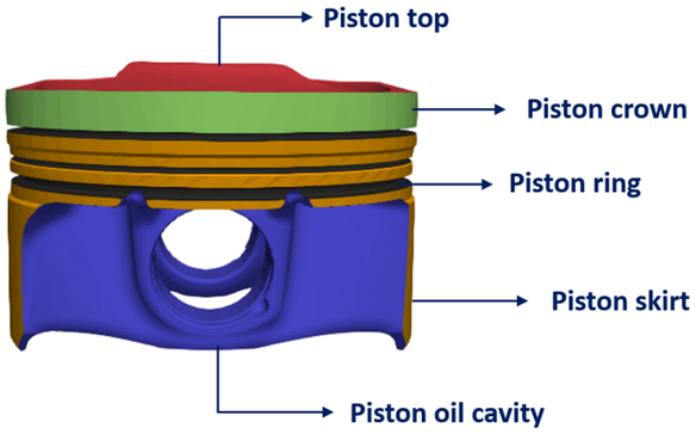

Figure 5.3: *Piston regions considered for boundary conditions in the CHT solid domain. Piston top represent the fluid/solid interface wall for the calculations.*

For the piston skirt, the heat transfer coefficient between the oil splashed and the lower block is calculated with the correlation [153]:

$$h_{skirt} = h_{REF}\left(\frac{N}{2000}\right)\left(\frac{\nu\,(T = 90°C)}{\nu(T)}\right)^{0.5} \tag{5.3.1}$$

where h_{REF} value is 350W/m^{2}K used in the literature [155, 156], ν is the oil viscosity and N is the engine speed.

For the oil cavity, the heat transfer coefficient is calculated with the equation 5.3.2

$$h_{coO} = \frac{2Nuk_{oil}}{De} \tag{5.3.2}$$

In the latter equation k_{oil} is the thermal conductivity of the oil, ν is the oil viscosity and N is the engine speed.

The Nusselt number Nu is calculated using the empirical formula from Bush and modified by French [157]:

$$Nu = 2.027\,(\text{Re}_B)^{0.466}\,(\text{De}/\text{H})^{0.3}(\text{Pr})^{0.33}\left(\mu_f/\mu_m\right)^{0.14} \tag{5.3.3}$$

where Re_B is the Reynolds number, De is the equivalent diameter of the cooling cavity, H is the average height of cavity, μ_f is the cooling oil viscosity at average temperature, μ_m is the cooling oil viscosity at the metal surface temperature. The factor $\left(\frac{\mu_f}{\mu_m}\right)$ set to one since the surface temperature is unknown.

The Re_B is determined by:

$$Re_B = \frac{\omega_B De}{\nu} \tag{5.3.4}$$

As the piston is in motion during the engine cycle, there is a transient effect on the oscillating velocity of cooling oil in the cooling cavity, In order to simplify the problem, this effect has been omitted [158]. The oscillating velocity of the cooling oil ω_B is calculated by equation 5.3.5.

$$\omega_B = \frac{NH}{30} \tag{5.3.5}$$

According to the literature, most of the total heat transfer happens in the cooling oil cavity. Due to the reciprocating motion of the piston, the cooling oil has a strong impact on the piston, which results in a high surface heat transfer coefficient.

The values considered as boundary conditions on the piston solid regions for each operating point are shown in Table 5.6.

Table 5.6: *Boundary conditions for the piston outer surface.*

2000 rpm - 4 bar		
Outer solid wall	$T[K]$	$h[W/(m^2K)]$
Piston crown	659	450
Piston ring	493	500
Piston skirt	423	435
Piston cavity	383	2148
3000 rpm - 7 bar		
Outer solid wall	$T[K]$	$h[W/(m^2K)]$
Piston crown	591	407
Piston ring	493	500
Piston skirt	423	525
Piston cavity	383	3766

For the cylinder head inner wall in contact with the gas, the boundary conditions on both sides of the fluid/solid interfaces are analogous to the ones imposed on the piston. For the outer wall a convection boundary condition taking into account the heat transfer coefficient and the temperature of the cooling system is imposed, as indicated in Fig. 5.4. The cooling temperature was obtained from the data provided by IFPEN, while the heat transfer coefficient is estimated with the Dittus-Boelter correlation for pipe flows explained in chapter 3.

In order to perform the CHT for the full cylinder head it is necessary to model the heat conduction between the valves guides and the head, and the heat transfer through the coolant system. Due to the CHT long computational times and the available resources, it was not possible to consider the whole domain for the cylinder head. Therefore, the geometry was simplified by considering just a solid part of the cylinder head above the gas exposed surface.

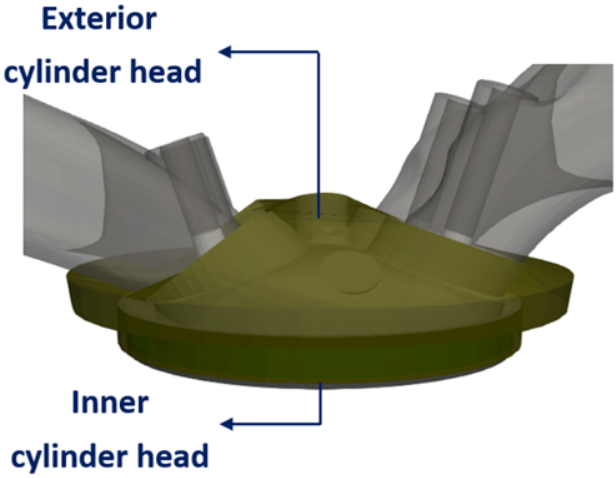

Figure 5.4: *Cylinder head regions considered for boundary conditions in the CHT solid domain. Inner cylinder head is the fluid/solid interface wall for the calculations.*

5.4. Combustion set-up validation

First the combustion parameters need to be adjusted by performing a full cycle CFD calculation without CHT. Once adjusted, the same parameters are used for the CFD-CHT calculation for all the study cases. Several cycles are needed for convergence of the CFD, measured by the adjustment of the calculated pressure traces to the experimentally measured at IFPEN. This ensures that the injection and combustion parameters have been properly set.

For this step, the solid domain is not considered and the piston and cylinder head gas exposed surfaces are treated as isothermal walls with the temperatures indicated in Table 5.4. Moreover, since the metallic configuration is the baseline case for each operating point, the multiple-cycle CFD calibration was performed for these layouts.

For each operating condition, 6 engine cycles were calculated. The validation of the CFD of the metallic engine results was made by comparison with the experimental measurements of the pressure traces provided by IFPEN.

In Fig. 5.5 the simulated traces are compared with the experimental ones. It should be noted that with the combustion settings used in the simulations, the calculated pressure traces of the converged cycles are underestimated

with respect to the averaged experimental pressure. Further improvements might be achieved with better calibration, but this would be computationally very time-consuming. Considering that the numerical pressure traces of the converged cycles of the multicycle calculation fit within the experimental dispersion, it was decided to do the CHT calculation with these combustion settings.

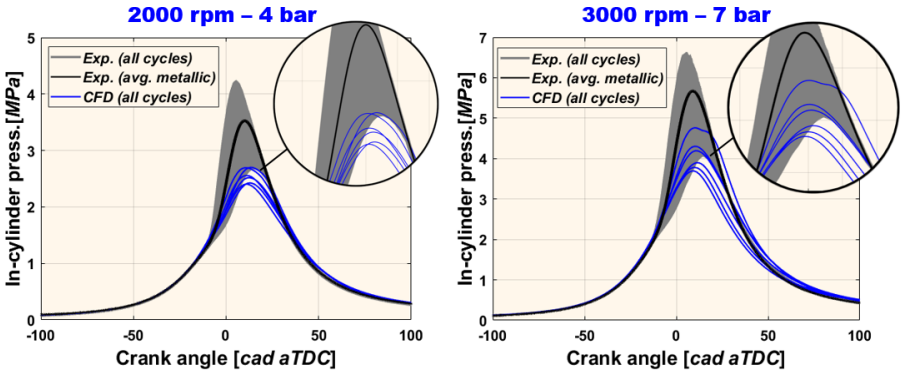

Figure 5.5: *CFD Calculated in-cylinder pressure traces for metallic and coated engines compared to experimental measurements for metallic engine at 2000 rpm-4 bar (left) and 3000 rpm -7 bar (right).*

In general the adjustment of the injection and combustion parameters is reasonably good for both operating conditions. However, for the operation point 2000 rpm - 4 bar the pressure traces are closer to the lowest experimental measured pressure.

5.4.1. CFD-CHT Validation

As explained previously, the same CFD settings are used for combustion process in the CHT calculations. Though the settings are tuned for the metallic engine configuration, they are assumed to remain unchanged for the coated configurations. In reality the coating affects the combustion process also, but the pressure traces measured at IFPEN for both the aluminium and coated engines are practically identical, with less than 1 bar difference in peak pressure (see Fig. 5.6) for both operating points.

The first step in the CFD-CHT calculations is to ensure adequate convergence of the cycles by comparing the pressure traces with the experimentally measured ones provided by IFPEN. Again, the calculated pressure traces fit within the experimental dispersion.

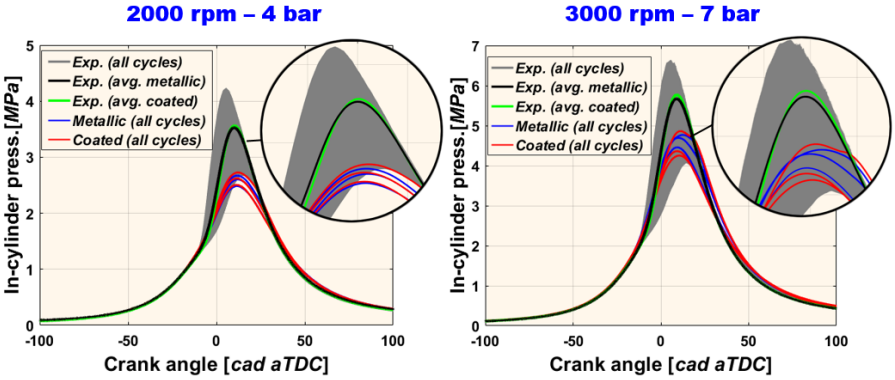

Figure 5.6: *CHT Calculated in-cylinder pressure traces for metallic and coated engines compared to experimental measurements for metallic engine at 2000 rpm-4 bar (left) and 3000 rpm -7 bar (right).*

Fig. 5.6 shows the in-cylinder pressure traces obtained with the CFD-CHT simulations of both engine configurations (metallic and coated) and for both operation conditions. They are compared with the experimental data of the engine provided by IFPEN for the two operating points.

- **Operation condition 2000 rpm-4 bar**

  Fig. 5.6(left) shows the last three converged cycles (all in all seven cycles were needed) calculated for each configuration (coated and uncoated). All the simulated cycles are close to the lower values of the experimental cyclic dispersion of the engine. The maximum dispersion at peak firing over the 300 experimental cycles performed is $+2\sigma = 4.8$ bar. The differences observed between the metallic and coated engines are in the same order of magnitude as the experimental values, about 1-2.5 bar. Clearly, the coating has little influence on the pressure traces, as is also observed experimentally.

- **Operation condition 3000 rpm-7 bar**

  Seven cycles were performed for this operation point, and the last three converged cycles are displayed in the Fig. 5.6(right). In this case, all the simulated cycles fit within the experimental cyclic dispersion of the engine. The maximum dispersion at peak firing over 300 cycles is $+2\sigma = 9.2$ bar. The differences observed between the metallic and coated engines are also relatively small, about 2-5 bar. It seems that the coating slightly affects the pressure traces.

In general, the traces for both operating points are closer to the lowest pressure trace measured experimentally. This may indicate that the combustion parameters would need additional tuning and would require some more iterations. In fact, difficulties were encountered to fit the combustion process. However, gasoline engines have a large cyclic dispersion as shown in Fig. 5.6, and the experimental averaged in-cylinder pressure trace is based on 300 measured cycles. Numerically, it is not realistic to calculate 300 cycles, so that it was considered that the combustion model parameters were well adjusted when the last three converged cycles were within the experimental cyclic dispersion. The maximum difference between the average experimental in-cylinder pressures and the calculated ones (3 converged cycles) is of the order of 10 bar for both operating points, while the cyclic dispersion itself is about 20 bar.

5.4.2. Combustion velocity

Fig. 5.7 presents the RoHR and the rate of burned fuel mass comparison for both engine configurations at the two operating conditions. The curves are the averages for the converged cycles.

For the low load operating point (2000 rpm – 4 bar) there are no significant changes in the slope of the rate of heat release that indicate that knock may appear in both engine configurations. Even that it was not possible to obtain a better tuning of the combustion model for this case within the limits of reasonable changes, it has to be stated that knock was not observed experimentally neither. Moreover, the traces of the fuel burned mass indicate a similar behavior for both configurations. However, the figure shows that the fuel is burning slightly faster in the coated case.

At 3000 rpm – 7 bar the rate of heat release for the coated case is very similar to the uncoated result, with a slightly lower maximum value. Contrary to the previous point, the average fuel burning rate of the converged simulated cycles is higher for the metallic engine. This may explain that in two of the cycles the in-cylinder pressure is higher for the metallic engine. This tendency was also observed in the engine high load condition [134], where the combustion process was calculated without CHT. However, the difference in maximum RoHR is of the order of 2%, and considering that there are uncertainties linked to the numerical calculations and to the cyclic dispersion, it is difficult to conclude.

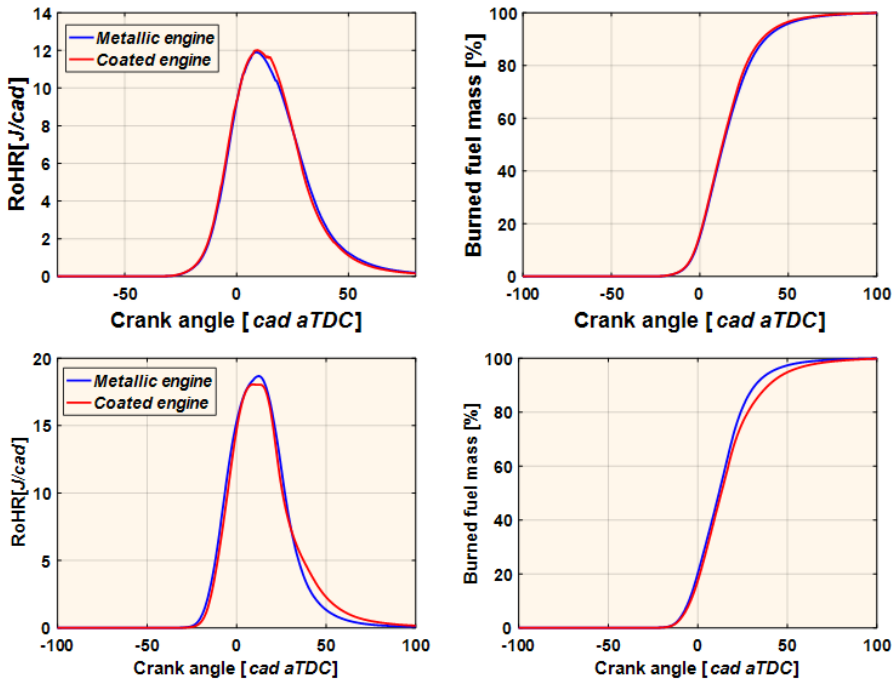

Figure 5.7: *Rate of heat release (left) and burned fuel mass (right) comparison between metallic and coated engines at 2000 rpm-4 bar (top) and 3000 rpm -7 bar (bottom).*

5.5. Results of heat transfer analysis

This section presents an in-depth analysis of the heat transfer in the combustion chamber in order to evaluate the effect of applying a thermal coating on gas exposed surfaces. Therefore, the spatial temperature distribution, the temporal temperature evolution and the heat balance are evaluated.

5.5.1. Wall temperature swing

The evolution of the average wall temperatures during the engine cycle is displayed in Fig. 5.8 for the CHT calculated surfaces. Note that the average is made only with the converged cycles values. In the same plot the results are also compared with the results obtained with the 1D Heat Transfer Model

(1DHTM) using as inputs the gas temperatures and heat transfer coefficients (HTC) from the CHT calculations. Though there are some differences, the CHT calculations reproduce the wall temperature swing in all configurations. As expected, the surface temperature swings on the insulated piston and cylinder head are both higher due to the application of the coating.

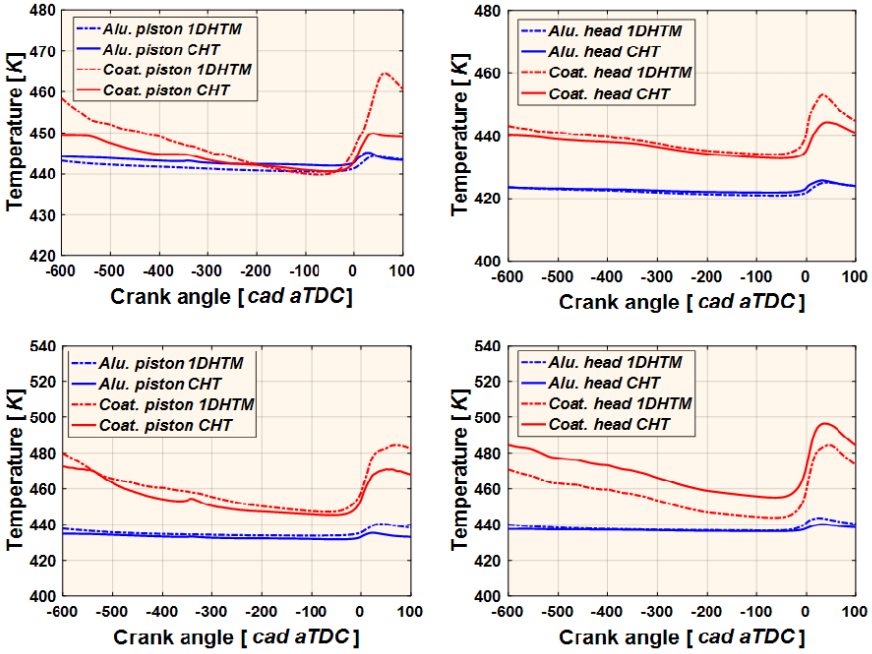

Figure 5.8: *Temporal evolution of wall temperature for the piston (left) and cylinder head (right) at 2000 rpm - 4 bar (top) and 3000 rpm - 7 bar (bottom).*

Operation condition 2000 rpm-4 bar

- For both configurations the average temperature level and evolution on the piston surface calculated with the CHT are similar to the ones predicted by the 1DHTM, including the maximum temperature. As expected, significant differences are not observed in the metallic configuration between both models due to the high capacitance of the aluminium. The differences in temperature between the CHT and the 1DHTM simulations during the whole cycle for the coated piston are about 3.1% for the maximum temperature value and -0.1% for the minimum temperature.

- The traces for the cylinder head follow the same tendency with both models in the metallic configuration. However, differences in the coated configuration of about 2% for the maximum temperature value and 0.3% for the minimum temperature are observed.
- The maximum of the averaged temperature swings on the piston and cylinder head surfaces are listed in Table 5.7. It seems that the maximum swing is obtained on the coated head surface, though the CHT seems to under-predict the wall temperature swing with respect to the 1DHTM.
- The peak wall temperature of the piston calculated with the CHT approach is reached earlier that the one calculated with the 1DHTM (about 37 cad) in both configurations. For the cylinder head, the peak wall temperature is reached almost at the same time (40 cad). The delay between both model is about 5 cad and it may be related with the one-dimensional assumption of the 1DHTM.

Table 5.7: *Thermal gradient on the gas exposed surfaces at 2000 rpm - 4 bar.*

Engine surface	Max. temperature swing predicted by 1D HTM [K]	Max. averaged temperature swing predicted by CHT [K]
Aluminium piston	3.7	3.1
Coated piston	24.6	9.4
Aluminium head	4.3	3.8
Coated head	19.0	11.5

Operation condition 3000 rpm -7 bar

- As for the previous point, the average temperature level and evolution on the piston surface calculated with the CHT are similar to the ones predicted by the 1D HTM, although the CHT approach tends to predict lower maximum temperature in the coated configuration (about 10 K, representing 2.4% in the case of the piston).
- The traces for the cylinder head follow the same tendency with both models. For this surface the difference between the models is slightly larger along the cycle, by about 3%.
- The maximum temperature swings on the surfaces are listed in Table 5.8. As for the previous point, the temperature swing is larger on the coated cylinder head surface than on the coated piston surface.

- Also, in this case, the average temperature of the coated surfaces is hotter by about 10 to 15 K respect to the metallic surfaces.
- The instant of the peak wall temperature follows the same tendency as the previous operations point. In the CHT calculations the peak is reached earlier (about 60 cad) that the one calculated with the 1DHTM with about 5 cad of delay, while for the cylinder head the traces are almost in phase (41 cad).

Table 5.8: *Thermal gradient on the gas exposed surfaces at 3000 rpm - 7 bar.*

Engine surface	Max. temperature swing predicted by 1D HTM [K]	Max. averaged temperature swing predicted by CHT [K]
Aluminium piston	6.4	3.6
Coated piston	37.3	27.7
Aluminium head	6.9	3.8
Coated head	40.8	35.6

5.5.2. Wall temperature distribution on piston

As seen in Fig. 5.9, which shows the temperature spatial distribution over the solid piston at 10 cad aTDC, higher wall temperatures are reached for the coated piston. For both configurations (aluminium and coated) the piston top is the hottest surface at the two operation conditions, as is expected, considering that this surface is directly exposed to the hot combustion gas. Also remarkable is that for the aluminium piston, the temperature gradient is mostly axial, the coolest part being naturally the piston oil cavity, which is in direct contact with the cooling oil. For the coated piston, there is clearly some radial temperature gradient also, meaning that some radial heat transfer takes place, which would not be taken into account by the 1D HTM model.

More details are given in Fig. 5.10 and Fig. 5.11, which display the spatial temperature distributions on the piston surface exposed to the gas for the metallic and the coated engine for the two operation conditions, at three different crank angles of the combustion phase.

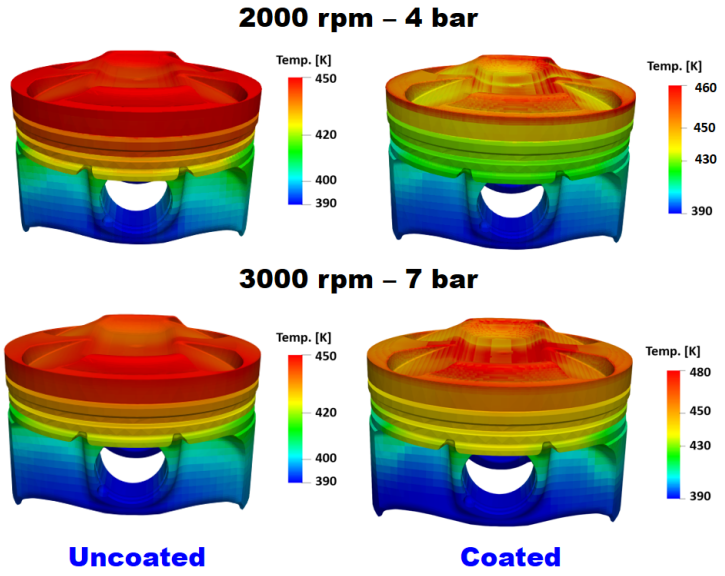

Figure 5.9: *Temperature wall distribution in the solid piston (10 CAD) at 2000 rpm-4 bar (top) and 3000 rpm -7 bar (bottom).*

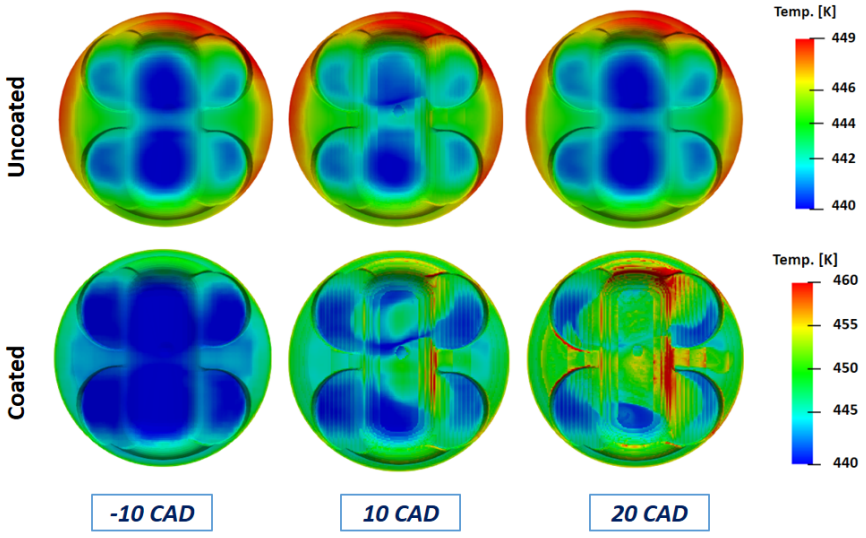

Figure 5.10: *Temperature distribution on top piston surface during the combustion at 2000 rpm - 4 bar: uncoated engine (top) and coated engine (bottom).*

Operation condition 2000 rpm - 4 bar (Fig. 5.10)

- The hottest spots are located in the periphery of the piston for both engine configurations. However, at 20 cad aTDC the center of the piston is hotter in the coated configuration.
- The maximum thermal gradient on the aluminium piston top surface is about 9 K, while for the coated piston it is about 20 K (at 20 cad), as indicated by the colour scale. However, it is to be noted that this may be larger between 20 cad and 50 cad, since the maximum peak temperature is reached at 38 cad.
- For the aluminium engine, there are hardly any differences between the three instants plotted, in agreement with the very low temperature swing observed in Fig. 5.8.
- For the coated engine configuration instead, the three snapshots show the quick response of the material (temperature swing). The peak mean temperature snapshot, which would be at 38 cad is not shown here because the storage limitation of the cluster.
- In both configurations, there are some asymmetries in the temperature distribution, of just 4K in the aluminium case (red and green), larger (about 10 K) for the coated engine at 10 cad. This will be explained later by the asymmetries in the gas temperature distribution in the combustion chamber.
- These asymmetries are more clearly visible at 20 cad for the coated engine, where temperature values are higher.

Operation condition 3000 rpm - 7 bar (Fig. 5.11)

- For both configurations, the hottest area on the piston surface is located in the lower part, probably due to the non-uniform progress of the flame front.
- The maximum thermal gradient on the aluminium piston top surface is about 20 K at 20 cad, while for the coated piston it is about 80 K at the same instant.
- As for the previous point there are hardly any differences between the three instants plotted for the aluminium engine, in agreement with the very low temperature swing observed in Fig. 5.8.
- The snapshot of the coated engine at 20 cad shows an average temperature close to the mean peak temperature (61 cad).

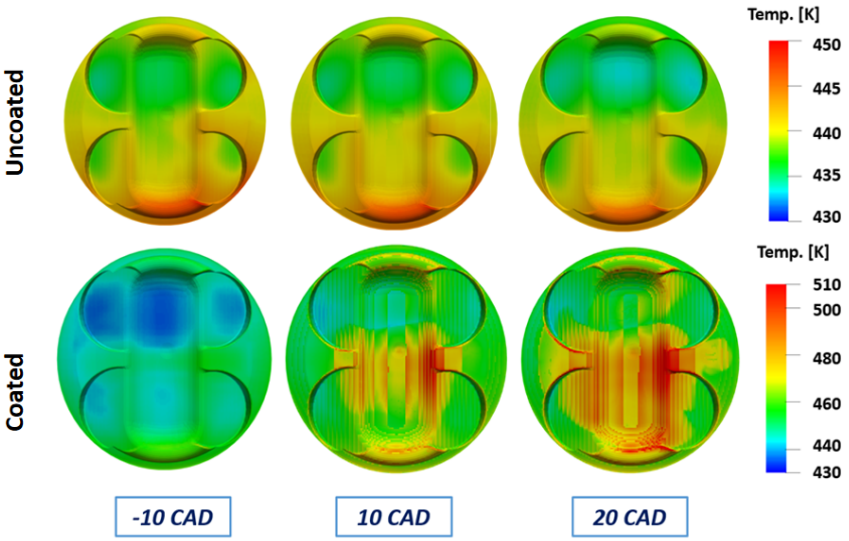

Figure 5.11: *Temperature distribution on top piston surface during the combustion at 3000 rpm - 7 bar: uncoated engine (top) and coated engine (bottom).*

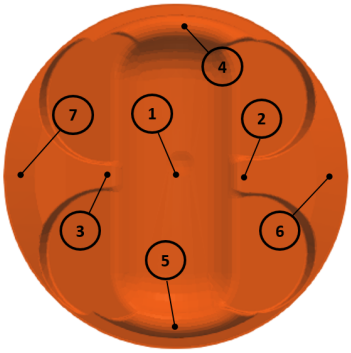

Figure 5.12: *Location of the monitor points on solid piston.*

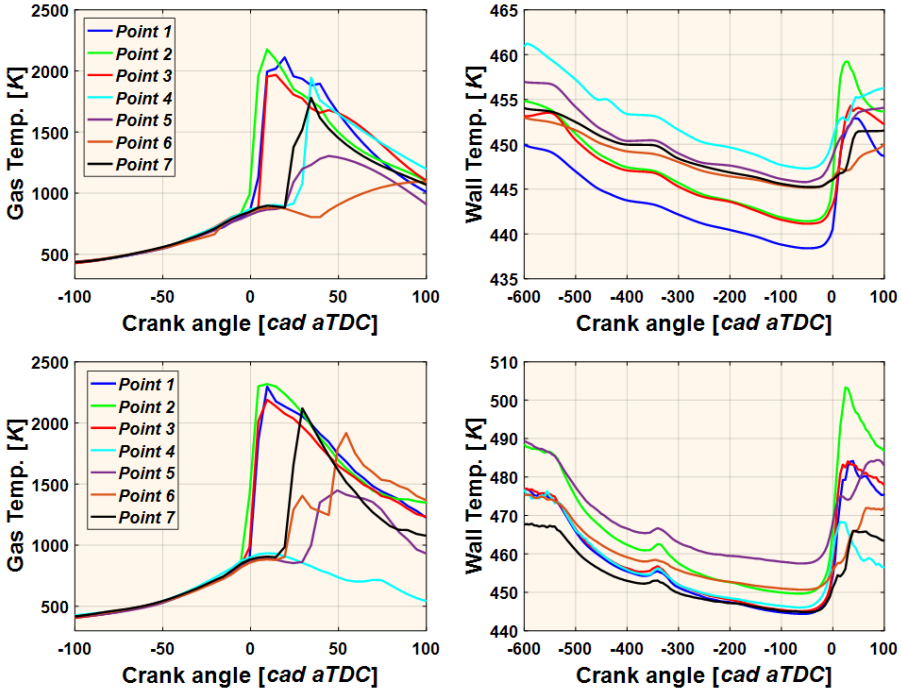

Figure 5.13: *Close-up of the near-wall gas temperature evolution and top surface temperature evolution at some spatially located points for the coated piston at 2000 rpm - 4 bar and 3000 rpm -7 bar.*

In order to complete the wall temperature study of the coated piston top surface, seven monitor points have been selected. The location of the points is indicated in Fig. 5.12. Furthermore, Fig. 5.13 shows the temperature evolution at the monitor points on the piston surface that can be correlated to the gas temperature evolution at the same locations.

According to Fig. 5.13, the points 1 (piston centre), 2 and 3 located in the middle of the top surface reach their maximum temperature at around 20 cad, while the temperature of the points located at the periphery culminates later, at about 40 to 50 cad. This shift can be correlated to the shift in gas temperature close to the wall: indeed, the gas temperature close to the central points 1, 2 and 3 reaches its maximum sooner (at between 5 cad and 10 cad) than the gas at the periphery (at between 20 cad and 60 cad). As may be expected, the time lag is larger for the solid response due to the inertia of the wall.

The figure allows deducing that the flame propagation is not uniform, since at the same cad, the various points have different temperatures, with significant variations, e.g. at 45 cad, point 4 on the top periphery has about 500 K of difference with the point 5 right opposite at the bottom periphery (hotter at 2000 rpm - 4 bar and cooler at 3000 rpm - 7 bar). This is naturally transferred to the wall temperature:

- At 2000 rpm - 4 bar at point 5 the temperature is 3 K cooler than at point 4 at about 60 cad
- At 3000 rpm - 7 bar at point 5 the temperature is 20 K hotter than at point 4 at about 60 cad

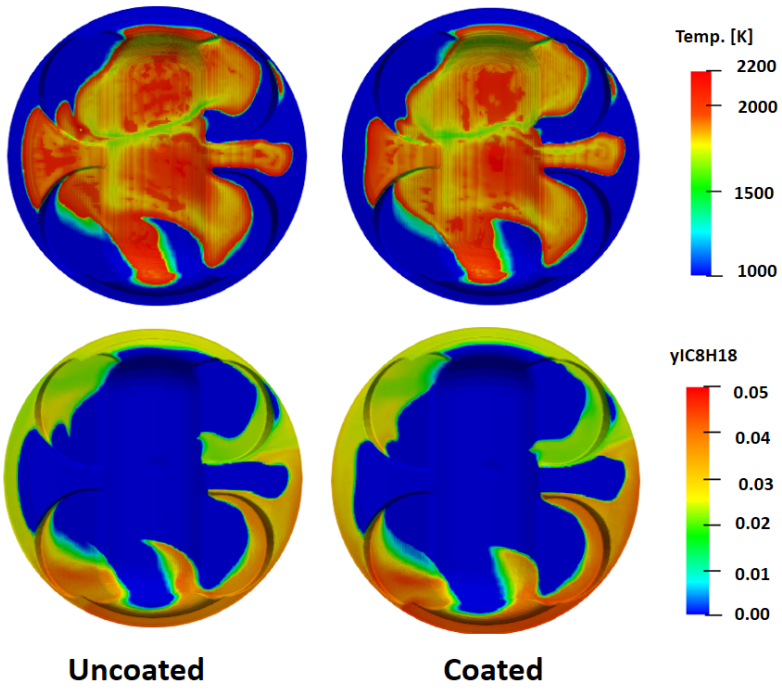

Figure 5.14: *Gas temperature field (top) close to piston top surface and burned mass fuel fraction (bottom) at 2000 rpm - 4 bar at 20 CAD: uncoated piston (left) and coated piston (right).*

Figures 5.14 and 5.15 further illustrate the non-uniformity of the gas temperature field close to the coated piston surface at 20 cad and for both operation conditions of the engine. The gas temperature follows the burned gases distribution and shows that the combustion takes longer to extend to the periphery.

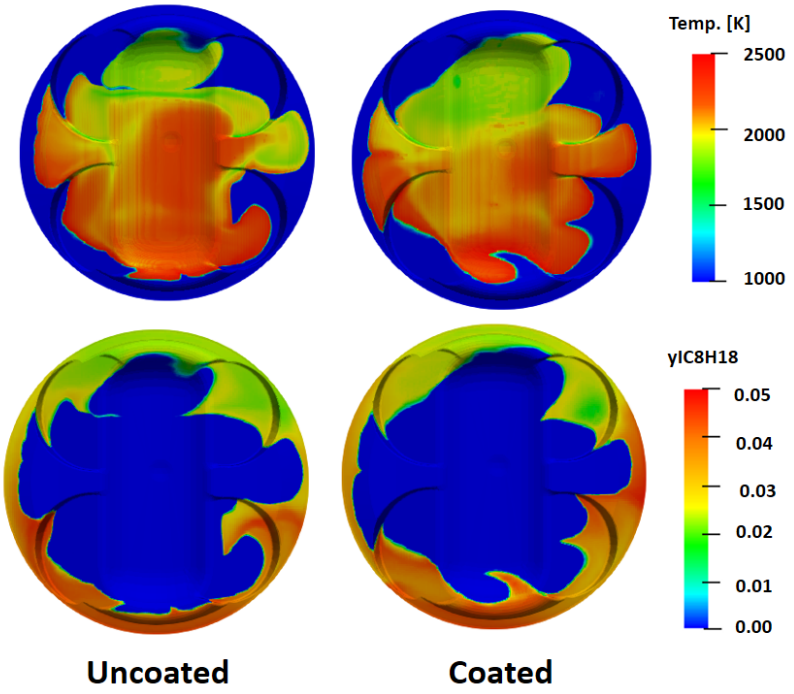

Figure 5.15: *Gas temperature field (top) close to piston top surface and burned mass fuel fraction (bottom) at 3000 rpm - 7 bar at 20 CAD: uncoated piston (left) and coated piston (right).*

5.5.3. Wall temperature distribution on cylinder head

Fig. 5.16 and Fig. 5.17 show the wall temperature distribution on the cylinder head at various crank angles during combustion. The hottest spots are located at the centre of the wall for both operation conditions, while the periphery remains cooler. The effect of the flame front propagation is amplified with the coating layer. Additional comments about the figures follow below.

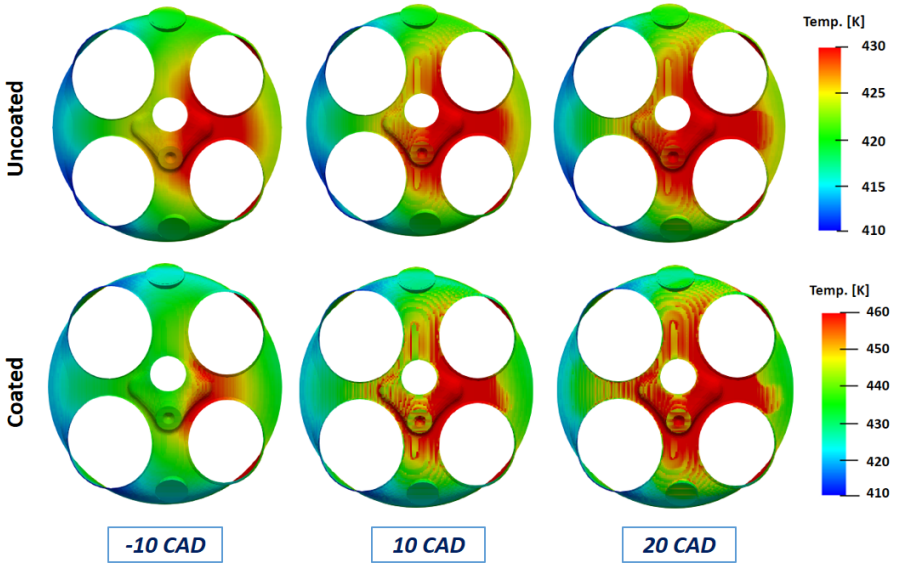

Figure 5.16: *Temperature distribution on top piston surface during the combustion at 2000 rpm - 4 bar: uncoated engine (top) and coated engine (bottom). Intake valves at the left side and exhaust valves at the right side of the cylinder head.*

Operation condition 2000 rpm - 4 bar (Fig. 5.16)

- The hottest spots are located at the centre of the wall, while the periphery remains cooler.
- The maximum thermal gradient on the coated surface is about 50 K, which is about double of the gradient observed on the piston surface.
- Rapid warming of the surface is observed as combustion develops and as is expected from the temperature swing shown in Fig. 5.8.
- The spatial temperature distribution shows that the surface is hotter around the exhaust valves ports.

Operation condition 3000 rpm - 7 bar (Fig. 5.17)

- The hottest spots are again located around the central area of the wall, while the periphery remains cooler.
- As expected, the maximum thermal gradient in the uncoated cylinder head is small (35 K) compared to that of the coated one (80 K).
- The maximum thermal gradient in the coated configuration is about 80 K.

- As happened also on the piston surface, the temperature distribution on the metallic cylinder head does not change much between -10 cad and 20 cad, while the warm-up is clearly visible for the coated cylinder head.
- Also, in the coated configuration, a clear asymmetry of the temperature distribution is also visible, as in the case of the 2000 rpm – 4 bar point.

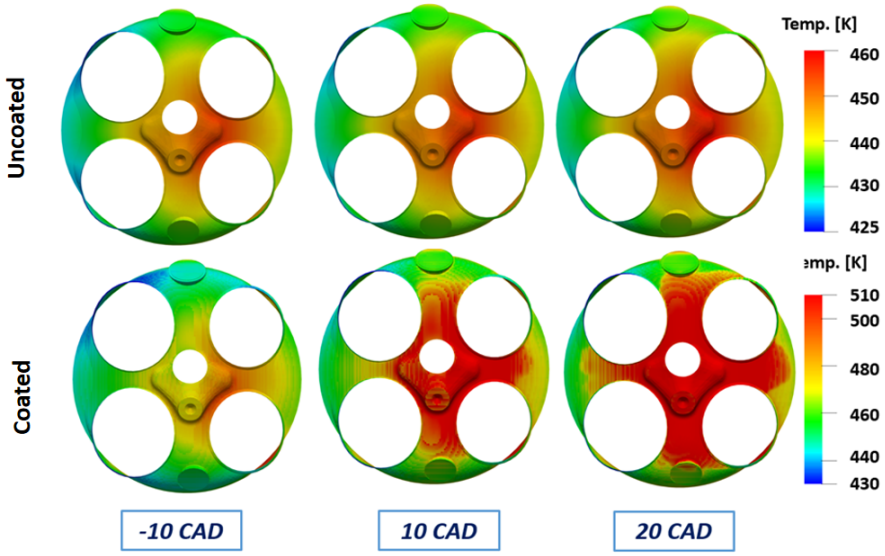

Figure 5.17: *Temperature distribution on top piston surface during the combustion at 3000 rpm - 7 bar: uncoated engine (top) and coated engine (bottom). Intake valves at the left side and exhaust valves at the right side of the cylinder head.*

Figures 5.18 and 5.19 further illustrate the non-uniformity of the gas temperature field close to the coated cylinder head surface at 20 cad and for both operation conditions. The gas temperature follows the burned gases distribution and shows that the asymmetry observed in the surface temperature distribution is explained by the non-uniform flame front propagation. The gas is also hotter on the exhaust valves side (right of cylinder head in figure).

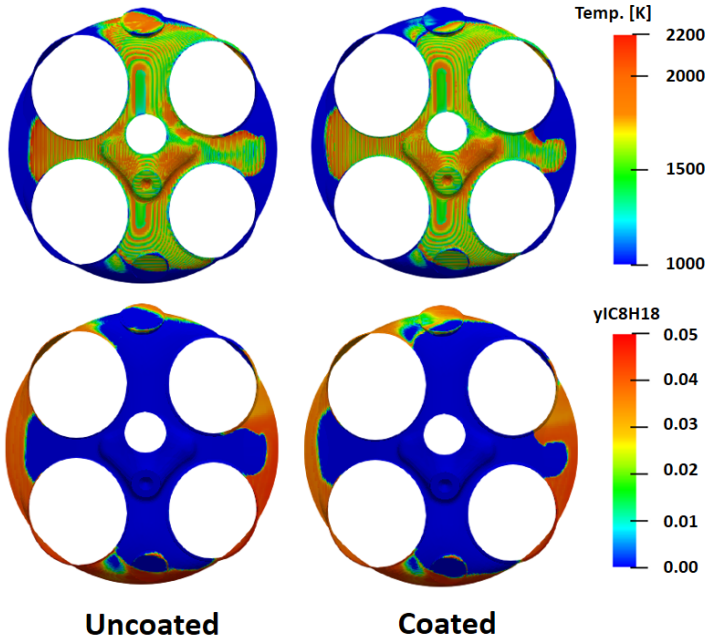

Figure 5.18: *Gas temperature field (top) close to cylinder head gas exposed surface and burned mass fuel fraction (bottom) at 2000 rpm - 4 bar at 20 CAD: uncoated piston (left) and coated piston (right).*

The flame front propagation for the two operating points seems quite similar in the two configurations (metallic and coated engine). However, in Figs. 5.14, 5.15, 5.18 and 5.19 it is difficult to observe possible differences. In order to determine a possible effect of the coating on the combustion, the flame fronts of the two configurations have been overlapped on the same snapshot (Figs. 5.20 and 5.21).

Fig. 5.20 shows that at 2000 rpm - 4 bar the shape of the flame is very similar on piston and cylinder head. On the other hand, Fig. 5.21 shows that at 3000 rpm - 7 bar in the coated configuration the flame takes longer to extend along the gas exposed surfaces and confirms what is shown in Fig. 5.7. Nonetheless, due to the cyclic dispersion in SI engines and the properties of the coating employed for the coated engine configuration, it is not possible to confirm if there is an impact of the coating on the flame front propagation.

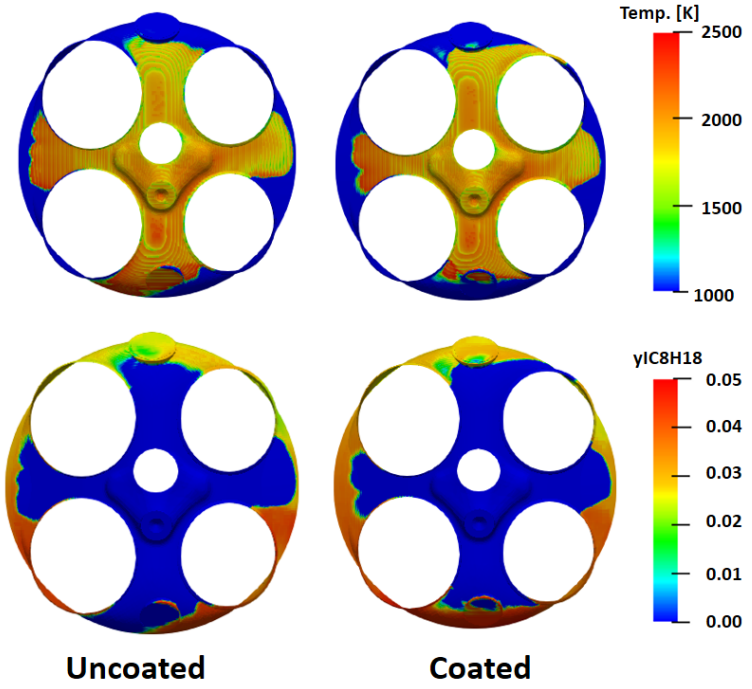

Figure 5.19: *Gas temperature field (top) close to cylinder head gas exposed surface and burned mass fuel fraction (bottom) at 3000 rpm - 7 bar at 20 CAD: uncoated piston (left) and coated piston (right).*

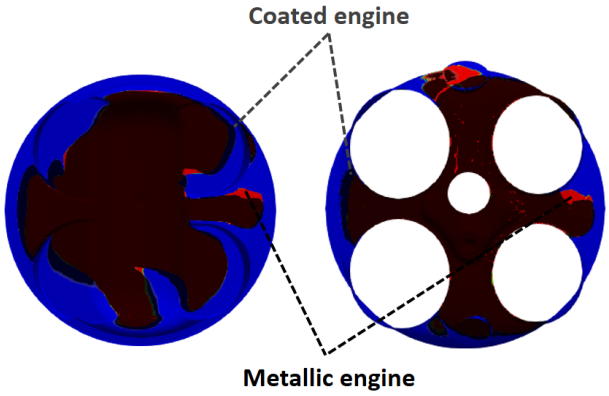

Figure 5.20: *Flame front propagation at the gas exposed surfaces at 2000 rpm - 4 bar on the top piston (left) and cylinder head (right): flame front propagation in the metallic engine (red color) and in the coated engine (black color).*

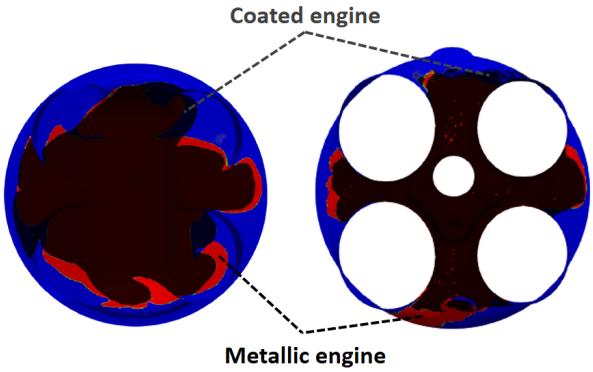

Figure 5.21: *Flame front propagation at the gas exposed surfaces at 3000 rpm - 7 bar on the top piston (left) and cylinder head (right): flame front propagation in the metallic engine (red color) and in the coated engine (black color).*

5.6. Heat transfer balance

Fig. 5.22 compares the amount of heat transferred through each of the combustion chamber walls for the metallic and coated engines. Most of the heat is transferred through the cylinder head, also for the coated case. It is also interesting to note that the total heat transferred for the low load point is about 4.5% higher than for the high load point for the metallic engine, slightly more for the coated engine (7.4%). The heat transfer balance is quantified in Table 5.9 and Table 5.10 for the two operation points.

Operation condition 2000 rpm - 4 bar

At 2000 rpm – 4 bar the heat transferred to the coated piston wall is the same as to the aluminium piston. On the other hand, though it seems that the heat transferred to the coated cylinder head has decreased by about -0.7% with respect to the metallic engine case. The balance shows a similar heat transferred through the liner and the piston. Looking into more detail at the heat transfer through the cylinder head surface, about 63% of it goes through the surface itself, while 37% goes through the exhaust and intake valves, and this for both the coated and uncoated engines.

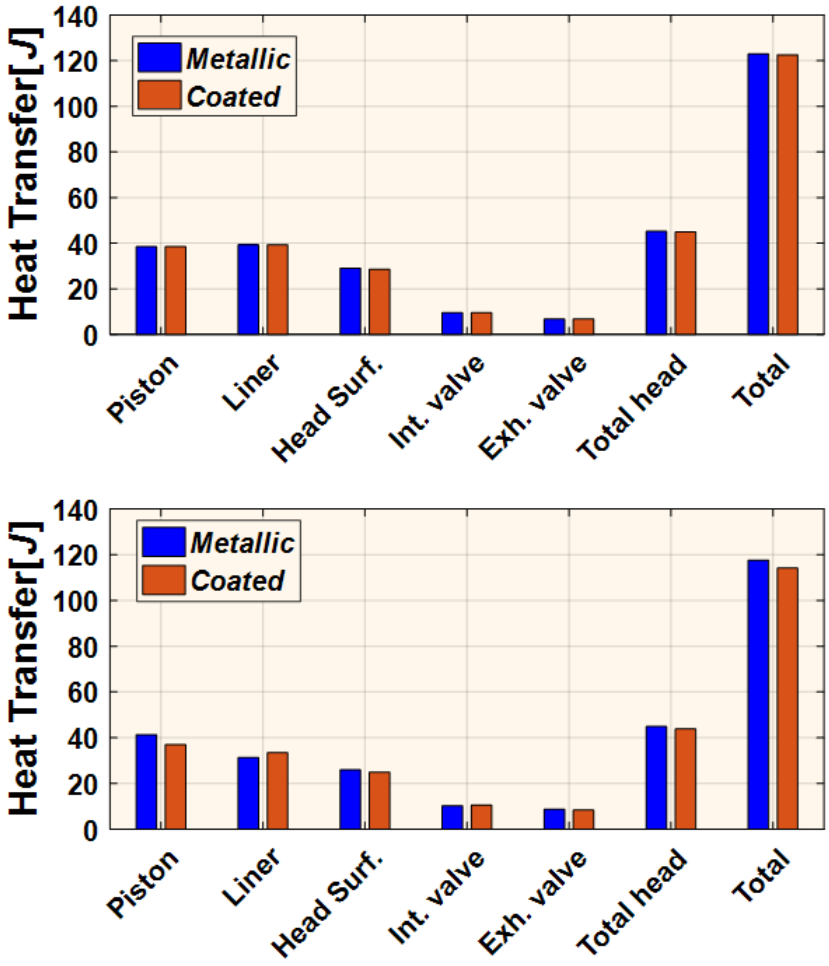

Figure 5.22: *Heat transfer balance: comparison between metallic (blue bars) and coated engines (orange bars) at 2000 rpm-4 bar (top) and 3000 rpm -7 bar (bottom).*

Globally, the heat transferred to the walls of the combustion chamber wall is 0.3% lower for the coated engine. According to this results, the coating has no significant impact on the total heat transfer of the engine at low load operation condition.

Table 5.9: *Heat transfer in the combustion chamber at 2000 rpm - 4 bar.*

Engine part	HT Metallic engine [J]	Coated engine [J]	Difference [%]
Piston	38.4	38.4	0
Head surface	29.0	28.6	-1.6
Intake valves	9.4	9.5	0.8
Exhaust valves	6.7	6.8	1.0
Total cylinder head	45.2	44.9	-0.7
Liner	39.3	39.3	-0.1
Total engine HT	122.9	122.6	-0.3

Operation condition 3000 rpm - 7 bar

For the operation point at 3000 rpm – 7 bar, the balance is very different: there is a reduction of 10.7% and 2.5% in the heat transferred to the coated piston and cylinder head respectively. As there is an increase of 6.4% through the liner wall, the total heat transfer through the combustion chamber walls decreases by almost 3%. The explanation for the largest reduction through the coated piston surface is probably due to two factors: first, the (physical) coating layer on the piston is thicker with respect to that on the cylinder head (see Table 4.1), and also there is less coated surface on the cylinder head, since no coating is applied on the valves. Even so, the detailed balance of heat transfer through the coated cylinder head does not differ significantly from that of the aluminium head. 57% of the cylinder heat transfer happens through the coated surface, while the rest (43%) leaves through the valves. This is practically the same balance as for the aluminium engine (58% versus 42%).

Table 5.10: *Heat transfer in the combustion chamber at 3000 rpm - 7 bar.*

Engine part	HT Metallic engine [J]	Coated engine [J]	Difference [%]
Piston	41.3	39.6	-10.7
Head surface	25.9	25.0	-3.5
Intake valves	10.2	10.5	2.9
Exhaust valves	8.7	8.4	-3.5
Total cylinder head	44.9	43.8	-2.5
Liner	31.4	33.4	6.4
Total engine HT	117.6	114.2	-2.9

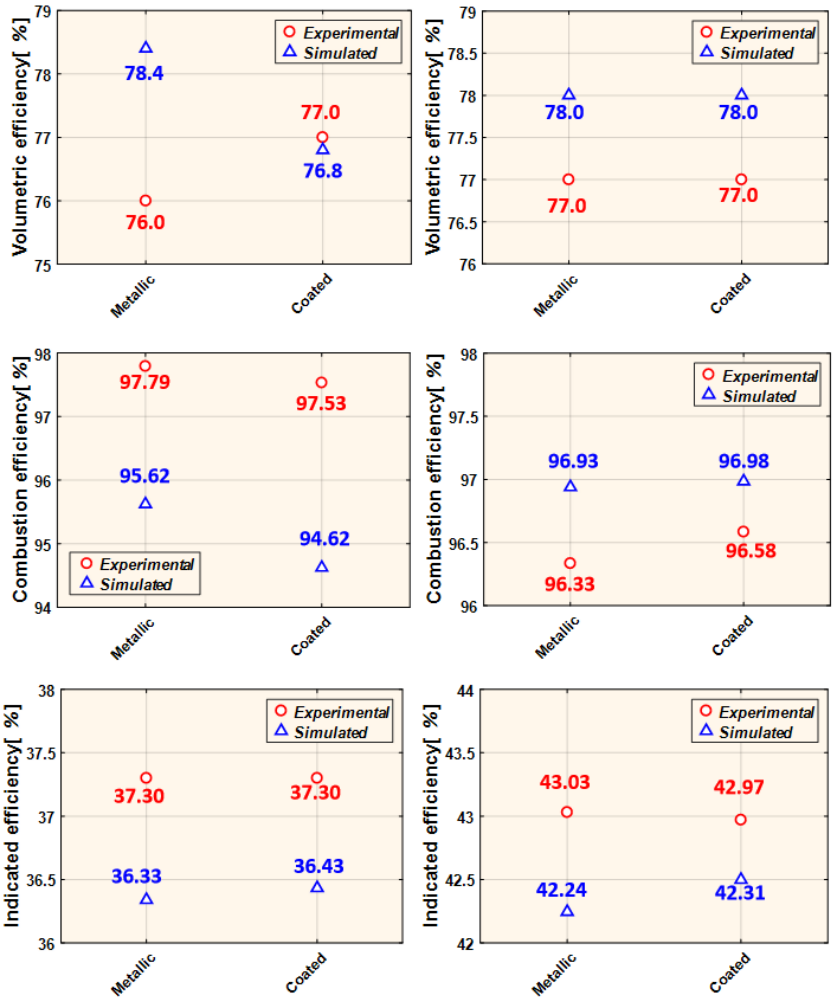

Figure 5.23: *Comparison between the metallic and coated engines. Volumetric, combustion and indicated efficiencies at 2000 rpm-4 bar (left) and 3000 rpm -7 bar (right).*

5.7. Impact of the coating on the engine efficiencies

The engine volumetric, combustion and indicated efficiencies for the metallic and coated engine configurations at both operating conditions are presented in Fig. 5.23. The numerical and experimental values were calculated with the following expressions:

- Volumetric efficiency

$$\eta_{\text{vol}} = \frac{m_{air}}{\rho \cdot V_T} \cdot 100 \tag{5.7.1}$$

where m_{air} is mass of trapped air in the combustion chamber at the IVC, ρ is the density of the air upstream and V_T is the maximum volume of the cylinder.

- Combustion efficiency

$$\eta_{\text{comb}} = \left(1 - \frac{m_{HC}}{m_{\text{fuel}}} - \frac{m_{CO}}{4 \cdot m_{\text{fuel}}}\right) \cdot 100 \tag{5.7.2}$$

where m_{HC} represents the mass of unburned, HC emissions, m_{CO} is the mass of CO and m_{fuel} is the injected mass fuel.

- Indicated efficiency

$$\eta_{\text{in}} = \frac{W}{m_{\text{fuel}} \cdot Cp} \cdot 100 \tag{5.7.3}$$

where W is the indicated work of the engine, and Cp is the calorific power of the fuel.

The experimental results provided by IFPEN are also plotted on Fig. 5.23. As may be observed, in terms of absolute values, the numerical results are in good agreement with the experimental measurements. However, the tendencies shown are different, as detailed below for each operation point, the problem being that the differences are so small, that they are in the range of measurements and calculation uncertainties.

Operation condition 2000 rpm - 4 bar

- The simulated volumetric efficiency decreases by 1.6 % in the coated configuration, while in the experimental test it is increasing by 1 %.
- By applying the coating layer on the piston and cylinder head there is a loss of 0.57% in the combustion efficiency. By comparison, the experimental tests show a slightly lower decrease of 0.26%.
- The CHT calculations predict a loss of 0.43% in indicated efficiency in the coated engine, while no impact of the coating has been observed experimentally.

Operation condition 3000 rpm - 7 bar

- Both experiments and calculations agree that there is no impact of the coating on the volumetric efficiency at this operation point.
- Contrary to what is observed for the low load point, the coating seems to provide a very low gain of 0.05% in the simulated combustion efficiency, significantly lower than the one resulting from the measurements (0.26%).
- In the experimental test the coating seems to induce a loss of 0.14% in indicated efficiency, while the CHT results predict a gain of 0.17%.

5.8. Fuel consumption and pollutant emissions

The measured and calculated values of isfc (indicated specific fuel consumption) are compared in the Table 5.11 in order to evaluate the possible effects of the coating on fuel consumption.

Table 5.11: *Fuel consumption for gasoline engine.*

2000 rpm - 4 bar			
	Metallic	Coated	Diff. [%]
Measured isfc $[g/kWh]$	232.7	238.5	2.5
Predicted isfc $[g/kWh]$	239.1	238.5	-0.3
3000 rpm - 7 bar			
	Metallic	Coated	Diff.
Measured isfc $[g/kWh]$	201.9	202.2	0.1
Predicted isfc $[g/kWh]$	205.6	204.4	-0.6

For the operating condition 2000 rpm – 4, the CHT calculations yielded isfc values similar to the experimental ones. However, it can be seen that with the coating the isfc increases by 2.5 % experimentally, while the simulations predict a slight reduction of 0.3%.

An increase in the isfc of about 0.1 % was determined experimentally in the coated configuration at 3000 rpm - 7 bar. In the CHT calculations, the coated walls led to a 0.6 % reduction in fuel consumption in this operating condition.

Finally, in tables 5.12, 5.13 and 5.14, the pollutant emissions for each operating point are analyzed:

Table 5.12: *Analysis of HC emissions for gasoline engine.*

2000 rpm - 4 bar			
	Metallic	Coated	Diff. [%]
Measured isHC $[g/kWh]$	7.0	7.8	11.4
Predicted isHC $[g/kWh]$	1.2	3.1	166
3000 rpm - 7 bar			
	Metallic	Coated	Diff.
Measured isHC $[g/kWh]$	6.8	6.2	-8.8
Predicted isHC $[g/kWh]$	5.2	4.7	-9.6

Table 5.13: *Analysis of CO emissions for gasoline engine.*

2000 rpm - 4 bar			
	Metallic	Coated	Diff. [%]
Measured isCO $[g/kWh]$	2.9	3.2	10.3
Predicted isCO $[g/kWh]$	36.9	48.7	32.0
3000 rpm - 7 bar			
	Metallic	Coated	Diff.
Measured isCO $[g/kWh]$	2.4	2.7	12.5
Predicted isCO $[g/kWh]$	5.2	4.7	-9.6

Table 5.14: *Analysis of NO_x emissions for gasoline engine.*

2000 rpm - 4 bar			
	Metallic	Coated	Diff. [%]
Measured isNO_x [g/kWh]	16.0	19.4	21.3
Predicted isNO_x [g/kWh]	3.4	2.5	-26.5
3000 rpm - 7 bar			
	Metallic	Coated	Diff.
Measured isNO_x [g/kWh]	14.5	13.5	-6.9
Predicted isNO_x [g/kWh]	12.0	11.9	-0.8

Operation condition 2000 rpm - 4 bar

- Both experimental and numerical results show that the coating increases HC emissions. According to the measurements, this increase is 11.4 %, while in the calculations the values are tripled with respect to the metallic one.
- The application of the coating seems to increase CO emissions in the gasoline engine. Experimentally this increase is 10.3 % and numerically it is 32 %.
- NOx emissions increase by 21.3 % experimentally. On the other hand, CHT calculations show a reduction of -26.5%.

Clearly, the predicted emissions values show a significant deviation at 2000 rpm -4 bar, which may be related to the fact that in the CFD the fuel converted in energy is less than the experimental one as shown in Fig. 5.23, with differences of about 2%.

Operation condition 3000 rpm - 7 bar

- The HC emissions calculated with the CHT are similar to the values measured on the physical engine. Experimentally, a reduction of 8.8% was observed due to the effect of the coating. In the CHT calculations this reduction was 9.6%.
- The calculated CO emissions double those measured in the engine. Experimentally, an increase of 12.5% was found with the coating, while in the CHT calculations the application of coating reduced by 9.6% the CO emissions.

- A reduction in NOx emissions as consequence of the coating was found in both cases, experimentally and numerically. In the first case the reduction was 6.9% and in the CHT calculations it was 0.8%.

Due to the important computational resources needed to perform the CHT simulations, especially at low speed, the calculation of emissions was not considered a priority for the combustion calibration. However, at 3000 rpm - 7 bar the calculated HC and CO emissions are in agreement with the experimental data. Regarding NOx emissions, the simulations predicted a reduction for the coated configuration greater than the experiments by 6.1%. This differences could be associated with the difficulty to calibrate the engine keeping exactly the same conditions in both engine configurations.

5.9. Summary

This chapter presents the engine full cycle CFD-CHT calculations performed to assess the impact on engine performance of coating the piston top surface and the cylinder head. The methodology, validation and results are thoroughly described. In particular, a complete heat transfer analysis is made and the heat losses through the walls of the engine combustion chamber are assessed for the whole engine cycle. This study has been performed with the commercial software CONVERGE and the main conclusions of the CHT calculations may be summarized as follows:

- The first step was to perform a CFD calculation of the conventional metallic engine (without coating insulation) for two operation conditions: low load operating point (2000 rpm, 4 bar IMEP, $=1.2$) and medium load operation point (3000 rpm, 7 bar, $=1.4$) to validate the combustion settings.
- Once validated, the same cases were calculated with the CHT model for two engine configurations: uncoated and coated engine. In the two operation points, the CHT approach was applied to both the piston and the cylinder head. The analysis of the results has allowed evaluating the impact of the coating on the heat losses and engine efficiencies.
- The validation of the temperature swing has been carried out by comparing the mean wall temperature on the combustion gas exposed surface of the piston with the mean temperature obtained with a well-validated 1D heat transfer model. Though both models are obviously very different in nature, the CHT calculated temporal evolution of the piston wall temperature follows a very similar tendency to that

obtained with the 1D model. Furthermore, the average temperature level throughout the engine cycle shows only 1% maximum difference between both models in the metallic engine configuration. However, this differences are higher in the coated configuration, with maximum differences of the order 3%.

- The CHT simulations have provided very useful information concerning the local heat transfer through the walls of the solid parts, as well as the temporal evolution and spatial distribution of the surfaces temperatures. In particular, they have clearly shown that that there is some radial heat transfer that is never taken into account by 0D-1D models, nor in combustion CFD calculations, and this affects the surface temperature distribution. This effect is more visible for the coated engine. This in turn has an impact on the combustion process that is not seen with isothermal CFD calculations. Asymmetries have been observed in the spatial temperature, more obvious on the coated piston surface, but also on the cylinder head at both operation points. These seem to be related to the non-uniform advance of the flame front, and to the presence of hotter gas in the vicinity of the exhaust pipes.
- The coating plays its role, in the sense that the insulation ensures that the wall follows the trend of the gas temperature temporal evolution in the combustion chamber (temperature swing), which the metallic piston hardly does. This has some impact on the heat losses: at 3000 rpm - 7 bar, there is a reduction of about 3%, though this tendency is not confirmed for the 2000 rpm – 4 bar case. However, the coating seems to have either practically no effect or a negative impact on volumetric and combustion efficiencies. In the case of the indicated efficiencies, a gain of 0.10% is predicted for the low load point, while a very slight gain of 0.17% is predicted for the other point. The calculated efficiencies agree quantitatively very closely with the experimental values provided by IFPEN, but not always in terms of tendencies. The major problem is that the differences are so small, that they are in the range of measurements and calculation uncertainties.
- The CHT calculations yield very good results in terms of engine performance during the whole engine cycle. However, it is important to remark that it is necessary to set suitable boundary conditions on the solid regions, since they have a high impact on the temperature distribution in the solid parts of the engine.

- A maximum increase of 2.5% in fuel consumption was obtained experimentally, while the CHT simulations predicted a maximum reduction of about 0.6% at 3000 rpm- 7 bar. In terms of emissions, the results for 3000 rpm - 7 bar are in agreement with the experimental values. At 2000 rpm - 4 bar there are important differences that could be related to the less efficient combustion of the CHT as the combustion model was not calibrated for emissions prediction.

5.A. Appendix: Mesh independence study for the SI engine

In order to find the best mesh for the CFD-CHT simulations in the SI engine, the base grid size of the mesh was varied from 4 - 2 mm in the CFD computational domain. Fig. 5.24 shows that the in-cylinder pressure fits with the experimental dispersion of the engine when the base grid size is 2 mm. Clearly, a higher base grid size does not allow to reproduce properly the combustion process. Thus, for the CHT calculations on the SI engine a base cell size of 2 mm was employed.

Since the calculations times in higher regimes are shorter, the mesh convergence is presented for the medium load operation point (3000 rpm - 7 bar).

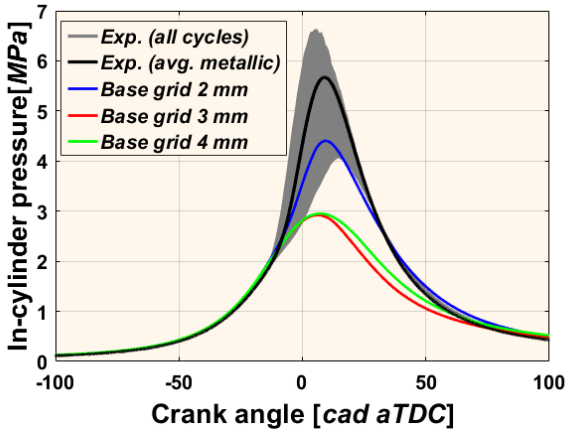

Figure 5.24: *Mesh independence study to define the base grid size for the CHT calculations on the SI engine. Operation point 3000 rpm - 7 bar.*

5.B. Appendix: Solid domain convergence

The CONVERGE supercycle approach has been used to solve the solid domain in the CHT simulations. This methodology aims to significantly reduce the solid convergence time, as explained in Chapter 3.

In this regard, for the convergence of the solid the temperature of the gas exposed surfaces in the combustion chamber was considered as a criterion. Fig. 5.25 shows that after 2989.4 cad (5 cycles) the wall temperature follows the same trend during each cycle. However, this temperature profile yielded by the super-cycling is a temperature value of a steady state. Then, it that does not represent the temperature swing of the material. Therefore, additional transient cycles must be performed (deactivating super-cycling). Due to long calculation times and difficulties in storing the data over multiple cycles, the wall temperature results are presented from the EVO, where the last super-cycling stage ends.

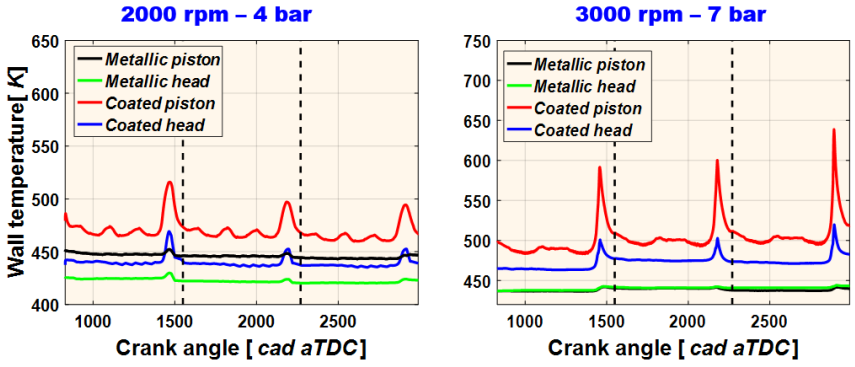

Figure 5.25: *Convergence of the solid domain with the super-cycling for both operation conditions: 2000 rpm - 4 bar (left) and 3000 rpm - 7 bar (right).*

CHAPTER 6

Optimization strategies

Though simulations using three-dimensional CFD can provide precise and instantaneous information about the flow within the engine (temperature, pressure, velocity distributions), they require temperature boundary conditions for the engine walls, which are typically assumed as being constant throughout the engine cycle. This may affect the combustion process, thus leading to inaccurate results [98]. Imposing appropriate wall temperature boundary conditions is not an easy task, and it may require some iterative process. However, such calculations with given surface temperature are not sufficient when the focus is on analyzing the heat transfer within the engine solid components. Indeed, CFD alone does not permit to calculate the heat fluxes through the engine walls, since they are imposed by the boundary conditions.

On the other hand, the CHT method offers a much better alternative. It is a coupled approach that solves simultaneously the fluid and the solid regions in a unique computational iterative process [96]. It therefore yields at the same time all the flow characteristics within the engine, as well as a more precise calculation of the heat fluxes through the walls. In addition, other important variables, such as the temperature distribution on any gas exposed surface of the engine, including peak temperatures, the local and instantaneous heat transfer coefficient, and the near wall velocities are also known. Heat losses are adequately identified and this knowledge may help improve engine design.

Though the CHT approach appears to be the best solution for heat transfer analysis in engines, the calculations in the previous chapter proved that the CHT simulations are very time consuming and require important computational resources.

The main purpose of this chapter is to propose different methods that allow optimizing the calculation time of the CHT simulations in ICEs. The idea is to perform CHT simulations with the less possible cells number in the domain without affecting the results. The study is performed for a 4-stroke compression ignition (CI) engine. Moreover, these strategies are employed to perform CHT calculations in uncoated and coated engine configurations. The objective is to evaluate the suitability of the optimization techniques to study the heat transfer through coated combustion chamber walls in ICEs.

6.1. Numerical setup

6.1.1. Case definition

As seen in the previous chapter, the computational domain for the CFD calculation is formed by the combustion chamber with the intake and exhaust manifolds. The solid piston is also included for the CHT calculations.

Table 6.1: *Engine specifications.*

Engine type	HSDI CI Diesel engine
Number of cylinders [-]	4-in line
Bore - Stroke [mm]	75.0-88.3
Connecting rod [mm]	137.1
Compression ratio	18:1
Number of valves [-]	2 intake and 2 exhaust

The main features of the Diesel engine used for this study are presented in Table 6.1. Moreover, the calculations are performed for two engine configurations:

- Conventional Diesel engine (aluminium piston):

$$k = 144 W/(mK)\ ,\ c = 2438 kJ/(m^3 K)$$

- Diesel engine with the piston top coated with the coating 3 from Table 4.2 (the best thermal coating nowadays).

The computational domain of the Diesel engine employed in this chapter is displayed in Fig. 6.1. The main difference with the SI engine is that intake/exhaust valves are flat in order to create swirl motion into the cylinder [159]. In addition, there are some differences in the piston design described in section 6.1.3.

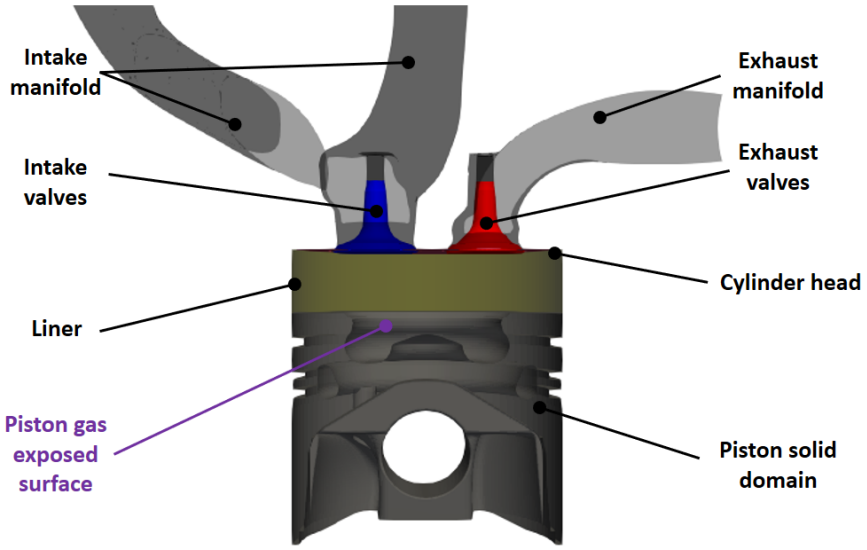

Figure 6.1: *Computational domain for CHT calculations in CI engine. Gas exposed surfaces of the piston represent the fluid/solid interface wall for the CHT simulations.*

Considering the long computational times of CHT calculations, a high speed - medium load operation point was selected for the simulations, since experience with the SI calculations (Chapter 5) has shown that convergence is faster for high speed. The details about this engine operation condition are listed in Table 6.2.

Table 6.2: *Specifications of the operation conditions to perform the CHT calculations.*

High speed - medium load	
Torque [Nm]	23.7
Engine speed [rpm]	3500
Number of injections [-]	1
Air-fuel ratio $\lambda[-]$	1.0
Injection pressure [MPa]	97

6.1.2. Mesh and model set-up

The mesh was generated by CONVERGE using a modified base grid for the computational domain. In spite of the facility of the software to generate the mesh at run-time, there is a limitation to set the size of the embedding layers. In this regard, CONVERGE defines the size of the embedded layer according to:

$$embed\_scale = \frac{dx\_base}{2^n} \tag{6.1.1}$$

where dx is the base cell size and n is the embedded scale. However, the software does not allow to set decimal numbers in the embedded scale. Consequently, in some cases the target size of the embedded layer cannot be achieved.

Usually, in CFD calculations it is assumed that $dx\_base = dy\_base = dz\_base$. According to Gomez-Soriano [140], a base cell size of 3 mm is enough to model the combustion process in the Diesel engine. However, this value for all the dimensions in the base grid will bring problems to limit the cell count and allow the description of the thick coating layer with an integer number of cells. Hence, a mesh base grid with the dimensions: $dx\_base = 3mm$, $dy\_base = 3mm$ and $dz\_base = 2mm$ is proposed. This mesh will allow to model the coating layer with the number of nodes defined in Chapter 4 for the equivalent material 3. From the computational point of view, this approach is better than using a cubic base grid of 2 mm when it is not needed (Appendix 6.A).

To refine the mesh for better accuracy of the results, the base grid size is reduced in specific regions where the physical processes are more complex. In particular, cell size is reduced to 0.75 mm at the liner, while for piston and cylinder head a 0.5 mm refinement was employed. Due to the previous explanation, it is not possible to reduce the cell size to 0.5 mm in all the combustion chamber walls. For spray modeling, an injector shaped refinement of 0.375/0.25 mm was used at the injector location. Furthermore, the AMR approach has been activated to refine the mesh in zones of the combustion chamber where the velocity and temperature gradients are highest. For these calculations the sub grid scales criterion applied in the SI engine was modified as is explained in section 6.2.2. The base computational mesh employed for the calculations is displayed in Fig. 6.2.

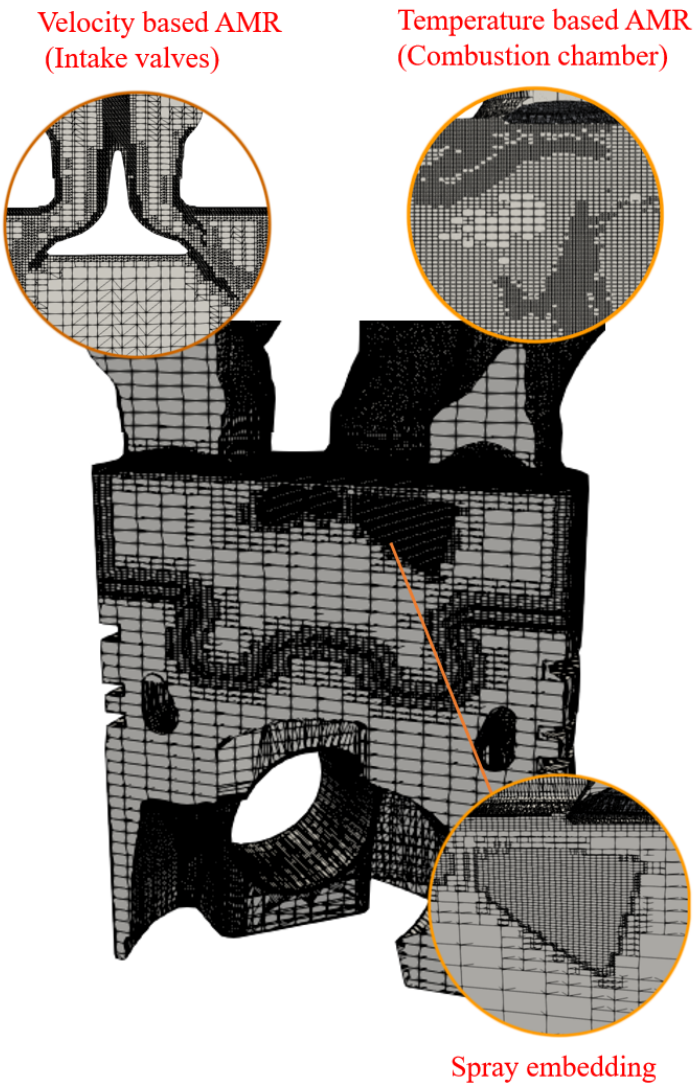

Figure 6.2: *Mesh characterization of the CI engine.*

For the fuel injection the same models employed for the SI engine have been considered. The Diesel fuel was characterized by the DIESEL2 fuel surrogate [160] that has been used by several authors for spray modeling in CI engines [140, 161]. This surrogate is available in the CONVERGE liquid library.

The combustion process is simulated using the SAGE combustion model. The empirical Hiroyasu soot model [145] and the extended Zeldovich mechanism [18] were employed for the calculation of emissions and NOx formation, respectively. The RNG (renormalization group) k-ϵ model is used for turbulence combined with the O'Rourke and Amsden heat transfer wall model [104, 105]. This model was chosen on the basis of the previous study carried out in the chapters 3 and 5.

As in the previous chapter, the strategy for relaxing the Courant number (CFL) from EVO to IVC [148] is used to optimize the calculation time. The Courant number limit for the calculations in the Diesel engine are shown in Table 6.3.

Table 6.3: *Maximum CFL limits for the calculations in the CI engine.*

Intake region			
CAD	max_cfl_u	max_cfl_nu	max_cfl_mach
-610.0	5.0	5.0	50
-374.0	2.0	5.0	50
-147.0	5.0	2.5	50
110.0	5.0	5.0	50
Exhaust region			
CAD	max_cfl_u	max_cfl_nu	max_cfl_mach
-610.0	2.0	5.0	50
-353.0	5.0	5.0	50
-147.0	5.0	2.5	50
110.0	5.0	5.0	50
In-cylinder region			
CAD	max_cfl_u	max_cfl_nu	max_cfl_mach
-610.0	2.0	5.0	50
-147.0	1.0	2.5	50
110.0	2.0	5.0	50

6.1.3. Boundary conditions for CI engine

For the CFD calculations without CHT, the boundary conditions of temperatures for all the gas exposed surfaces (piston, liner, cylinder head) during the engine cycle were set consistently with experimental data acquired by means of thermocouples and are displayed in Table 6.4.

Table 6.4: *Boundary conditions for the isothermal walls obtained with the 1D-HTM.*

3500 rpm - 8.57 bar	
$T_{piston}[K]$	454
$T_{head}[K]$	406
$T_{liner}[K]$	389

For the CHT calculations the liner and cylinder head temperature boundary conditions are fixed in the same way. The piston wall temperature is calculated with the conjugate heat transfer model of CONVERGE [102]. For this, the required boundary conditions at the inner surface in contact with the gas are the material physical properties. For the outer wall of the piston, the convection coefficient and temperature of the environment surrounding the piston regions are needed as boundary conditions.

Additional boundary conditions such as the fuel mass, injection rate and intake/exhaust ports pressure and temperature are imposed in the same way as in the the SI engine. In this case, the values were obtained from experimental tests in the Diesel Engine carried out at CMT facilities. Table 6.5 shows the conditions at the intake and exhaust manifolds.

Table 6.5: *Boundary conditions in the intake and exhaust ports for the calculations in the CI engine.*

3500 rpm - 8.57 bar	
$P_{int}[bar]$	1.71
$T_{int}[K]$	328.28
$P_{exh}[bar]$	1.72
$T_{exh}[K]$	794.9

6.1.4. CHT solid domain in CI engine

For the CHT calculations, the piston is the same as the one employed for the validation in Chapter 3. The boundary conditions are imposed in the solid domain following the same approach of Chapter 5. The piston is divided into several regions, although the boundary condition are different since the study cases have unrelated purposes. Moreover, the combustion gas exposed surface of the piston is divided in two regions in order to be able to coat the piston top.

In general, it is more difficult to determine the boundary conditions in a Diesel engine due to the cooling gallery inside the piston. Hence, the CONVERGE proposed division of the piston is not the most suitable and a more detailed division on the solid needs to be considered as shown in Fig. 6.3-bounds-CI. As in the previous chapter, empirical correlations are available in the literature for the boundary conditions of a Diesel engine piston. The boundary conditions employed for the solid domain are listed below:

- Piston top: Contact with the combustion gas, h and T given by the calculation itself (Convection)
- Piston bowl: Contact with the combustion gas, h and T given by the calculation itself (Convection)
- Piston top land [21]: Contact with combustion gas near the liner wall, h and T given by the calculation (Convection)
- Piston ring 1,2 and 3[21]: Piston segments (Convection)
- Skirt between rings[21]: Contact with oil (Convection)
- Piston skirt [154]: Contact with oil (Convection)
- Piston pin [154]: Contact with cooling oil
- Piston inner cavity [154]: Contact with cooling oil
- Piston gallery [154]: Contact with cooling oil

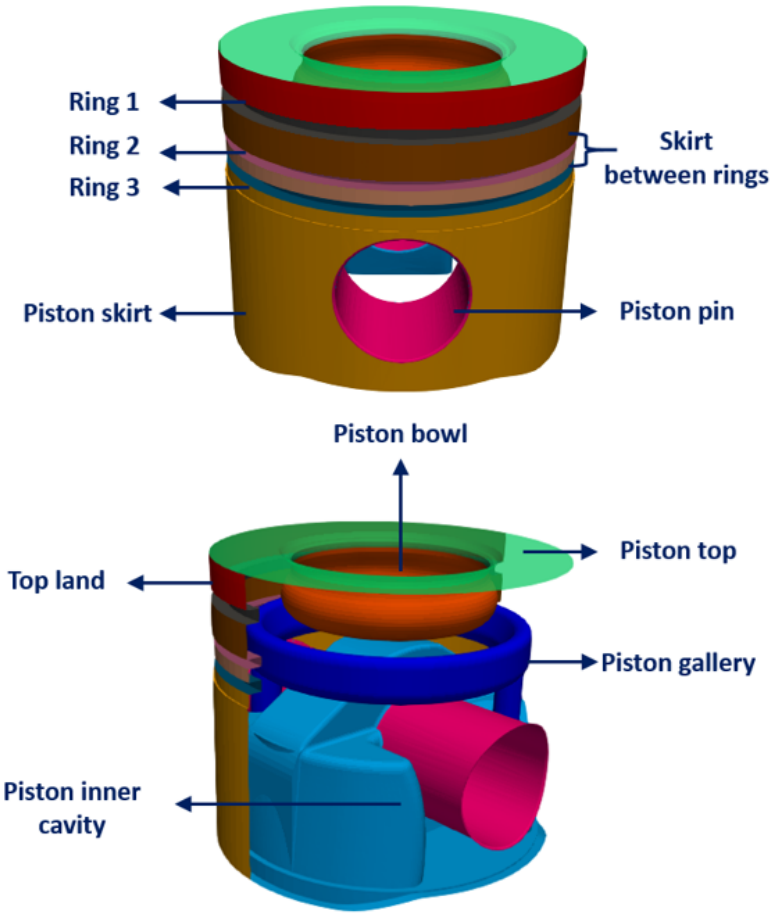

Figure 6.3: *Piston regions considered for boundary conditions in the CHT solid domain. Piston top and piston bowl represent the fluid/solid interface walls for the calculations.*

Fig. 6.3 shows the solid engine piston with the sub-divisions considered for the calculations. The piston top and piston bowl represent the fluid/solid interface walls in the domain and the values for h and T are calculated by

the software. For the skirt and the gallery have been used equations 5.3.1 and 5.3.2, respectively. On the other hand, the other boundary conditions were estimated as follows:

- Piston top land

The temperature was calculated with CONVERGE and the heat transfer coefficient was determined with eq. 6.1.2:

$$h = \frac{k_{\text{gas}}}{\delta} \tag{6.1.2}$$

where k_{gas} is the gas thermal conductivity and δ is the crevice clearance.

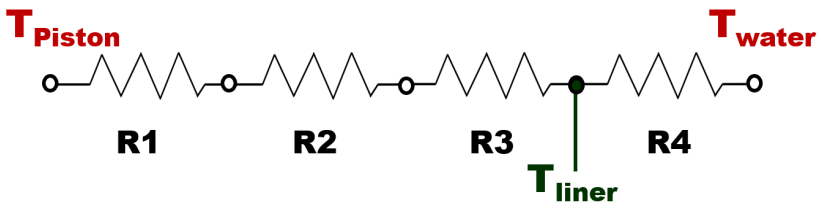

Figure 6.4: *Thermal circuit employed for the calculation of the boundary conditions at the piston rings.*

- Piston rings

For the piston rings the thermal circuit proposed by Esfahanian et al. [21] and display in Fig. 6.4 was employed, considering only conduction through the piston rings. The circuit is comprised by the following thermal resistances:

$$R_1 = \frac{\ln(r_2/r_1)}{2\pi H_1 k_{\text{ring}}} \tag{6.1.3}$$

$$R_2 = \frac{\ln(r_3/r_2)}{2\pi H_2 k_{\text{oil}}} \tag{6.1.4}$$

$$R_3 = \frac{\ln\left(r_4/r_3\right)}{2\pi H_3 k_{\text{block}}} \tag{6.1.5}$$

$$R_4 = \frac{1}{h_{\text{water}} A_{\text{s}}} \tag{6.1.6}$$

where r_1, r_2, r_3 and r_4 are the inner radius, outer radius, bore radius and inner radius of the water jacket, respectively. H_1, H_2 and H_3 are width of the paths for each thermal resistance. Finally, A_s is the effective area of the water jacket.

According to the authors, the thermal resistance R_2 is too small to have an impact on the circuit and can be neglected. For the thermal resistance R_4 the heat transfer coefficient is needed. However this value is different for every cylinder (4-in line engine) and it is not available. Then, the thermal circuit is used until the liner (R_3).

The heat transfer coefficient at the piston rings is determined with the expression 6.1.7:

$$h_{\text{ring}} = \frac{1}{R_{\text{tot}} A_{\text{eff}}} \tag{6.1.7}$$

where R_{tot} is the sum of the thermal resistances and A_{eff} is the effective area of the ring

Finally, the liner temperature was considered as the reference temperature and it was manually adjusted for each ring.

- Skirt between the piston rings

The recommended value of 115 W/(m/K) [21] was taken as the heat transfer coefficient for the skirt between the piston rings with the reference temperature of the oil.

- Piston pin and piston inner cavity

For the piston pin and the piston inner cavity a reference of 612.5 W/(m/K) from a piston with a similar configuration [154] has been considered, while the temperature was referenced to cooling oil.

The empirical correlations have shown to yield good estimations of boundary conditions for the engine piston [162]. However, additional tuning may be required for better results. Finally, the final boundary conditions employed for the CHT calculations are listed on Table 6.6.

Table 6.6: *Boundary conditions for the CI engine piston outer surface.*

Outer solid wall	$T[K]$	$h[W/(m^2K)]$
Piston top land	451	91
Ring 1	421	1108
Ring 2	381	828
Ring 3	371	984
Skirt between rings	363	115
Piston pin	363	612.5
Piston inner cavity	363	612.5
Piston gallery	374	6384

6.2. Customized meshing approach

In order to reduce the CHT calculation time, which is about 10 days/cycle using 32 cores on the UPV cluster, new alternatives must be implemented to optimize the CHT simulations without affecting the results. In this regard, a method to optimize the domain and number of cells in the mesh is proposed.

6.2.1. Coarsen surface mesh

As explained in the previous chapters, in CONVERGE the mesh is generated at runtime using the surface mesh. For stationary geometries, CONVERGE performs this process once at the start of the simulation and again whenever the geometry is refined or coarsened. For moving geometries, CONVERGE performs the grid generation process at each time-step. The creators of CONVERGE designed the grid generation process to be computationally efficient and minimize CPU usage for this portion of the simulation.

Fig. 6.5 shows a very refined surface mesh of the engine (top) with the default geometry file. A coarser surface mesh for the intake and exhaust ports could help speeding up the simulation. Indeed, when coarsening the valves as in Fig. 6.5 (bottom) some improvements are achieved regarding the memory usage and the size of the output files. The intake/exhaust valves system of the original surface mesh has 232646 entities while the coarsen surface mesh has 72252 entities. Though this difference does not change the overall amount of cells in the domain. However, the size of the output files (post files) is reduced by 9%.

Since the CHT calculations are very time consuming, large storage capacities are required to save the cells information. In this regard, when the resources are limited, information from previous cycles must be deleted to preserve the information from the last cycles. Hence, it is important to reduce the files size as much as possible.

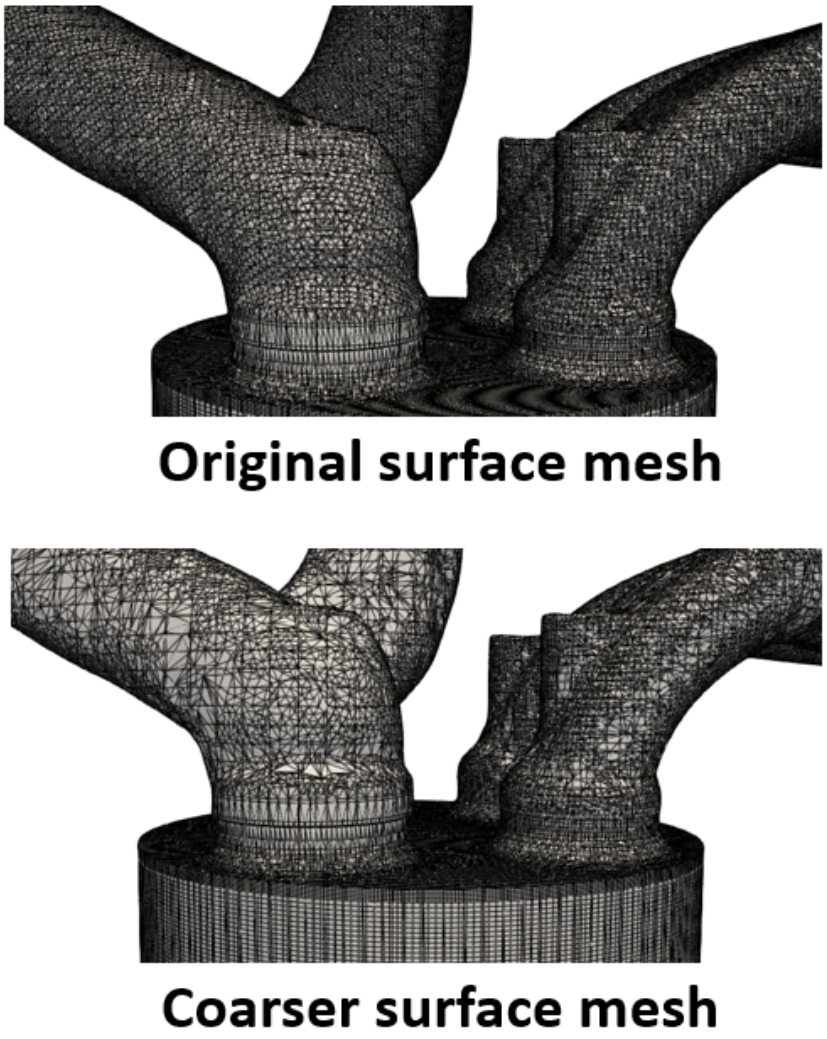

Figure 6.5: *CONVERGE mesh surface generation in the intake/exhaust valves: original mesh surface (top) and coarser mesh surface (bottom).*

6.2.2. y+ Embedding

In order to optimize the CHT calculations and limit cell count, a strategy aiming at achieving a desired value of near-wall y+ using the AMR approach was employed. The method consists in defining the maximum and minimum y+ target on selected boundaries to allow the refinement of cells by the AMR algorithm only where and when is needed, thus reducing the computational weight of the simulation compared to a fixed embedding strategy. Although the numerical resolution of the thermal and kinetic boundary layers would be the preferred choice in CHT simulations, this strategy is computationally expensive especially when multiple engine cycles need to be simulated. The wall-function approach was therefore adopted in the study, with standard wall functions, and the y+ was targeted to be between 30 and 300 following available best practices [24,25]. In particular, a permanent AMR was adopted on the fluid side of the combustion chamber walls (piston, liner and cylinder head) to achieve the target y+, with a minimum cell size set to 0.75/0.5 mm. This setting is consistent with the local grid refinement adopted in coating layer, in which cell size was set to 0.75/0.5 mm, which assured that the grid on the solid side of the fluid-solid interface is equal or finer than the one in the fluid side [22].

According to Bredberg [163] if the y+ value of a cell adjacent to a wall falls outside of the range for the chosen model, law-of-the-wall models will no longer produce physically realistic results.

From the post-processing point of view, this method has the disadvantage that the resolution in the near wall cells on the fluid is lost. Therefore, images like those shown in Figs. 5.14, 5.15, 5.18 and 5.19 cannot be visualized with this approach.

6.2.3. Approach validation

To apply the proposed approach it is necessary to verify that with the changes in the mesh, there are no changes in in-cylinder gas properties. Both refinement approaches, the fixed refinement applied in Chapter 5 and the y+ based AMR refinement are compared in Fig. 6.6. Clearly, there are no significant differences in the in-cylinder pressure and the in-cylinder temperature. Furthermore, in both methods the fuel injection is modeled.

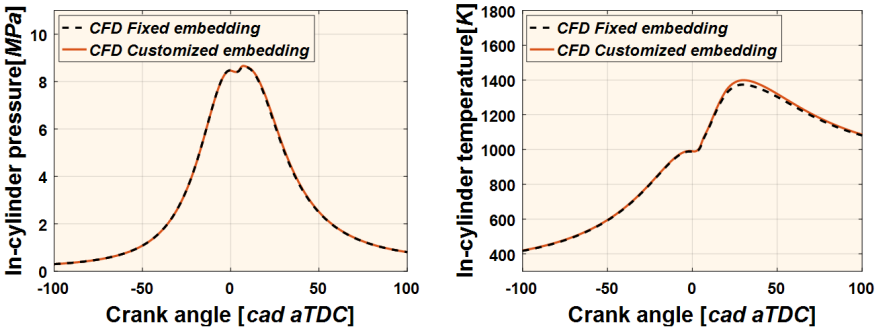

Figure 6.6: *In-cylinder pressure trace (left) and in-cylinder temperature (right) comparison between the fixed embedding approach and the customized meshing approach.*

Moreover, there is an important difference in the cells number and consequently in the calculation time between both approaches. Using a fixed embedding there are 561403 cells in the calculation base domain (with no AMR), while the customized meshing approach yields 198653 cells in the whole domain. This implies a reduction of almost a third (1/3) in the total number of cells. The gain in the calculation time is about 30-40%. In addition, less cells in the computational domain leads to a reduction in the computational resources consumption, such as processor power and RAM (Random-Access Memory) requirements.

Since this approach only concerns the mesh of the computational domain, it is valid for any type of ICE.

For the CHT calculations, the computational domain considered included the solid walls also, so that not only the heat transfer from gas to wall was considered, but also that within the wall. These CHT calculations are performed for the same operation point (3500 rpm - 23.7 Nm). Following the methodology of Chapter 5, the solid region is initialized with the temperature obtained from the 1D lumped model in order to accelerate the solid convergence.

In contrast with the SI engines, the significant cyclic dispersion observed in the previous chapter is not present in Diesel engines. However, it is necessary to perform several cycles for the convergence of both the fluid and the solid domains. The convergence criteria used for the CHT calculations were the in-cylinder pressure for the fluid phase, and the wall temperature at the fluid-solid interface surface for the solid phase (Appendix 6.B).

6.3. Results

In this section the results obtained for metallic and coated piston are compared in order to determine the impact of the coating on engine performance.

6.3.1. Combustion analysis

As explained above, the cyclic dispersion of gasoline engines is not present in Diesel engines. So that, the in-cylinder pressure does not change cycle to cycle. However, numerically multiple cycles calculations are still required to ensure the solid domain convergence. In Fig. 6.7 the in-cylinder pressure traces obtained for each configuration are compared. Both traces are almost over imposed throughout the engine cycle. However, the coated engine trace is slightly above the metallic one near TDC and at peak pressure. The maximum difference between pressures is about 0.7 bar.

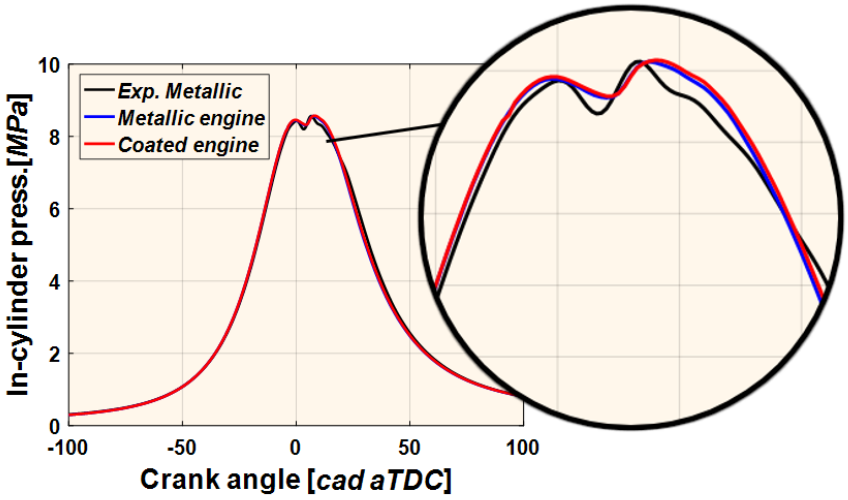

Figure 6.7: *Calculated in-cylinder pressure traces for metallic and coated Diesel engines. Zoom in the figure shows in more detail the differences between both configurations.*

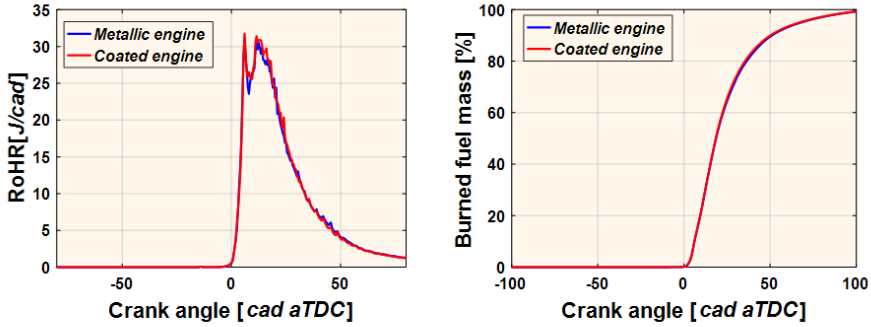

Figure 6.8: *Rate of heat release (left) and burned fuel mass (right) comparison between metallic and coated Diesel engines.*

Fig. 6.8 shows the RoHR calculated from both CHT simulations. There are some differences, with lower peak values of RoHR in the coated engine configuration as consequence of the coating layer. The burned fuel mass along the engine cycle is also displayed in Fig.6.8. It can be noticed that the coated piston top shows slightly higher energy release rate during the first part of the combustion, between 0 CAD aTDC and roughly 25 CAD aTDC. Afterwards the rate of heat release becomes lower for the coated piston top, during the expansion stroke. These characteristics highlights that the coated piston top shows a faster combustion development compared to the standard metallic piston, which is possibly a consequence of the lower combustion heat losses during early combustion. These characteristics highlights that the coated piston top shows a faster combustion development compared to the standard metallic piston, which is possibly a consequence of the lower combustion heat losses during early combustion. This is confirmed by data in Table 2 where characteristic combustion angles are compared for the two configurations studied. The MFB50 (Mass Fraction Burnt 50%) crank angle is almost identical between the metallic and the coated piston configurations, however the MFB10-90 (Mass Fraction Burnt 10%-90%) crank angle highlights a significantly faster combustion development with the coated piston.

Table 6.7: *Combustion velocity features. Mass of burned fuel 50% and mass of burned fuel from 10% to 90%.*

	Metallic engine	Coated engine
MBF50 [cad aTDC]	19.2	19.1
MBF10-90 [degrees]	45.1	43.3

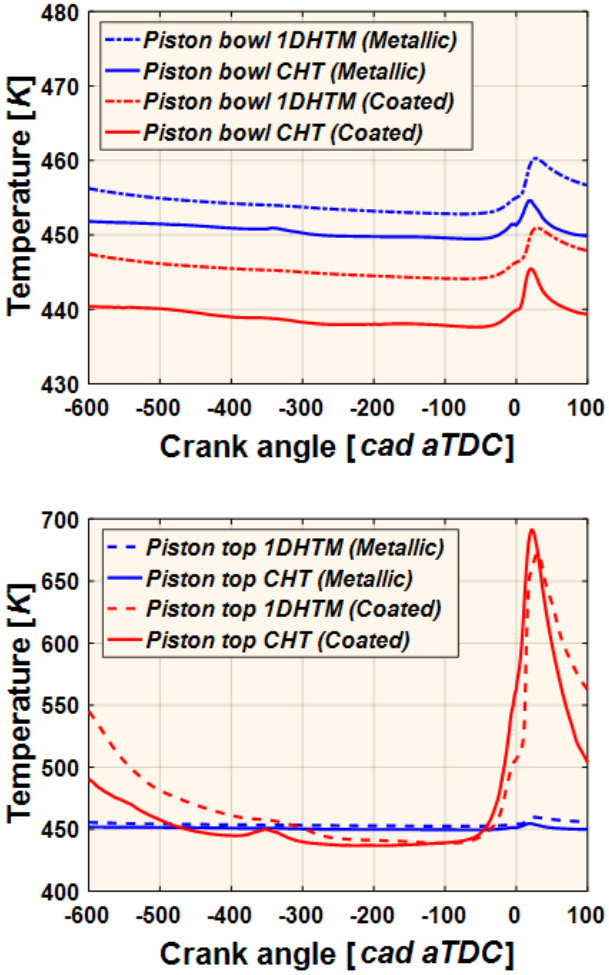

Figure 6.9: *Wall temporal temperature evolution of the fluid/solid interface surfaces on Diesel piston: piston bowl (left) and piston top (right).*

6.3.2. Wall temperature results

Even though several cycles were needed to converge the solid domain, the final mean temperature of the piston gas exposed surface is very close to the initial assumption on the solid. The converged mean temperatures of the fluid/solid interfaces walls (piston bowl and piston top) are shown in Fig. 6.9:

- The piston bowls of both configurations show similar mean temperature levels and temperature swings. However, the temperature of the coated configuration is around 5 K lower.
- The temperature swing of the coated piston top is higher than the metallic configuration as expected. The maximum difference is about 265 K.
- The mean wall temperature levels calculated with the CHT are lower than those of the 1D-HTM.

Table 6.8 shows the maximum temperature swing for each gas exposed surface of the solid piston. Clearly, some differences are observed between the maximum temperature swings calculated with both models. The differences are due to the models are different in nature. In fact, the heat transfer in the 1D-HTM is simplified and it does not consider the radial heat transfer.

Table 6.8: *Thermal gradient on the gas exposed surfaces for CI engine.*

Engine surface	Max. temperature swing predicted by 1D HTM [K]	Max. averaged temperature swing predicted by CHT [K]
Piston bowl (Metallic engine)	7.5	6.1
Piston bowl (Coated engine)	6.8	8.3
Piston top (Metallic engine)	7.2	6.1
Piston top (Coated engine)	234.0	264.6

To further analyze the effect of the coating layer, the spatial temperature distribution of the solid piston for both configurations is displayed in Fig. 6.10. As expected, the higher wall temperatures are reached for the coated engine configuration. Similarly, as in the SI engine (Chapter 5), the combustion gas exposed surface of the piston is hottest for both engine configurations. The coolest part of the piston is located in the inner cavity and the piston skirt. Moreover, the temperature distribution is mostly axisymmetric as shown in Chapter 3 and Chapter 5. The spatial temperature distribution calculated on the piston are in agreement with the results found by other authors [154].

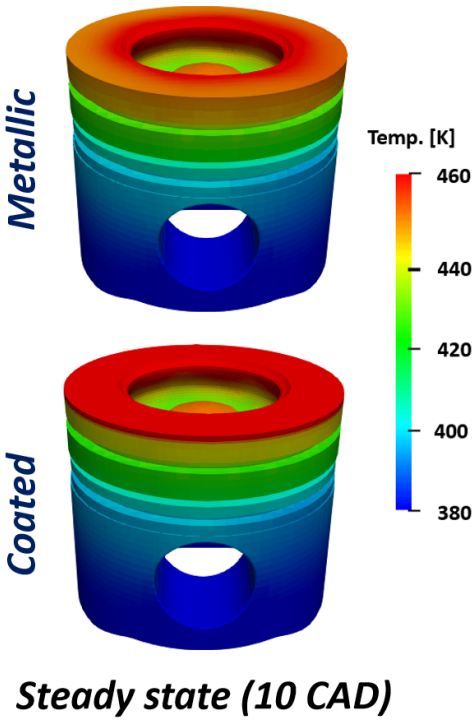

Figure 6.10: *Temperature wall distribution in the Diesel solid piston (10 CAD): conventional metallic piston (left) and coated piston (right).*

A more accurate way of looking at the piston wall temperature consists in monitoring its evolution by plotting several snapshots of the piston gas exposed surface near TDC, as shown in Fig. 6.11. Observations regarding Fig. 6.11 are listed below:

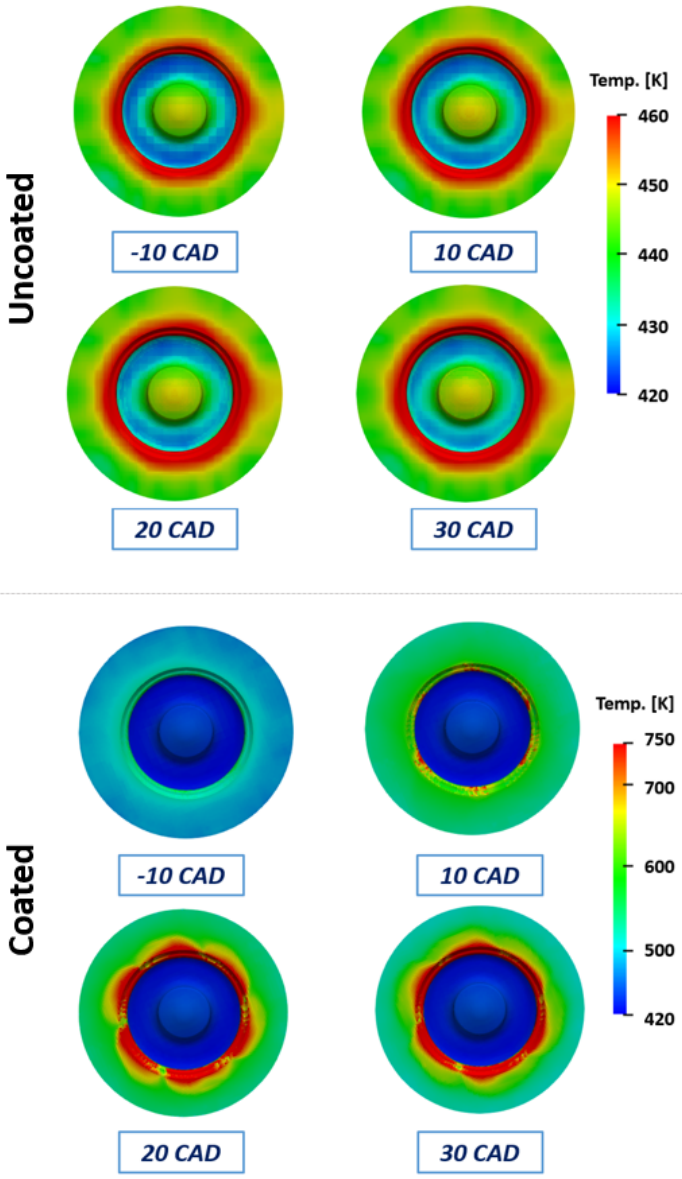

Figure 6.11: *Temperature distribution on piston gas exposed surfaces during the combustion: Metallic engine (top) and coated engine (bottom).*

- For both configurations, the hottest area on the piston surface is located at the center rim of the piston top.

- The maximum thermal gradient on the metallic piston top surface is about 40 K at 20 cad, while for the coated piston it is about 330 K at the same instant.
- In the metallic engine configuration there are no significant differences between the four snapshots of the cycle. As explained in Chapter 5, this trend is due to the high thermal conductivity of the aluminium.
- The coldest zones in both configurations are in the piston bowl, as consequence of the cooling oil gallery.

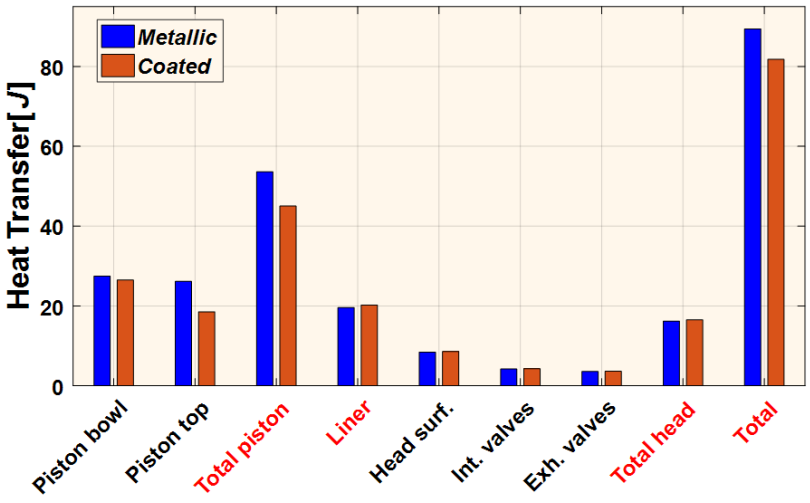

Figure 6.12: *Heat transfer balance comparison between metallic and coated Diesel engines.*

6.3.3. Heat transfer results

To analyze the effect of the coating on the heat losses, the heat transfer to each wall of the combustion chamber is quantified for both engine configurations, and presented in Fig. 6.12. The total heat transferred through all the walls of the combustion chamber is lower for the coated engine configuration (8.8%). Considering the heat transfer through each wall separately, the heat transferred to the piston presents the highest values in both configurations. The largest difference is observed for the piston top (29.1%) due to the temperature swing of the coating layer. As in both calculations the liner and cylinder head are assumed isothermal with the same temperature, there are small differences in heat transfer between these surfaces. It is worth

noting that the total heat transfer through the piston represents 60% and 55% of the total heat transfer through the in-cylinder walls in the metallic and coated configurations, respectively. The heat balance is in agreement with the one found by some authors in Diesel engines [101]. The differences in heat transfer for both configurations are listed in Table 6.9.

Table 6.9: *Heat transfer in the combustion chamber in CI engine at medium load.*

Engine part	HT Metallic engine [J]	Coated engine [J]	Difference [%]
Piston bowl	27.46	26.50	-3.50
Piston top	26.16	18.53	-29.17
Total piston	53.62	45.03	-16.02
Liner	19.58	20.23	3.32
Head surface	8.43	8.61	2.14
Intake valves	4.20	4.30	2.38
Exhaust valves	3.57	3.63	1.68
Total head	25.8	26.3	1.7
Total engine HT	89.41	81.80	-8.81

According to the heat balance shown in the Fig. 6.12 the application of the thermal coating seems to slightly affect the heat transfer through the uncoated combustion chamber walls (liner, head and valves). To explain these differences, the gas temperature and the heat transfer coefficient in two of the uncoated walls (Piston bowl and Liner) are shown in Fig. 6.13.

For the piston bowl, the highest differences are observed in the heat HTC during the combustion phase. Indeed, the HTC near the uncoated piston is higher than the coated piston, leading to higher heat transfer. Although the temperatures in the coated configuration are higher during the exhaust phase (-610 cad to – 450 cad), the HTC has a greater influence on heat losses for this surface.

In the liner surface, the HTC traces are almost over imposed throughout the full engine cycle. However, higher temperatures in the coated configuration during exhaust and combustion are observed. Consequently, the heat losses through the liner are higher in the configuration with coated piston top (Table 6.9).

Summarizing, the in-cylinder gas temperature of the combustion chamber slightly increases due to the higher wall temperatures of the coated surface (Fig. 10). However, the coating seems to affect only the HTC of the gas near the piston because high wall temperatures (Fig. 10) cause the fuel to burn before reaching the surface (Table 6.7).

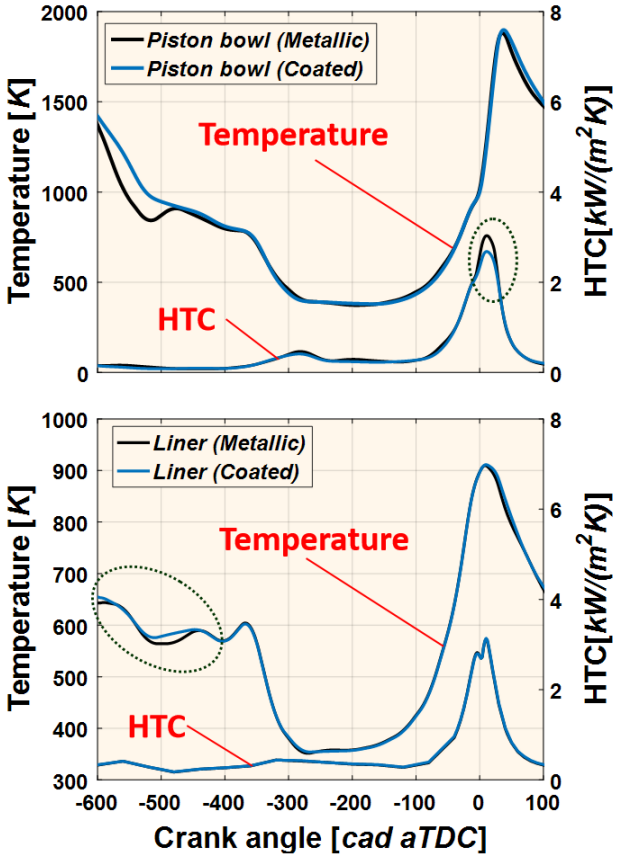

Figure 6.13: *Near wall gas temperature and heat transfer coefficient HTC of the piston bowl (top) and liner (bottom). Highest differences are highlighted with dashed circles.*

6.4. Fuel consumption, pollutant emissions and engine efficiencies

Results regarding fuel consumption and polluting emissions in the Diessel engine are shown in Table 6.10. Although experimental values are not available for this operating point, the CHT calculations lead to reasonable values according to the literature [140].

Applying the coating on the piston reduces fuel consumption by 1.3 %. These results confirm the benefits that thermal coatings could provide in the fuel consumption alleged by other authors [75].

Regarding emissions, with the coated piston, HC and CO emissions were reduced by 12.5 % and 45 %, respectively. On the other hand, NOx emissions increased by 9.5 % in the coating configuration.

As seen in Fig. 6.7 the in-cylinder pressure is higher for the coated piston top, which leads to higher in-cylinder gas temperature as observed in Fig 6.13. Therefore the NOx emissions are higher for this configuration [49].

Table 6.10: *Fuel consumption and pollutant emissions for Diesel engine.*

	Metallic	Coated	Diff. [%]
Predicted isfc $[g/kWh]$	200.5	197.8	-1.3
Predicted isHC $[g/kWh]$	0.64	0.56	-12.5
Predicted isCO $[g/kWh]$	11.6	6.3	-45.7
Predicted isNO_x [g/kWh]	1.26	1.38	9.5

Finally, the engine efficiencies are compared in Table 6.11 (Eqs. 5.7.1, 5.7.2 and 5.7.3). The reduction of 4 % in heat losses seems to improve the indicated efficiency of the engine which is higher for the coated configuration. This effect seems to be related with the increase in combustion efficiency due to the coating layer. Regarding the volumetric efficiency, there is no negative impact due to the lower temperatures on the piston during the intake phase (6.9).

Table 6.11: *Comparison between the metallic and coated Diesel engines. Volumetric, combustion and indicated efficiencies.*

Efficiency	Metallic engine	Coated engine
Volumetric efficiency [%]	96.4	96.4
Combustion efficiency [%]	98.2	98.9
Indicated efficiency [%]	39.03	39.58

6.5. Summary

In this chapter, two strategies that allow optimizing the CHT calculation in internal combustion engines are presented. The simulations are performed for a 4-stroke CI engine and considering the heat transfer to the solid piston only. The most important findings from this chapter are summarized below:

- In order to optimize the CHT calculations time a customized meshing approach was employed.

- The customized meshing approach consists in replacing a fixed embedding refinement for a y+ strategy using the AMR approach of CONVERGE. The method is based on defining the maximum and minimum y+ targets for meshing the combustion chamber walls. This approach models the engine cycle by refining the cells in the domain only when and where needed. Thus, the total number of cells in the domain is significantly reduced. Furthermore, this technique was further optimized by coarsening the surface mesh of the intake and exhaust valves. As result, the calculation time and the size of the output files were reduced.
- The equivalent material methodology was applied in combination with the optimized mesh strategy to study the heat transfer in a Diesel engine with coated piston top. The results show a better resolution than those found by applying the fixed refinement strategy used in the gasoline engine.
- The greatest heat losses in a Diesel engine occur in the piston due to the impact of the fuel jet. Therefore, it is the wall where the application of a thermal coating may lead to some benefits on the engine performance.
- Due to the application of a coating with lower conductivity and lower heat capacitance, the temperature swing is higher than that of the coating used in the gasoline engine. Thus, the temperature gradient between the gas and the surface is smaller, reducing total heat losses through the combustion chamber by about 9%. This reduction in heat losses seems to yield improvements of 0.7%, and 0.5% in the combustion and indicated efficiencies, respectively.
- The application of the coating on the piston top led to a reduction in fuel consumption of about 1.3%. Regarding the emissions, the amounts of HC and CO were lower in the coated configuration, while NOx emissions increased by 9.5% due to the higher in-cylinder temperature.

6.A. Appendix: Mesh independence study for the CI engine

In order to find the best mesh for the CFD-CHT simulations in the SI engine, three different mesh configurations have been evaluated to model the combustion process:

- Mesh 1: $dx\_base = dy\_base = dz\_base = 2$ mm
- Mesh 2: $dx\_base = dy\_base = 3$ mm , $dz\_base = 2$ mm
- Mesh 3: $dx\_base = dy\_base = dz\_base = 4$ mm

Fig. 6.14 shows that the in-cylinder pressure calculated with mesh 1 and mesh 2 fits with the experimental trace of the engine. A higher base grid size (Mesh 3)increases the differences between the experimental and simulated pressures. The maximum error with respect to the experimental pressure is -0.6%, 1.2% and 4.9% for mesh 1, mesh 2 and mesh 3, respectively. Clearly, mesh 1 and mesh 2 are the most suitable configurations. However, mesh 2 consumes less computational time (about 40% faster). Then, for the CHT calculations on the CI engine the mesh 2 configuration was employed.

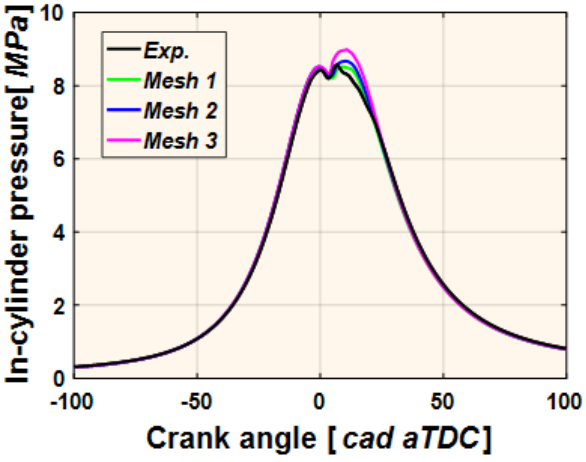

Figure 6.14: *Mesh independence study to define the base grid size for the CHT calculations on the CI engine.*

6.B. Appendix: Solid domain convergence of the Diesel engine

The super-cycling CONVERGE approach used in previous chapters has been employed to calculate the steady state temperature of the solid. As in the gasoline engine, the wall temperature of the combustion gas exposed surfaces was considered. Since there is no cyclic dispersion in Diesel engines, there are no variations cycle to cycle in the gas properties that affect the wall temperature evolution of the piston bowl and piston top.

Fig. 6.15 shows that after 2270 cad (4 cycles) the wall temperature of the surfaces follows the same trend during each cycle. Nonetheless, in order to determine the temperature swing of the surfaces additional transient cycles need to be performed. This simulations start from the EVO of the last super-cycling cycle as seen in Fg. 6.9.

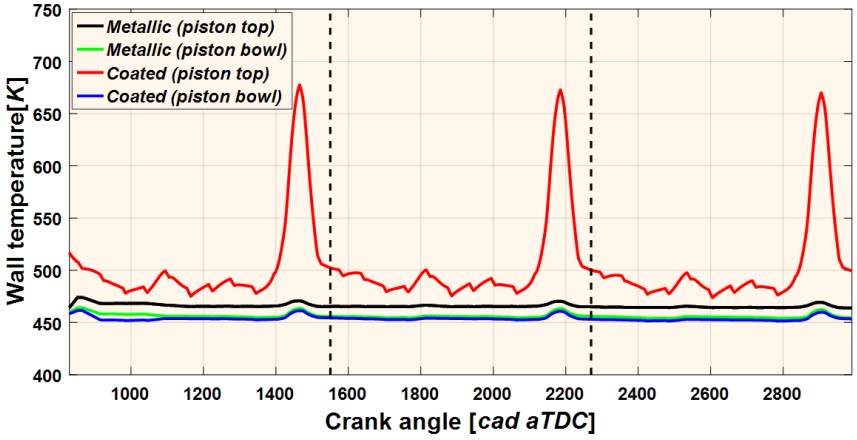

Figure 6.15: *Convergence of the solid domain in the CI engine. Wall temperature evolution of the fluid/solid interface surfaces (piston top and piston bowl).*

CHAPTER 7

Conclusions and future works

This chapter presents the summary of the research work carried out in this doctoral thesis. Likewise, the main conclusions obtained in the previous chapters are reported, highlighting the contributions made in the study of heat losses in ICE by means of CHT calculations.

Finally, some future works that could contribute to improve the existing know-how on the CFD-CHT calculation in ICE are discussed, using the knowledge and numerical strategies developed in the previous chapters.

7.1. Conclusions

In Chapter 1, the main objective of this thesis was established as the study of heat losses through the solid walls of the combustion chamber in an ICE. This purpose is based on the need to develop more efficient and cleaner combustion engines; one way is to improve their thermal efficiency. For this, it is necessary to have engineering tools that allow assessing the heat losses in the engine and thus create new technologies that allow to reduce them. In this regard, this thesis has given an important focus to engines with combustion chamber walls coated with the most novel insulating materials, which have arisen in the industry in recent years.

From the literature review carried out in Chapter 2, an overview on heat transfer in internal combustion engines is given, as long as the alternatives that have been proposed in recent decades to reduce heat losses. In addition, it is outlined that all the components in the engine intended for thermal management have an interaction that affects the heat transfer through the solid walls of the combustion chamber. From these findings and developments in thermal management and heat transfer at ICE, it arises the concept of engines with combustion chamber walls coated with thermal insulation

materials. The new generation of these materials are characterized by low thermal conductivities and low heat capacities. Nonetheless, the study of this type of engines by means of experimental and numerical techniques has been challenging for the manufacturers, due to the fragility of the coatings and their thin thickness. Numerical methods seem less expensive and suitable during the early design stages. In particular, the CHT calculations appear to be one of the most suitable approaches for studying heat losses in ICEs. Therefore, in this thesis the CHT calculation is used as the main tool to study the heat transfer in ICEs with coated walls.

In order to achieve the main objective of this thesis, specific tasks were carried out. The summary of these tasks and the main findings derived from their completion are summarized below.

- **Validation of the conjugate heat transfer 3D-CHT calculation to study the heat losses in ICEs**

  The CONVERGE computational tool to perform CHT calculations was evaluated through simple cases in Chapter 3. First, simple geometries were used comparing the results with analytic values. Then, steady state tests were performed in a metallic piston to determine the temperatures in the solid, which were compared with experimental measurements obtained with thermocouples. For the calculations the software Super-Cycling approach was employed. The simulations allowed validating that, with the CHT interface of CONVERGE, reasonable results can be obtained in steady state for metallic solids.

  In this same chapter it was confirmed that the roughness has no influence on heat transfer in the range of values similar to those of thermal coatings. Therefore, it is not required to consider this parameter to perform the CHT simulations in ICEs.

  Furthermore, in Chapters 5 and 6 the results of the CHT calculations are compared with experimental measurements carried out on a gasoline engine and a Diesel engine, respectively. The results showed that the 3D-CHT approach is reliable to study the heat transfer in both configurations (coated and uncoated engines)

- **Developing new numerical strategies to study the behavior of advanced insulation coatings applied on the combustion chamber walls in an ICE.**

  A strategy for modeling heat transfer in ICE with coated combustion chamber walls has been presented in Chapter 4. This approach consists in determining the properties of a thicker equivalent material, with a behavior similar to that of a thin thermal coating. The most important contributions of this methodology are listed below:

  - The results obtained with the 1D-HTM showed that by fixing some parameters, such as the equivalent coating thickness and number of mesh layers (nodes) and performing a DoE analysis, the proposed approach yields a temporal evolution of temperature and heat flux similar to that of the real coating.
  - It is possible to model the wall temperature swing of the thermal coating applying the equivalent material methodology in the 3D-CHT calculation as observed in Chapters 5 and 6.
  - To obtain accurate results, it is necessary to ensure that the mesh of the 3D-CHT calculation considers the same thickness and number of cells as in the 1D-HTM.
  - Currently, there is a significant uncertainty about the reliability of experimental techniques to determine the impact of thermal coatings on ICE. Thus, this tool constitutes an important contribution that can help to determine the accuracy of experimental techniques and improve them.
  - Though the new generation of thermal coatings are able to follow instantaneously the in-cylinder gas temperature in the combustion chamber, some considerations must be taken into account for their application in ICEs. In Chapter 5 was observed that a material with low thermal conductivity may not be enough to obtain a thermal gain in the engine. The insulation material must also have a low heat capacitance as seen in previous studies [129]. In general, the ideal coating should have the lowest possible values of thermal conductivity and heat capacitance.
  - Since most of the heat losses occur through the piston and cylinder head, the greatest benefits can be obtained by coating most of these surfaces. However, the insulating materials must be able to withstand the thermal conditions in the combustion chamber and not detach or disintegrate during the engine operation.

- **Optimization of the 3D calculation tools for saving computational resources.**

  Working on this thesis it was determined that CHT calculations are very time consuming. Hence, some optimization strategies have been developed in the frame of this work to accelerate the CFD-CHT calculations. In this regard, important contributions and findings have been presented in Chapter 6 for a better use of the computational resources.

  - Usually, conventional CAE softwares convert the base geometry of the engine into very fine surfaces, which are employed by CONVERGE. In particular, this refinement is quite considerable in the intake and exhaust valves. It was demonstrated that coarsening the surface mesh in these regions reduced the size of the output files and yielded to some improvement in RAM consumption.
  - According to previous background in CFD combustion modeling, a fixed refinement is employed on the combustion chamber walls to model the SI engine. However, a customized mesh approach was employed to model the CI engine in order to reduce the computational time of the CHT calculations. In this regard, the latter approach appears to be a better strategy to address the CHT calculations of the heat losses in ICEs. From the computational point of view, this y+ based AMR embedding strategy allowed to considerably reduce the number of cells in the domain, saving computational resources and without affecting the accuracy of the results.
  - The simulations carried out in Chapters 5 and 6 indicated that CHT calculations were faster for high speed operating conditions ($\geq$ 3000 RPM). For this reason, the times in the calibration process were significantly reduced as well.

7.2. Recommendations

From the experience acquired with this doctoral thesis, the following recommendations to perform CHT calculations are presented:

- When this thesis was proposed, the implementation of the CHT in CONVERGE was very recent. In addition, there was no previous background at CMT facilities on this type of simulation. Consequently, many errors due to inexperience took place in the project at the beginning.

According to the knowledge obtained, the first step before performing CHT simulations is to establish a planning scheme to achieve a balance between available resources and target objectives. Based on this balance, it can be determined which simplifications can be made to the achievement of results. It is important to know the quality/quantity of processors, RAM and storage capacity available. The fact of depending on an external computing cluster shared with the entire university can often complicate the accessibility of these resources.

- CHT calculations implies long computational times, but they also consume significant storage resources. Due to this limitation, an important amount of information must be trashed as the only alternative of saving specific information. This often means a loss of information, especially when it could be interesting to observe the cycle-to-cycle evolution of some variables. Nowadays, storage and management of data is a hot topic in the engineering world. From the experience of this thesis, it is suggested to invest R&D efforts in this matter, both for CHT calculations and for any type of calculation that leads to large output files.

7.3. Future works

Over the next years, ICEs are expected to continue to be the main propulsion system in transport vehicles. In this regard, it will be important to develop new alternatives that help to reduce heat losses and increase engine efficiency. The study of heat transfer by means of CHT calculation is a challenging task due to the complexity of the processes that take place in an ICE. Although important contributions have been made in this thesis in this regard, there is still much room for improvement. To achieve this target, the following suggestions are presented below:

- Since the y+ based AMR embedding approach seems to be the most suitable for modeling heat losses in ICEs, the use of this approach is also proposed to model gasoline engines. Since SI engines may require a finer mesh than CI engines, it might be interesting to apply this refinement configuration to all engine walls, including intake/exhaust valves and ports.

- The equivalent material methodology has proven its usefulness and validity to make CHT calculations with very thin coating layers. In this regard, it is proposed to apply this methodology to model the application of thermal coatings in other parts of the engine, such as

valves and exhaust exhaust. However, it is important to always comply the condition of properly setting the thickness and the number of nodes. This target is not trivial, and advanced CAD (Computer-aided design) modeling techniques may be required.

- The knowledge provided in this thesis about CHT calculations can be used in different engineering applications for propulsive systems in transportation such as:
  - The CHT can be used to model the cooling of batteries and heat transfer in heat exchangers for electric and hybrid vehicles. This is an important issue nowadays.
  - Since thermal coatings research will continue over the next years, the methodology developed in the frame of this thesis can be used to study further improvements in coatings applied in gasoline, marine and industrial engines that may help reducing further heat losses.
  - To perform thermal analysis of gas turbines components. The thermal stresses in the components can be studied to improve the design of the parts by using CHT calculations. In addition, the contributions made for studying thin coating layers can be used to model the application of TBCs to improve the turbines performance.

Bibliography

[1] A. Broatch, P. Olmeda, X. Margot, and J. Escalona. “New approach to study the heat transfer in internal combustion engines by 3D modelling”. International Journal of Thermal Sciences 138, 2019, pp. 405–415.

[2] A. Broatch, X. Margot, J. Garcia-Tiscar, and J. Escalona. “Validation and Analysis of Heat Losses Prediction Using Conjugate Heat Transfer Simulation for an Internal Combustion Engine”. In: 14th International Conference on Engines & Vehicles. SAE International, 2019 (cited in p. 79).

[3] P. Olmeda, X. Margot, P. Quintero, and J. Escalona. “Numerical approach to define a thermodynamically equivalent material for the Conjugate Heat Transfer simulation of very thin coating layers”. International Journal of Heat and Mass Transfer 162, 2020, p. 120377 (cited in p. 49).

[4] A. Broatch, P. Olmeda, X. Margot, and J. Escalona. “Conjugate Heat Transfer study of the impact of "thermo-swing" coatings on Internal Combustion Engines heat losses”. International Journal of Engine Research 138, 2020, pp. 405–415 (cited in p. 79).

[5] X. Margot, J. Escalona, and A. Bianco. “Development of a Novel Numerical Methodology for the Assessment of Insulating Coating Performance in Internal Combustion Engines”. Submitted to SAE WCX World Congress Experience, 2021.

[6] P. Olmeda, X. Margot, P. Quintero, and J. Escalona. “Reply to short communication ‘Comment on “Numerical approach to define a thermodynamically equivalent material for the conjugate heat transfer simulation of very thin coating layers" by P. Olmeda, X. Margot, P. Quintero, J. Escalona, International Journal of Heat and Mass Transfer, Vol. 162(2020) 120377 " by Jaal Ghandhi and Georgios Koutsakis”. International Journal of Heat and Mass Transfer, 2021.

[7] X. Margot, J. Gomez-Soriano, P. Quintero, and J. Escalona. “Implementation of 1D-3D integrated model for thermal prediction in internal combustion engines ”. Submitted to Applied Thermal Engineering, 2020.

[8] Proposal: Efficient Additivated Gasoline Lean Engine EAGLE. Horizon 2020 GV-02-2016, GA No. 724084. European Commission. 2016 (cited in pp. 1, 2, 4).

[9] C. Medina. "Biografıas: Arquımedes, Felice Matteucci y Eugenio Barsanti". Revista Prisma Tecnológico 5 (1), 2014, pp. 53–54 (cited in p. 2).

[10] M. Moyer. "Internal-combustion engine.(Cover story)". Scientific American 301 (3), 2009, pp. 97–97 (cited in p. 2).

[11] E. F. Somerscales and A. Zagotta. History of the internal combustion engine. Tech. rep. New York, NY (United States); American Society of Mechanical Engineers, 1989 (cited in p. 2).

[12] M. Weiss, P. Bonnel, J. Kühlwein, A. Provenza, et al. "Will Euro 6 reduce the NOx emissions of new diesel cars?–Insights from on-road tests with Portable Emissions Measurement Systems (PEMS)". Atmospheric Environment 62, 2012, pp. 657–665 (cited in p. 3).

[13] R. O'Driscoll, M. E. Stettler, N. Molden, T. Oxley, and H. M. ApSimon. "Real world CO2 and NOx emissions from 149 Euro 5 and 6 diesel, gasoline and hybrid passenger cars". Science of the total environment 621, 2018, pp. 282–290 (cited in p. 3).

[14] R. Giannelli and E. Nam. Medium and heavy duty diesel vehicle modeling using a fuel consumption methodology. 2004 (cited in p. 3).

[15] D. Chalet, M. Lesage, M. Cormerais, and T. Marimbordes. "Nodal modelling for advanced thermal-management of internal combustion engine". Applied energy 190, 2017, pp. 99–113 (cited in p. 8).

[16] L. Bates, D. Bradley, G. Paczko, and N. Peters. "Engine hot spots: Modes of auto-ignition and reaction propagation". Combustion and Flame 166, 2016, pp. 80–85 (cited in p. 8).

[17] Z. Wang, H. Liu, and R. D. Reitz. "Knocking combustion in spark-ignition engines". Progress in Energy and Combustion Science 61, 2017, pp. 78–112 (cited in p. 8).

[18] J. B. Heywood. "Combustion engine fundamentals". 1st Edition. Estados Unidos, 1988 (cited in pp. 8, 9, 84, 128).

[19] Z. Wang, H. Liu, T. Song, Y. Qi, et al. "Relationship between super-knock and pre-ignition". International Journal of Engine Research 16 (2), 2015, pp. 166–180 (cited in p. 8).

[20] T. Castiglione, S. Bova, and M. Belli. "A novel approach to the thermal management of internal combustion engines". Energy Procedia 126, 2017, pp. 883–890 (cited in p. 8).

[21] V. Esfahanian, A. Javaheri, and M. Ghaffarpour. "Thermal analysis of an SI engine piston using different combustion boundary condition treatments". Applied Thermal Engineering 26 (2-3), 2006, pp. 277–287 (cited in pp. 8, 130, 132, 133).

[22] A. H. Committee. ASM Handbook, Properties and Selection: Irons, Steels, and High-Performance Alloys. Vol. 1. ASM International, 1990 (cited in p. 8).

[23] A. K. Agarwal, S. K. Goyal, and D. K. Srivastava. "Time resolved numerical modeling of oil jet cooling of a medium duty diesel engine piston". International Communications in Heat and Mass Transfer 38 (8), 2011, pp. 1080–1085 (cited in p. 8).

[24] J. H. Chastain and J. R. Wagner. Advanced thermal management for internal combustion engines-valve design, component testing and block redesign. Tech. rep. SAE Technical Paper, 2006 (cited in p. 8).

[25] A. Vagenas, J. Hawley, C. Brace, and M. Ward. On-vehicle controllable cooling jets. Tech. rep. SAE Technical Paper, 2004 (cited in p. 8).

[26] K. Tanaka, K. Arase, and A. Kitayama. Development of Oil-Cooled Engine for Optimization of Engine Cooling System. Tech. rep. SAE Technical Paper, 2016 (cited in p. 9).

[27] A. Torregrosa, A. Broatch, P. Olmeda, and C. Romero. "Assessment of the influence of different cooling system configurations on engine warm-up, emissions and fuel consumption". International Journal of Automotive Technology 9 (4), 2008, pp. 447–458 (cited in p. 9).

[28] R. Cipollone, D. Di Battista, and M. Mauriello. "Effects of oil warm up acceleration on the fuel consumption of reciprocating internal combustion engines". Energy Procedia 82, 2015, pp. 1–8 (cited in p. 9).

[29] R. S. Benson and N. D. Whitehouse. Internal combustion engines: a detailed introduction to the thermodynamics of spark and compression ignition engines, their design and development. Vol. 1. Oxford: Pergamon Press, 1979 (cited in p. 9).

[30] C. Ferguson. Internal combustion engines. New York: Wiley, 1986 (cited in p. 9).

[31] Thermodynamics, F. M. Group, and W. Annand. "Heat transfer in the cylinders of reciprocating internal combustion engines". Proceedings of the Institution of Mechanical Engineers 177 (1), 1963, pp. 973–996 (cited in pp. 9, 11).

[32] C. C. J. French. "Piston Cooling". In: 1972 Automotive Engineering Congress and Exposition. SAE International, 1972 (cited in p. 9).

[33] G. Woschni. A universally applicable equation for the instantaneous heat transfer coefficient in the internal combustion engine. Tech. rep. SAE Technical paper, 1967 (cited in pp. 9, 11, 20).

[34] W. Seale and D. Taylor. "Spatial variation of heat transfer to pistons and liners of some medium speed diesel engines". Proceedings of the Institution of Mechanical Engineers 185 (1), 1970, pp. 203–218 (cited in p. 10).

[35] G. Sitkei. Heat transfer and thermal loading in internal combustion engines. Akademiai Kiado, 1974 (cited in p. 10).

[36] R. Prasad and N. Samria. "Transient heat transfer analysis in an internal combustion engine piston". Computers & Structures 34 (5), 1990, pp. 787–793 (cited in p. 10).

[37] D. Kouremenos, C. Rakopoulos, and D. Hountalas. "Thermodynamic analysis of indirect injection diesel engines by two-zone modeling of combustion". Transactions of the ASME, Journal of Engineering for Gas Turbines and Power, 1990 (cited in p. 10).

[38] C. Rakopoulos. "Influence of ambient temperature and humidity on the performance and emissions of nitric oxide and smoke of high speed diesel engines in the Athens/Greece region". Energy Conversion and Management 31 (5), 1991, pp. 447–458 (cited in p. 10).

[39] C. Rakopoulos and G. Mavropoulos. "Study of the steady and transient temperature field and heat flow in the combustion chamber components of a medium speed diesel engine using finite element analyses". International journal of energy research 20 (5), 1996, pp. 437–464 (cited in p. 10).

[40] C. Rakopoulos and G. Mavropoulos. "Components heat transfer studies in a low heat rejection DI diesel engine using a hybrid thermostructural finite element model". Applied thermal engineering 18 (5), 1998, pp. 301–316 (cited in p. 10).

[41] C. Rakopoulos and G. Mavropoulos. "Modelling the transient heat transfer in the ceramic combustion chamber walls of a low heat rejection diesel engine". International journal of vehicle design 22 (3-4), 1999, pp. 195–215 (cited in p. 10).

[42] C. Rakopoulos and G. Mavropoulos. "Experimental instantaneous heat fluxes in the cylinder head and exhaust manifold of an air-cooled diesel engine". Energy Conversion and Management 41 (12), 2000, pp. 1265–1281 (cited in p. 10).

[43] C. Rakopoulos, D. Rakopoulos, G. Mavropoulos, and E. Giakoumis. "Experimental and theoretical study of the short term response temperature transients in the cylinder walls of a diesel engine at various operating conditions". Applied Thermal Engineering 24 (5-6), 2004, pp. 679–702 (cited in p. 10).

[44] C. Rakopoulos and G. Mavropoulos. "Experimental evaluation of local instantaneous heat transfer characteristics in the combustion chamber of air-cooled direct injection diesel engine". Energy 33 (7), 2008, pp. 1084–1099 (cited in p. 10).

[45] A. Alkidas and J. Myers. "Transient heat-flux measurements in the combustion chamber of a spark-ignition engine". Trans ASME J Heat Transfer, 1982 (cited in p. 10).

[46] Y. Enomoto and S. Furuhama. "A study of the local heat transfer coefficient on the combustion chamber walls of a four-stroke gasoline engine". JSME international journal. Ser. 2, Fluids engineering, heat transfer, power, combustion, thermophysical properties 32 (1), 1989, pp. 107–114 (cited in p. 11).

[47] J. Chang, O. Güralp, Z. Filipi, D. Assanis, et al. "New heat transfer correlation for an HCCI engine derived from measurements of instantaneous surface heat flux". SAE transactions, 2004, pp. 1576–1593 (cited in p. 11).

[48] S. Broekaert, T. De Cuyper, M. De Paepe, and S. Verhelst. Experimental Investigation and Modelling of the In-Cylinder Heat Transfer during Ringing Combustion in an HCCI Engine. Tech. rep. SAE Technical Paper, 2017 (cited in p. 11).

[49] R. Thring. "Low heat rejection engines". SAE transactions, 1986, pp. 377–383 (cited in pp. 12–14, 147).

[50] W. Bryzik and R. Kamo. "TACOM/Cummins adiabatic engine program". SAE transactions, 1983, pp. 1063–1087 (cited in p. 12).

[51] S. Jaichandar and P. Tamilporai. Low heat rejection engines–an overview. Tech. rep. SAE Technical Paper, 2003 (cited in p. 13).

[52] C. H. Moore and J. L. Hoehne. "Combustion chamber insulation effect on the performance of a low heat rejection Cummins V-903 engine". SAE transactions, 1986, pp. 415–426 (cited in p. 13).

[53] Y. Miyairi. "Computer simulation of an LHR DI diesel engine". SAE transactions, 1988, pp. 282–294 (cited in p. 13).

[54] J. Tovell. "The reduction of heat losses to the diesel engine cooling system". SAE transactions, 1983, pp. 1088–1097 (cited in p. 13).

[55] L. Bruns, W. Bryzik, and R. Kamo. Performance Assessment of US. Army Truck with Adiabatic Diesel Engine. Tech. rep. SAE Technical Paper, 1989 (cited in p. 13).

[56] S. Colgate. "Partial adiabatic cycle heat loss". In: Intersociety energy conversion engineering conference. 21. 1986, pp. 331–335 (cited in p. 13).

[57] W. Wade, P. Havstad, E. Ounsted, F. Trinkler, and I. Garwin. "Fuel economy opportunities with an uncooled DI diesel engine". SAE transactions, 1984, pp. 743–756 (cited in p. 13).

[58] W. K. Cheng, V. W. Wong, and F. Gao. Heat transfer measurement comparisons in insulated and non-insulated diesel engines. Tech. rep. SAE Technical Paper, 1989 (cited in p. 13).

[59] T. Morel, S. Wahiduzzaman, and E. F. Fort. "Heat transfer experiments in an insulated diesel". SAE transactions, 1988, pp. 261–281 (cited in p. 14).

[60] G. Woschni, W. Spindler, and K. Kolesa. "Heat insulation of combustion chamber walls—a measure to decrease the fuel consumption of IC engines?" SAE transactions, 1987, pp. 269–279 (cited in p. 14).

[61] D. W. Dickey, S. Vinyard, and R. Keribar. The effect of insulated combustion chamber surfaces on direct-injected Diesel engine performance, emissions, and combustion. Tech. rep. SAE Technical Paper, 1989 (cited in p. 14).

[62] S. Furuhama and Y. Enomoto. "Heat transfer into ceramic combustion wall of internal combustion engines". SAE transactions, 1987, pp. 38–53 (cited in p. 14).

[63] S. Henningsen. "Evaluation of emissions and heat-release characteristics from a simulated low-heat-rejection diesel engine". SAE transactions, 1987, pp. 811–826 (cited in p. 14).

[64] A. Alkidas. "Performance and emissions achievements with an uncooled heavy-duty, single-cylinder diesel engine". SAE Transactions, 1989, pp. 137–148 (cited in p. 14).

[65] R. Kamo, D. N. Assanis, and W. Bryzik. "Thin thermal barrier coatings for engines". SAE Transactions, 1989, pp. 131–136 (cited in p. 14).

[66] T. D. Bennett and F. Yu. "A nondestructive technique for determining thermal properties of thermal barrier coatings". Journal of applied physics 97 (1), 2005, p. 013520 (cited in p. 15).

[67] S. M. Meier and D. Gupta. "The evolution of thermal barrier coatings in gas turbine engine applications". ASME. J. Eng. Gas Turbines Power 116 (1), 1994, pp. 250–257 (cited in p. 15).

[68] D. N. Assanis. "Thin thermal barrier coatings for internal combustion engine components". International Journal of Materials and Product Technology 4 (3), 1989, pp. 232–243 (cited in p. 15).

[69] R. Kamo, W. Bryzik, M. Reid, and M. Woods. "Coatings for improving engine performance". SAE transactions, 1997, pp. 354–363 (cited in p. 15).

[70] R. A. Miller and D. Zhu. "Lower-Conductivity Thermal-Barrier Coatings". NASA Glenn Research Center; Cleveland, OH, United States, 2003 (cited in p. 15).

[71] D. Zhu and R. A. Miller. "Development of advanced low conductivity thermal barrier coatings". International Journal of Applied Ceramic Technology 1 (1), 2004, pp. 86–94 (cited in p. 15).

[72] D. N. Assanis and T. Mathur. "The effect of thin ceramic coatings on spark-ignition engine performance". SAE transactions, 1990, pp. 981–990 (cited in p. 15).

[73] T. Powell, R. O'Donnell, M. Hoffman, and Z. Filipi. "Impact of a yttria-stabilized zirconia thermal barrier coating on HCCI engine combustion, emissions, and efficiency". Journal of Engineering for Gas Turbines and Power 139 (11), 2017 (cited in p. 15).

[74] S. Caputo, F. Millo, G. Cifali, and F. C. Pesce. "Numerical investigation on the effects of different thermal insulation strategies for a passenger car diesel engine". SAE International Journal of Engines 10 (4), 2017, pp. 2154–2165 (cited in p. 15).

[75] S. Caputo, F. Millo, G. Boccardo, A. Piano, G. Cifali, and F. C. Pesce. "Numerical and experimental investigation of a piston thermal barrier coating for an automotive diesel engine application". Applied Thermal Engineering 162, 2019, p. 114233 (cited in pp. 16, 146).

[76] Y. Wang, T. Ma, L. Liu, and M. Yao. "Numerical Investigation of the Effect of Thermal Barrier Coating on Combustion and Emissions in a Diesel Engine". Applied Thermal Engineering, 2020, p. 116497 (cited in p. 16).

[77] H. Kosaka, Y. Wakisaka, Y. Nomura, Y. Hotta, et al. "Concept of "temperature swing heat insulation" in combustion chamber walls, and appropriate thermo-physical properties for heat insulation coat". SAE International Journal of Engines 6 (1), 2013, pp. 142–149 (cited in p. 16).

[78] A. Kikusato, K. Terahata, K. Jin, and Y. Daisho. "A Numerical Simulation Study on Improving the Thermal Efficiency of a Spark Ignited Engine—Part 2: Predicting Instantaneous Combustion Chamber Wall Temperatures, Heat Losses and Knock—". SAE International Journal of Engines 7 (1), 2014, pp. 87–95 (cited in pp. 16, 17, 21, 58).

[79] T. Kogo, Y. Hamamura, K. Nakatani, T. Toda, A. Kawaguchi, and A. Shoji. High Efficiency Diesel Engine with Low Heat Loss Combustion Concept-Toyota's Inline 4-Cylinder 2.8-Liter ESTEC 1GD-FTV Engine. Tech. rep. SAE Technical Paper, 2016 (cited in p. 16).

[80] K. Fukui, Y. Wakisaka, K. Nishikawa, Y. Hattori, H. Kosaka, and A. Kawaguchi. Development of instantaneous temperature measurement technique for combustion chamber surface and verification of temperature swing concept. Tech. rep. SAE Technical Paper, 2016 (cited in p. 18).

[81] M. Andrie, S. Kokjohn, S. Paliwal, L. S. Kamo, A. Kamo, and D. Procknow. Low heat capacitance thermal barrier coatings for internal combustion engines. Tech. rep. SAE Technical Paper, 2019 (cited in pp. 18, 60).

[82] S. Moser, R. O'Donnell, M. Hoffman, E. Jordan, T. Powell, and Z. Filipi. Experimental Investigation of Low Cost, Low Thermal Conductivity Thermal Barrier Coating on HCCI Combustion, Efficiency, and Emissions. Tech. rep. SAE Technical Paper, 2020 (cited in p. 18).

[83] F. Carpenter and A. Colburn. "Proceedings of General Discussion on Heat Transfer". Inst. Mech. Engrs., London, England, 1951, pp. 1–7 (cited in p. 20).

[84] V. Gnielinski. "On heat transfer in tubes". International Journal of Heat and Mass Transfer 63, 2013, pp. 134–140 (cited in p. 20).

[85] F. Dittus and L. Boelter. "Heat transfer in automobile radiators of the tubular type". International Communications in Heat and Mass Transfer 12 (1), 1985, pp. 3–22 (cited in pp. 20, 28).

[86] E. N. Sieder and G. E. Tate. "Heat transfer and pressure drop of liquids in tubes". Industrial & Engineering Chemistry 28 (12), 1936, pp. 1429–1435 (cited in p. 20).

[87] S. Shaaban and J. Seume. "Analysis of turbocharger non-adiabatic performance". In: 8th International Conference on Turbochargers and Turbocharging. 2006, pp. 119–130 (cited in p. 20).

[88] A. Torregrosa, P. Olmeda, B. Degraeuwe, and M. Reyes. "A concise wall temperature model for DI Diesel engines". Applied Thermal Engineering 26 (11-12), 2006, pp. 1320–1327 (cited in p. 20).

[89] P. Olmeda, V. Dolz, F. Arnau, and M. Reyes-Belmonte. "Determination of heat flows inside turbochargers by means of a one dimensional lumped model". Mathematical and computer modelling 57 (7-8), 2013, pp. 1847–1852 (cited in p. 21).

[90] A. Broatch, P. Olmeda, A. Garcıa, J. Salvador-Iborra, and A. Warey. "Impact of swirl on in-cylinder heat transfer in a light-duty diesel engine". Energy 119, 2017, pp. 1010–1023 (cited in p. 21).

[91] A. Torregrosa, A. Broatch, P. Olmeda, J. Salvador-Iborra, and A. Warey. "Experimental study of the influence of exhaust gas recirculation on heat transfer in the firedeck of a direct injection diesel engine". Energy Conversion and Management 153, 2017, pp. 304–312 (cited in p. 21).

[92] D. N. Assanis and E. Badillo. "Transient analysis of piston-liner heat transfer in low-heat-rejection diesel engines". SAE transactions, 1988, pp. 295–305 (cited in p. 22).

[93] C. Borgnakke, V. S. Arpaci, and R. J. Tabaczynski. A model for the instantaneous heat transfer and turbulence in a spark ignition engine. Tech. rep. SAE Technical Paper, 1980 (cited in p. 22).

[94] T. Morel and R. Keribar. "A model for predicting spatially and time resolved convective heat transfer in bowl-in-piston combustion chambers". SAE transactions, 1985, pp. 77–93 (cited in p. 22).

[95] M. M. Patil, A. Pise, and N. Gokhale. Simulation of conjugate heat transfer (CHT) between engine head and cooling medium of diesel engine. Tech. rep. SAE Technical Paper, 2015 (cited in p. 22).

[96] Y. Li and S.-C. Kong. "Coupling conjugate heat transfer with in-cylinder combustion modeling for engine simulation". International journal of heat and mass transfer 54 (11-12), 2011, pp. 2467–2478 (cited in pp. 22, 23, 123).

[97] J. Xin, S. Shih, E. Itano, and Y. Maeda. "Integration of 3D combustion simulations and conjugate heat transfer analysis to quantitatively evaluate component temperatures". SAE transactions, 2003, pp. 2210–2220 (cited in p. 23).

[98] E. Urip, K. H. Liew, and S. Yang. "Modeling IC engine conjugate heat transfer using the KIVA code". Numerical Heat Transfer, Part A: Applications 52 (1), 2007, pp. 1–23 (cited in pp. 23, 123).

[99] O. Iqbal, K. Arora, and M. Sanka. "Thermal map of an IC engine via conjugate heat transfer: validation and test data correlation". SAE International Journal of Engines 7 (1), 2014, pp. 366–374 (cited in p. 23).

[100] P. Kundu, R. Scarcelli, S. Som, A. Ickes, et al. Modeling heat loss through pistons and effect of thermal boundary coatings in Diesel engine simulations using a conjugate heat transfer model. 2016. SAE Technical Paper (cited in pp. 23, 50, 87).

[101] A. Poubeau, A. Vauvy, F. Duffour, J.-M. Zaccardi, G. d. Paola, and M. Abramczuk. "Modeling investigation of thermal insulation approaches for low heat rejection Diesel engines using a conjugate heat transfer model". International Journal of Engine Research 20 (1), 2019, pp. 92–104 (cited in pp. 23, 145).

[102] "CONVERGENT SCIENCE Inc." CONVERGE 2.3 Theory Manual, 2018 (cited in pp. 27–29, 82–84, 88, 129).

[103] V. Yakhot and S. A. Orszag. "Renormalization group analysis of turbulence. I. Basic theory". Journal of scientific computing 1 (1), 1986, pp. 3–51 (cited in pp. 29, 84).

[104] P. O'rourke and A. Amsden. "A particle numerical model for wall film dynamics in port-injected engines". SAE transactions, 1996, pp. 2000–2013 (cited in pp. 29, 128).

[105] A. A. Amsden and M. Findley. KIVA-3V: A block-structured KIVA program for engines with vertical or canted valves. Tech. rep. Lawrence Livermore National Lab.(LLNL), Livermore, CA (United States), 1997 (cited in pp. 29, 84, 128).

[106] C. Angelberger, T. Poinsot, and B. Delhay. Improving near-wall combustion and wall heat transfer modeling in SI engine computations. Tech. rep. SAE Technical Paper, 1997 (cited in p. 29).

[107] Z. Han and R. D. Reitz. "A temperature wall function formulation for variable-density turbulent flows with application to engine convective heat transfer modeling". International journal of heat and mass transfer 40 (3), 1997, pp. 613–625 (cited in p. 29).

[108] T. C. J. Cousteix. Modeling and computation of boundary-layer flows. Springer, 2005 (cited in p. 30).

[109] X. Yu, G. Li, W. Dong, Z. Shang, et al. "Numerical study on effects of hydrogen direct injection on hydrogen mixture distribution, combustion and emissions of a gasoline/hydrogen SI engine under lean burn condition". International Journal of Hydrogen Energy 45 (3), 2020, pp. 2341–2350 (cited in p. 31).

[110] L. He, L. Jingyuan, Y. Xiumin, L. Mengliang, and Y. Tian. "Numerical study on combustion and emission characteristics of a PFI gasoline engine with hydrogen direct-injection". Energy Procedia 158, 2019, pp. 1449–1454 (cited in p. 31).

[111] P. Sharma and A. Dhar. "Compression ratio influence on combustion and emissions characteristic of hydrogen diesel dual fuel CI engine: Numerical Study". Fuel 222, 2018, pp. 852–858 (cited in p. 31).

[112] B. Wang, T. Li, L. Ge, and H. Ogawa. "Optimization of combustion chamber geometry for natural gas engines with diesel micro-pilot-induced ignition". Energy conversion and management 122, 2016, pp. 552–563 (cited in p. 31).

[113] G. Tripathi, P. Sharma, A. Dhar, and A. Sadiki. "Computational investigation of diesel injection strategies in hydrogen-diesel dual fuel engine". Sustainable Energy Technologies and Assessments 36, 2019, p. 100543 (cited in p. 31).

[114] M. R. Boldaji, B. Gainey, P. O'Donnell, J. Gohn, and B. Lawler. "Investigating the effect of spray included angle on thermally stratified compression ignition with wet ethanol using computational fluid dynamics". Applied Thermal Engineering 170, 2020, p. 114964 (cited in p. 31).

[115] A. Torregrosa, A. Broatch, P. Olmeda, J. Martı, et al. "A contribution to film coefficient estimation in piston cooling galleries". Experimental Thermal and Fluid Science 34 (2), 2010, pp. 142–151 (cited in pp. 35, 36).

[116] "Gamma Technologies Inc." GT-SUITE Theory Manual, 2019 (cited in pp. 38, 40).

[117] P. Gommel. "SAE 5W-30 engine oils as all-season multigrade oils for passenger cars", 1986 (cited in p. 38).

[118] S. D. Larson. "Phase studies of the two-component carbon dioxide-water system, involving the carbon dioxide hydrate". Ph. D. Thesis, Univ. of Michigan, 1955 (cited in p. 38).

[119] C. L. Yaws, H.-C. Yang, and X. Pan. "633 Organic chemicals: surface tension data". Chemical Engineering 98 (3), 1991, p. 140 (cited in p. 39).

[120] C. L. Yaws and P. C. Richmond. "Surface tension—Organic compounds". In: Thermophysical Properties of Chemicals and Hydrocarbons. Elsevier, 2009, pp. 686–781 (cited in p. 40).

[121] S. Peyghambarzadeh, S. Hashemabadi, S. Hoseini, and M. S. Jamnani. "Experimental study of heat transfer enhancement using water/ethylene glycol based nanofluids as a new coolant for car radiators". International communications in heat and mass transfer 38 (9), 2011, pp. 1283–1290 (cited in p. 40).

[122] P. Wang, R. Liang, Y. Yu, J. Zhang, J. Lv, and M. Bai. "The flow and heat transfer characteristics of engine oil inside the piston cooling gallery". Applied Thermal Engineering 115, 2017, pp. 620–629 (cited in p. 40).

[123] C. W. Hirt and B. D. Nichols. "Volume of fluid (VOF) method for the dynamics of free boundaries". Journal of computational physics 39 (1), 1981, pp. 201–225 (cited in p. 40).

[124] S. Muzaferija. "A two-fluid Navier-Stokes solver to simulate water entry". In: Proceedings of 22nd symposium on naval architecture, 1999. National Academy Press. 1999, pp. 638–651 (cited in p. 41).

[125] M. Leguille, F. Ravet, J. Le Moine, E. Pomraning, K. Richards, and P. K. Senecal. Coupled Fluid-Solid Simulation for the Prediction of Gas-Exposed Surface Temperature Distribution in a SI Engine. WCX™ 17: SAE World Congress Experience. SAE International, 2017 (cited in p. 50).

[126] M. Wu, Y. Pei, J. Qin, X. Li, and J. Zhou. Study on Methods of Coupling Numerical Simulation of Conjugate Heat Transfer and In-Cylinder Combustion Process in GDI Engine. WCX™ 17: SAE World Congress Experience. SAE International, 2017 (cited in p. 50).

[127] L. Zhang. "Parallel simulation of engine in-cylinder processes with conjugate heat transfer modeling". Applied Thermal Engineering 142, 2018, pp. 232–240 (cited in p. 50).

[128] D. Hummel, S. Beer, and A. Hornung. "A conjugate heat transfer model for unconstrained melting of macroencapsulated phase change materials subjected to external convection". International Journal of Heat and Mass Transfer 149, 2020, p. 119205 (cited in p. 50).

[129] A. Broatch, P. Olmeda, X. Margot, and J. Gomez-Soriano. "A one-dimensional modeling study on the effect of advanced insulation coatings on internal combustion engine efficiency". International Journal of Engine Research, 2020, p. 1468087420921584 (cited in pp. 52, 153).

[130] A. Bejan and A. D. Kraus. Heat transfer handbook. Vol. 1. John Wiley & Sons, 2003 (cited in pp. 56, 59).

[131] J. Chérel, J.-M. Zaccardi, B. Bouteiller, and A. Allimant. "Experimental assessment of new insulation coatings for lean burn spark-ignited engines". Oil & Gas Science and Technology–Revue d'IFP Energies nouvelles 75, 2020, p. 11 (cited in p. 60).

[132] F. Payri, J. Luján, J. Martın, and A. Abbad. "Digital signal processing of in-cylinder pressure for combustion diagnosis of internal combustion engines". Mechanical Systems and Signal Processing 24 (6), 2010, pp. 1767–1784 (cited in p. 61).

[133] F. Payri, P. Olmeda, J. Martın, and A. Garcıa. "A complete 0D thermodynamic predictive model for direct injection diesel engines". Applied Energy 88 (12), 2011, pp. 4632–4641 (cited in p. 61).

[134] A. Broatch, P. Olmeda, X. Margot, and J. Gómez-Soriano. "Numerical simulations for evaluating the impact of advanced insulation coatings on H2 additivated gasoline lean combustion in a turbocharged spark-ignited engine". Applied Thermal Engineering 148, 2019, pp. 674–683 (cited in pp. 80, 94).

[135] E. Pomraning, K. Richards, and P. Senecal. Modeling turbulent combustion using a RANS model, detailed chemistry, and adaptive mesh refinement. Tech. rep. SAE Technical Paper, 2014 (cited in p. 83).

[136] S. D. Givler, M. Raju, E. Pomraning, P. Senecal, N. Salman, and R. Reese. Gasoline combustion modeling of direct and port-fuel injected engines using a reduced chemical mechanism. Tech. rep. SAE Technical Paper, 2013 (cited in p. 83).

[137] R. Scarcelli, K. Richards, E. Pomraning, P. K. Senecal, J. M. Sevik, and T. Wallner. Cycle-to-cycle variations in multi-cycle engine RANS simulations. Tech. rep. Argonne National Lab.(ANL), Argonne, IL (United States), 2016 (cited in p. 83).

[138] A. Robert, S. Richard, O. Colin, L. Martinez, and L. De Francqueville. "LES prediction and analysis of knocking combustion in a spark ignition engine". Proceedings of the Combustion Institute 35 (3), 2015, pp. 2941–2948 (cited in p. 83).

[139] A. Robert, S. Richard, O. Colin, and T. Poinsot. "LES study of deflagration to detonation mechanisms in a downsized spark ignition engine". Combustion and Flame 162 (7), 2015, pp. 2788–2807 (cited in p. 83).

[140] J. Gómez Soriano. "Computational assessment of combustion noise of automotive compression-ignited engines". PhD thesis. 2018 (cited in pp. 84, 126, 127, 146).

[141] J. C. Beale and R. D. Reitz. "Modeling spray atomization with the Kelvin-Helmholtz/Rayleigh-Taylor hybrid model". Atomization and sprays 9 (6), 1999 (cited in p. 84).

[142] P. J. O'Rourke. Collective drop effects on vaporizing liquid sprays. Tech. rep. Los Alamos National Lab., NM (USA), 1981 (cited in p. 84).

[143] A. Amsden. "A computer program for chemically reactive flows with sprays". Report of Los Alamos National Laboratory, 1989 (cited in p. 84).

[144] P. Senecal, E. Pomraning, K. Richards, T. Briggs, et al. "Multi-dimensional modeling of direct-injection diesel spray liquid length and flame lift-off length using CFD and parallel detailed chemistry". SAE transactions, 2003, pp. 1331–1351 (cited in p. 84).

[145] H. Hiroyasu and T. Kadota. "Models for combustion and formation of nitric oxide and soot in direct injection diesel engines". SAE transactions, 1976, pp. 513–526 (cited in pp. 84, 128).

[146] O. Redlich and J. N. Kwong. "On the thermodynamics of solutions. V. An equation of state. Fugacities of gaseous solutions." Chemical reviews 44 (1), 1949, pp. 233–244 (cited in p. 84).

[147] R. I. Issa. "Solution of the implicitly discretised fluid flow equations by operator-splitting". Journal of computational physics 62 (1), 1986, pp. 40–65 (cited in p. 84).

[148] A. Broatch, X. Margot, R. Novella, and J. Gomez-Soriano. "Impact of the injector design on the combustion noise of gasoline partially premixed combustion in a 2-stroke engine". Applied Thermal Engineering 119, 2017, pp. 530–540 (cited in pp. 85, 128).

[149] F. Payri, P. Olmeda, J. Martin, and R. Carreño. "A new tool to perform global energy balances in DI diesel engines". SAE International Journal of Engines 7 (1), 2014, pp. 43–59 (cited in p. 86).

[150] A. J. Torregrosa, P. Olmeda, J. Martın, and C. Romero. "A tool for predicting the thermal performance of a diesel engine". Heat transfer engineering 32 (10), 2011, pp. 891–904 (cited in p. 86).

[151] P. Olmeda, J. Martın, R. Novella, and R. Carreño. "An adapted heat transfer model for engines with tumble motion". Applied Energy 158, 2015, pp. 190–202 (cited in p. 86).

[152] J. R. Serrano, P. Olmeda, F. J. Arnau, A. Dombrovsky, and L. Smith. "Analysis and methodology to characterize heat transfer phenomena in automotive turbochargers". Journal of engineering for gas turbines and power 137 (2), 2015 (cited in p. 86).

[153] L. Jarrier, J. Champoussin, R. Yu, and D. Gentile. Warm-up of a DI diesel engine: experiment and modeling. Tech. rep. SAE Technical Paper, 2000 (cited in p. 88).

[154] Y. Lu, X. Zhang, P. Xiang, and D. Dong. "Analysis of thermal temperature fields and thermal stress under steady temperature field of diesel engine piston". Applied thermal engineering 113, 2017, pp. 796–812 (cited in pp. 88, 130, 133, 141).

[155] J. A. Kaplan and J. B. Heywood. "Modeling the spark ignition engine warm-up process to predict component temperatures and hydrocarbon emissions". SAE transactions, 1991, pp. 361–376 (cited in p. 88).

[156] S. V. Bohac, D. M. Baker, and D. N. Assanis. "A global model for steady state and transient SI engine heat transfer studies". SAE transactions, 1996, pp. 196–214 (cited in p. 88).

[157] L. Gang. "FEM for Medium Speed Diesel Engine Combined Piston Analysis". Shanghai Jiaotong University (in Chinese), 2007 (cited in p. 89).

[158] W. Qianwen, Z. Jinchen, P. Min, X. Zhimin, H. Dingyun, and H. Yuping. "Numerical simulation of piston oscillating cooling and temperature field analysis (in chinese)". Veh. Eng. 2015, pp. 54–59 (cited in p. 89).

[159] A. Mohiuddin. "Investigation of the swirl effect on engine using designed swirl adapter". IIUM Engineering Journal 12 (3), 2011 (cited in p. 124).

[160] C. Habchi, F. A. Lafossas, P. Béard, and D. Broseta. "Formulation of a One-Component Fuel Lumping Model to Assess the Effects of Fuel Thermodynamic Properties on Internal Combustion Engine Mixture Preparation and Combustion". In: 2004 SAE Fuels Lubricants Meeting Exhibition. SAE International, 2004 (cited in p. 127).

[161] S. Molina, A. Garcıa, J. Pastor, E. Belarte, and I. Balloul. "Operating range extension of RCCI combustion concept from low to full load in a heavy-duty engine". Applied Energy 143, 2015, pp. 211–227 (cited in p. 127).

[162] M. Gonera and O. Sandin. "Thermal Analysis of a Diesel Piston and Cylinder Liner using the Inverse Heat Conduction Method". Goteborg, Sweden, Chalmers University Of Technology, 2015 (cited in p. 133).

[163] J. Bredberg. "On the wall boundary condition for turbulence models". Chalmers University of Technology, Department of Thermo and Fluid Dynamics. Internal Report 00/4. G oteborg, 2000 (cited in p. 136).

UNIVERSITAT POLITÈCNICA DE VALÈNCIA

DOCTORAL THESIS

MODELLING OF HEAT LOSSES THROUGH COATED CYLINDER WALLS AND THEIR IMPACT ON ENGINE PERFORMANCE

PRESENTED BY
Johan Enrique Escalona Cornejo

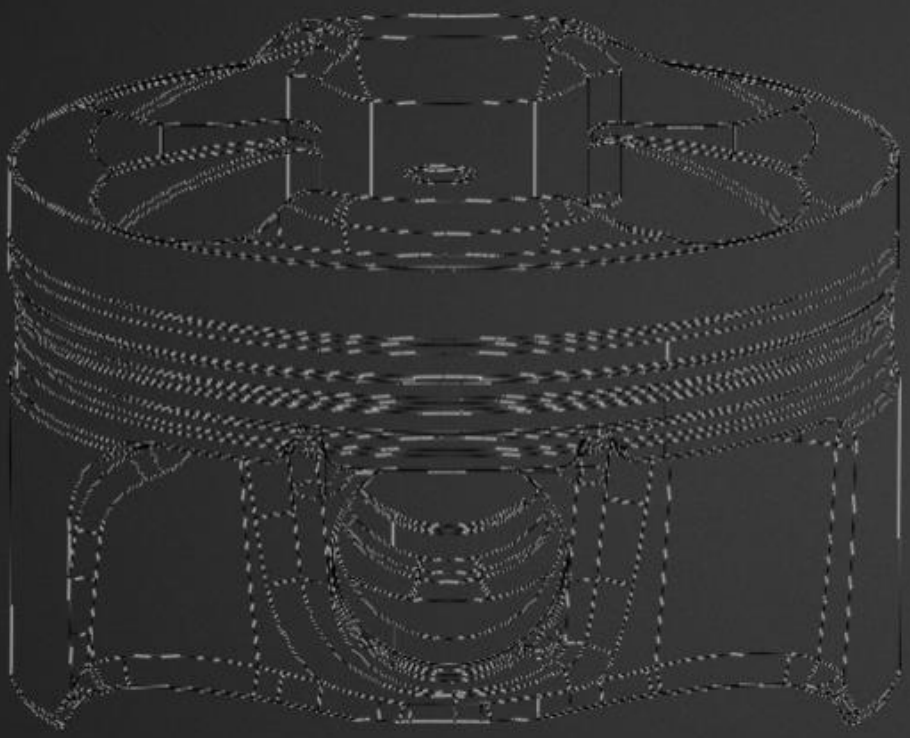

February 2021
DEPARTAMENTO DE MÁQUINAS Y MOTORES TÉRMICOS